

THESIS

OPTIMIZATION OF DAYTIME FUEL CONSUMPTION FOR A HYBRID DIESEL  
AND PHOTOVOLTAIC INDUSTRIAL MICRO-GRID

Submitted by

Stacey Dufrane

Department of Mechanical Engineering

In partial fulfillment of the requirements

For the Degree of Master of Science

Colorado State University

Fort Collins, Colorado

Spring 2017

Master's Committee:

Advisor: Anthony Marchese  
Co-Advisor: Daniel Zimmerle

Siddharth Suryanarayanan  
Thomas Bradley

Copyright by Stacey Dufrane 2017

All Rights Reserved

## ABSTRACT

### OPTIMIZATION OF DAYTIME FUEL CONSUMPTION FOR A HYBRID DIESEL AND PHOTOVOLTAIC INDUSTRIAL MICRO-GRID

The work to be presented will examine the optimization of daytime diesel fuel consumption for a hybrid diesel and photovoltaic (PV) industrial micro-grid with no energy storage. The micro-grid utilizes a control system developed to forecast PV transients and manage the diesel generators providing electrical supply to the micro-grid. The work focuses on optimization of daytime fuel consumption when PV generation is available. Simulations were utilized to minimize diesel consumption while maintaining secure operations by controlling both PV curtailment and diesel generation. The control system utilizes a cloud forecast system based upon sky imaging, developed by CSIRO (Australia), to predict the presence of cloud cover in concentric “rings” around the sun’s position in the sky. The control system utilizes these cloud detections to establish supervisory settings for PV and diesel generation. Work included methods to optimize control response for the number of rings around the sun, studied the use of two different sizes of generators to allow for increased PV utilization, and modification of generator controller settings to reduce fault occurrence. The work indicates that increasing the number of rings used to create the PV forecast has the greatest impact on reducing the number of faults, while having a minimal impact on the total diesel consumption. Additionally, increasing the total number of generators in the system increases PV utilization and decreases fuel consumption.

## ACKNOWLEDGEMENTS

There are several people who I would like to thank for their support while I was working on this project. This is not limited to faculty here at Colorado State University. I am grateful for all of their contributions and encouragement. First of all, I would like to acknowledge Daniel Zimmerle. Without his industry experience and partners outside of the university, I would not have the opportunity to work on this project. He has helped me learn new skills that I will not only use on this project, but for the rest of my career as an engineer. Next, I would like to acknowledge Jerry Duggan who worked as a software engineer on this project. He helped me learn how to validate test configurations that were crucial to the deployment of this system and helped me evaluate what was feasible for this system. I am confident that his expertise will lead to a smooth deployment of this system and I am grateful to have worked with him. I would also like to acknowledge Redavia who is the project sponsor. Without them, I would have not have had the opportunity to collaborate with Dan Zimmerle or CSIRO on this project. Next, I would like to thank Sam West as CSIRO for designing the cloud tracking system for this project. Next, I would like to acknowledge my academic advisor, Anthony Marchese. He gave me a lot of guidance on how to format my thesis, choose my committee members, and prepare for my defense. Although I have not worked closely with him in my academic pursuits, I am grateful for his insight. Lastly, I would like to thank Siddharth Suryanarayanan. I really enjoyed taking his electrical power systems course in the spring of 2015 and feel that he has taught me skills that I will use for my entire career. I would also like to thank all of the engineering faculty at Colorado State University who helped me complete all my coursework as part of the requirements for the degree of the master of science in mechanical engineering.

## TABLE OF CONTENTS

ABSTRACT.....	ii
ACKNOWLEDGEMENTS .....	iii
LIST OF TABLES .....	vi
LIST OF FIGURES .....	vii
NOMENCLATURE .....	ix
1 INTRODUCTION .....	1
1.1 SITE INFORMATION .....	2
1.2 GENERATOR OPERATION .....	5
1.2.1 LOAD MANAGEMENT.....	6
1.2.2 OPERATING RANGE DEFINITIONS .....	6
1.2.3 GENERATOR STATE MACHINE .....	8
1.2.4 GENERATOR FUEL CONSUMPTION .....	12
1.3 INDUSTRIAL LOADING PATTERNS .....	14
1.4 MICRO-GRID DEFINITION .....	18
1.5 CONNECTION STANDARDS .....	18
1.5.1 IEEE 1547: “STANDARD FOR INTERCONNECTING DISTRIBUTED RESOURCES WITH ELECTRIC POWER SYSTEMS” .....	19
1.5.2 IEEE 519-2014: “IEEE RECOMMENDED PRACTICE AND REQUIREMENTS FOR HARMONIC CONTROL IN ELECTRIC POWER SYSTEMS” .....	21
1.6 INTEGRATION OF PV SYSTEM USING INVERTERS.....	22
1.7 “INDUSTRY STANDARD” FOR PV UTILIZATION .....	23
1.8 PLANNED SYSTEM CONFIGURATION .....	27
1.8.1 CALCULATION OF THE MINIMUM GENERATORS ONLINE.....	28
1.8.2 CALCULATION OF MAXIMUM PV OUTPUT .....	29
1.9 EXISTING CLOUD TRACKING METHODS AND LIMITATIONS .....	31
1.9.1 INTRA-WEEK FORECASTS.....	31
1.9.2 INTRA-DAY FORECASTS.....	33
1.9.3 INTRA-HOUR FORECASTS .....	33
1.10 PROBLEM STATEMENT .....	35
2 METHODS .....	38
2.1 FORECAST INPUTS TO THE SUPERVISORY CONTROLLER.....	38
2.2 SYSTEM OVERVIEW .....	38
2.2.1 PV FORECASTING SYSTEFM.....	39
2.2.2 LOAD FORECASTING USING A MARKOV TRANSITION MATRIX .....	52
2.2.3 RESERVE CALCULATION .....	54
2.3 GENERATOR CONTROLS .....	56
2.3.1 ‘MIN NUM ON’ PARAMETER.....	57
2.3.2 LOAD-DEPENDENT START .....	58
2.3.3 LOAD-DEPENDENT STOP.....	58
2.3.4 FAULT PROTECTION METHODS .....	59
2.4 OPTIMIZATION TECHNIQUES .....	60
2.4.1 IMPROVEMENT OF PV FORECAST BASED ON NUMBER OF RINGS .....	60

2.4.2	USE OF SMALLER GENERATORS TO REDUCE FUEL CONSUMPTION....	63
3	RESULTS AND DISCUSSION.....	65
3.1	MODIFICATION OF PV FORECASTING SETTINGS.....	65
3.1.1	ANALYSIS OF PV FORECAST ERRORS .....	74
3.1.2	COMPARISON TO “INDUSTRY STANDARD” .....	82
3.1.3	COMPARISON TO “NO PV” CASE .....	84
3.2	INCREASING GENERATOR COUNT.....	87
3.2.1	RESULTS ASSUMING NO VARIANCE IN TREND LINES .....	87
3.2.2	RESULTS ASSUMING SEPARATE TREND LINES .....	95
3.2.3	RESULTS FOR TEN GENERATORS WITH VARIED RESERVE SETTINGS	96
4	CONCLUSION .....	99
4.1	RECOMMENDATIONS FOR FUTURE WORK.....	100
APPENDICES .....		102
4.2	LOAD MANAGEMENT.....	102
4.2.1	LOAD-DEPENDENT START.....	102
4.2.2	LOAD-DEPENDENT STOP.....	103
4.3	CONFIGURATION PARAMETERS.....	104

## LIST OF TABLES

TABLE 1-1: SPECIFICATIONS FOR CUMMINS QSK50 DQGAG .....	4
TABLE 1-2: FAULT DEFINITIONS .....	7
TABLE 1-3: REFERENCES TO STATES IN DEIF DOCUMENTATION .....	9
TABLE 1-4: CLASSIFICATION OF DEIF STATES .....	10
TABLE 1-5: SUMMARY OF IEEE STANDARD 1547 .....	19
TABLE 1-6: DESIGN TESTS OUTLINED BY IEEE STANDARD 1547.1.....	20
TABLE 1-7: STATE TRANSITION TABLE FOR RELAY BLOCK .....	25
TABLE 1-8: SPATIAL RESOLUTIONS FOR VARIOUS NWP FORECASTS .....	33
TABLE 2-1: INPUTS TO THE SANDIA MODEL.....	41
TABLE 2-2: DEFINITIONS OF VARIABLES USED IN FIGURE 2-5 .....	43
TABLE 2-3: SPECIFICATIONS FOR CUMMINS QSK50 DQGAG AND QSX15 DFEK .....	63
TABLE 3-1: RESULTS FOR KS TESTS COMPARING FAULT DISTRIBUTIONS .....	69
TABLE 3-2: MEAN ANNUAL VALUES FOR PV PENETRATION, FAULT COUNT, AND DAYTIME DIESEL CONSUMPTION FOR 6, 8, AND 10 RINGS ACROSS ALL ARRAY SIZES .....	71
TABLE 3-3: RESULTS FOR FAULT TYPES 1-4.....	82

## LIST OF FIGURES

FIGURE 1-1: SINGLE-LINE DIAGRAM FOR TANZANIA MICRO-GRID .....	3
FIGURE 1-2: POWER OUTPUT FOR THE MICRO-GRID FOR APPROX. 115 DAYS.....	5
FIGURE 1-3: OPERATING RANGE DEFINITIONS FOR THE GENERATORS .....	7
FIGURE 1-4: LOGIC USED IN THE GENERATOR CONTROLLER .....	9
FIGURE 1-5: GENERATOR STATE MACHINE .....	11
FIGURE 1-6: FUEL CONSUMPTION TREND LINE FOR CUMMINS QSK50 DQGAG .....	13
FIGURE 1-7: SPECIFIC FUEL CONSUMPTION FOR CUMMINS QSK50 DQGAG .....	14
FIGURE 1-8: RESIDENTIAL LOAD PROFILE FOR ONE DAY.....	15
FIGURE 1-9: HISTOGRAM FOR A RESIDENTIAL LOAD PROFILE.....	16
FIGURE 1-10: SAMPLE TWENTY-DAY LOAD PROFILE FOR THE TANZANIA MINE ..	17
FIGURE 1-11: LOAD HISTOGRAM FOR THE TANZANIA MINE .....	17
FIGURE 1-12: CURRENT DISTORTION LIMITS FROM IEEE STANDARD 519 .....	21
FIGURE 1-13: CURRENT CONTROL LOOP USED IN AN INVERTER .....	23
FIGURE 1-14: HYSTERESIS BEHAVIOR .....	26
FIGURE 1-15: SET-UP OF THE HYBRID DIESEL-PV MICRO-GRID .....	28
FIGURE 1-16: CONTROLLED PV RAMP USING SUPERVISORY CONTROLLER.....	30
FIGURE 1-17: TIME HORIZONS FOR VARIOUS NWP MODELS.....	32
FIGURE 1-18: EXAMPLE OF AN OVERLOADING EVENT.....	36
FIGURE 2-1: OVERVIEW OF THE CONTROLLER OPERATION .....	38
FIGURE 2-2: OUTLINE OF IMAGE PROCESSING PROCEDURE.....	40
FIGURE 2-3: PROCESSED IMAGE WITH RINGS CENTERED ON THE SUN .....	40
FIGURE 2-4: TILT AND AZIMUTH ANGLES FOR A SOUTH FACING ARRAY .....	42
FIGURE 2-5: FLOWCHART OUTLINING CALCULATION OF TOTAL IRRADIANCE ...	42
FIGURE 2-6: SOLAR AZIMUTH, ZENITH, AND ELEVATION ANGLES.....	44
FIGURE 2-7: ILLUSTRATION OF VARIOUS TYPES OF IRRADIANCE.....	45
FIGURE 2-8: CLEAR SKY PV FORECAST ERROR FOR CANBERRA ARRAY .....	46
FIGURE 2-9: ILLUSTRATION OF CLOUD EDGE EFFECT.....	46
FIGURE 2-10: SAMPLE IMAGE WITH WHITE CLOUD EDGES DUE TO REFRACTION	47
FIGURE 2-11: AMPLIFIED IRRADIATION DUE TO WHITE CLOUD EDGES .....	47
FIGURE 2-12: PV FORECASTING SUBSYSTEM .....	48
FIGURE 2-13: JITTER FILTER CONFIGURATION .....	49
FIGURE 2-14: THE CL (“CHICKEN LITTLE”) CONTROLLER STATE MACHINE.....	51
FIGURE 2-15: MARKOV TRANSITION MATRIX FOR TANZANIA DATA .....	54
FIGURE 2-16: MAXIMUM POWER TRANSIENTS.....	56
FIGURE 2-17: STATE MACHINE FOR THE GENERATOR LOAD CONTROLLER .....	59
FIGURE 2-18: PROCEDURE TO COMPILE A RANDOM YEAR .....	62
FIGURE 2-19: SPECIFIC FUEL CONSUMPTION FOR CUMMINS DQGAG AND DFEK ..	64
FIGURE 3-1: FAULT HISTOGRAM FOR PV=500 KW .....	65
FIGURE 3-2: FAULT HISTOGRAM FOR PV=1000 KW .....	66
FIGURE 3-3: FAULT HISTOGRAM FOR PV=1500 KW .....	66
FIGURE 3-4: FAULT HISTOGRAM FOR PV=2000 KW .....	67
FIGURE 3-5: FAULT HISTOGRAM FOR PV=2500 KW .....	67

FIGURE 3-6: FAULT HISTOGRAM FOR PV=3000 KW .....	68
FIGURE 3-7: COMPARISON OF FAULT OCCURRENCE FOR ALL ARRAY SIZES .....	70
FIGURE 3-8: DIESEL TOTALS FOR VARIOUS ARRAY SIZES AND RING SETTINGS ...	72
FIGURE 3-9: FRACTION OF PV UTILIZED FOR VARIOUS RING SETTINGS .....	73
FIGURE 3-10: EVENT CLASSIFICATION .....	75
FIGURE 3-11: FAULT OCCURRENCE BY DAY TYPE FOR 6 RING SIMULATIONS .....	76
FIGURE 3-12: CLASSIFICATION OF DAYS .....	77
FIGURE 3-13: SOLUTIONS FOR FAULT TYPES 1-4 .....	78
FIGURE 3-14: FAULTS CLEARED BY INCREASING NUMBER OF RINGS IN FORECAST FROM 6 TO 8 RINGS .....	80
FIGURE 3-15: FAULTS CLEARED BY INCREASING NUMBER OF RINGS IN FORECAST FROM 8 TO 10 RINGS .....	81
FIGURE 3-16: V1 TO I1 COMPARISON FOR DIESEL TOTAL .....	83
FIGURE 3-17: V1 TO I1 FRACTION OF PV UTILIZED.....	83
FIGURE 3-18: V1 TO I1 COMPARISON FOR NUMBER OF FAULTS.....	84
FIGURE 3-19: V1 TO “NO PV” COMPARISON FOR DIESEL TOTAL .....	85
FIGURE 3-20: DIESEL SAVINGS PER KW OF PV ADDED .....	86
FIGURE 3-21: V1 DIESEL TOTALS FOR THREE AND TEN GENERATORS .....	88
FIGURE 3-22: V1 FRACTION OF PV UTILIZED FOR THREE AND TEN GENERATORS	88
FIGURE 3-23: V1 GENERATOR CYCLES FOR THREE AND TEN GENERATORS.....	89
FIGURE 3-24: V1 FAULTS FOR THREE AND TEN GENERATORS .....	90
FIGURE 3-25: RELATIVE LOADING VS. THEORETICAL PVPEN PV=500 KW .....	91
FIGURE 3-26: RELATIVE LOADING VS. THEORETICAL PVPEN PV=1000 KW .....	91
FIGURE 3-27: RELATIVE LOADING VS. THEORETICAL PVPEN PV=1500 KW .....	92
FIGURE 3-28: RELATIVE LOADING VS. THEORETICAL PVPEN PV=2000 KW .....	92
FIGURE 3-29: GEN CYCLES VS. THEORETICAL PVPEN FOR PV=500 KW .....	93
FIGURE 3-30: GEN CYCLES VS. THEORETICAL PVPEN FOR PV=1000 KW .....	94
FIGURE 3-31: GEN CYCLES VS. THEORETICAL PVPEN FOR PV=1500 KW .....	94
FIGURE 3-32: GEN CYCLES VS. THEORETICAL PVPEN FOR PV=2000 KW .....	95
FIGURE 3-33: FUEL CONSUMPTION RESULTS USING DFEK AND DQGAG TREND LINES .....	96
FIGURE 3-34: V1 ANNUAL FAULT COUNTS FOR 3 GENERATOR SIMULATIONS AND 10 GENERATOR SIMULATIONS USING 450 KW RESERVE.....	97
FIGURE 3-35: V1 DIESEL TOTALS FOR 3 GENERATOR SIMULATIONS AND TEN GENERATOR SIMULATIONS USING 450 KW RESERVE .....	98

## NOMENCLATURE

$\alpha$  is the confidence level used to calculate a statistical confidence interval  
 $\phi$  is the normalized current  
 $\phi_b$  is a breakpoint in the normalized current  
 $\kappa$  is the fraction of PV energy utilized relative to the total PV available  
 $\psi$  is the normalized current transient  
 $\psi_{max}$  is the maximum normalized current transient  
 $\chi$  is PV penetration, or the total system load satisfied by PV on the interval  $[0, t_e]$   
 $\chi_{inst}$  is instantaneous PV penetration  
 $\chi_t$  is the theoretical PV penetration, or the resulting PV penetration if all PV were utilized  
 $CI_{min}$  is the minimum value on a confidence interval  
 $CI_{max}$  is the maximum value on a confidence interval  
 $f$  is a fraction that specifies the allowable ramp rate of PV after curtailment  
 $f_c$  is the estimated fraction of PV output if clouds are detected  
 $f_r$  is the fraction of load commanded to a generator  
 $f_x$  is the fraction of cloudiness outputted by the jitter filter  
 $F$  is the fuel input to the generators  
 $F_{inst}$  is the instantaneous fuel consumption  
 $F_{total}$  is the total diesel consumption on the interval  $[0, t_e]$   
 $FuelState$  is the current state of the generator  
 $H_a$  is the current hour of the day  
 $H_{end}$  is the hour of the day when the industry controller turns off  
 $H_{start}$  is the hour of the day when the industry controller turns on  
 $I$  is the current  
 $I_{max}$  is the maximum current observed in the load data  
 $J_x$  is the cloudiness state outputted by the jitter filter  
 $K_m$  is the jitter filter hold time  
 $K_t$  is the jitter filter trigger time  
 $\Delta L$  is the size of the load bins in the Markov Transition Matrix  
 $L$  is the total load on the system  
 $L_f$  is the forecasted load on the generators  
 $L_{f,ind}$  is the industry standard forecasted load on the generators  
 $L_i$  is the current load in the Markov Transition Matrix  
 $L_j$  is the load that is being evaluated for the next time step in the Markov Transition Matrix  
 $L_{max}$  is the maximum load observed in a load profile  
 $LD_{start}$  is the load dependent start threshold  
 $LD_{stop}$  is the load dependent stop threshold  
 $N$  is the dimension of the Markov Transition Matrix  
 $N_f$  is the desired number of generators online  
 $N_{f,ind}$  is the minimum number of generators the industry controller commands online  
 $N_o$  is the number of generators online  
 $N_{raw}$  is the raw number of generators required online

$N_{raw,r}$  is the raw number of generators required online rounded to the nearest integer  
 $p_a$  is the relative loading of a generator  
 $p_{a,o_n}$  is the  $n^{\text{th}}$  level of relative loading required to trigger overload protection  
 $p_{a,r_1}$  and  $p_{a,r_2}$  are the conditions that trigger reverse power faults in the generator controller if timers  $X_1$  and  $X_2$  have been exceeded  
 $p_{i,j}$  is the probability that the next load at the next time step,  $X_{m+1}$ , will equal another load level  
 $p_{min}$  is the minimum relative loading for a generator  
 $p_{max}$  is the maximum relative loading for a generator  
 $P$  is the load dispatched to each generator  
 $P_{avail}$  is the unused space on the generator system  
 $P_E$  is the power output of a generator  
 $P_{net}$  is the net load on the generators  
 $P_r$  is the continuous rating for a generator  
 $PV_a$  is PV output  
 $PV_{avail}$  is the available PV, assuming all PV is utilized  
 $PV_{clear}$  is the PV clear sky estimate  
 $PV_d$  is the total PV discarded  
 $PV_{est}$  is the estimated PV output  
 $PV_{est,ind}$  is the industry standard estimate of PV output for the next control period  
 $PV_{min,p_{max}}$  is the minimum PV that could be utilized assuming that the generators are operating at their maximum relative loading  
 $PV_{max,ind}$  is the maximum allowable PV output calculated by the industry controller  
 $PV_{max,p_{min}}$  is the maximum PV that could be utilized assuming that the generators are operating at their minimum relative loading  
 $PV_{max,up}$  is the maximum PV output, assuming that PV increases  
 $r_{in}$  is the input to the relay  
 $r_{out}$  is the output from the relay  
 $R_a$  is the current reserve on the generator system  
 $SFC$  is the specific fuel consumption  
 $t_e$  is the end time for which a variable is being evaluated  
 $t_{LD\ Start}$  is the number of consecutive time steps where the power available must fall below the load dependent start threshold for a 'START' command to be sent  
 $t_{LD\ Stop}$  is the number of consecutive time steps where the power available minus the rated power for one generator (theoretical new power available) must exceed the load dependent stop threshold for a 'STOP' command to be sent  
 $t_{NonnConnGens}$  is the number of consecutive time steps where the power available must exceed the load dependent start threshold after the initial 'START' command to force the generator into the 'COOLDOWN' state  
 $W$  is the width of the dead band  
 $x_{idle}$  is the idle fuel consumption of a generator.  
 $x_{rel\ load}$  is slope of the fuel consumption line as a fraction of relative load  
 $X_m$  is the current time being evaluated in the Markov Transition Matrix  
 $X_n$  is the  $n^{\text{th}}$  timer that must be exceeded to trigger overload protection  
 $X_1$  and  $X_2$  are the timers that must be exceeded for reverse power conditions to be triggered

$Z$  is the array for which the confidence interval is being calculated, with the samples sorted from smallest to largest

## 1 INTRODUCTION

This paper examines the optimization of daytime diesel fuel consumption for an industrial micro-grid located in Tanzania. The micro-grid owners would like to reduce operating costs by reducing the diesel consumption of the on-site diesel generators, which will in turn increase their profit. This will be accomplished by introducing a photovoltaic (PV) system to offset the load on the generators, as the de-loading of the generators will reduce their overall fuel consumption. To concentrate on the impact of the PV system, all analysis for this study considers only daytime diesel consumption as there is no PV output during nighttime hours.

To maximize diesel savings, it is desirable to maximize PV penetration. PV penetration is defined as energy penetration, as in Equation 1-1. It is expressed as the fraction of total load satisfied by PV for a given time period.

**Equation 1-1:**

$$\chi(t_e) = \frac{\int_0^{t_e} PV_a(t) dt}{\int_0^{t_e} L(t) dt}$$

Where:

$\chi(t_e)$  is the PV penetration on the interval  $[0, t_e]$

$PV_a(t)$  is the PV output at any time  $t$  on the interval  $[0, t_e]$

$L(t)$  is the total system load at any time  $t$  on the interval  $[0, t_e]$

While maximizing PV penetration is desirable, it is important to analyze the impact of the PV generation on the stability of the system. Variable cloud cover may cause PV output to drop as much as 75% in a matter of seconds.<sup>1</sup>As a result of this rapid change in PV output, the diesel

---

<sup>1</sup> A. Mills et al., "Understanding Variability and Uncertainty of Photovoltaics for Integration with the Electronic Power System", *The Electricity Journal*, Dec. 2009

generators may not be able to pick up the load carried by the PV system, which could cause unacceptable frequency or voltage transients, or may cause generation to stop, blacking out the system (see fault definitions in section 1.2.2). To successfully integrate high PV penetrations while maintaining low fault rates, it is crucial to anticipate rapid changes in PV output and adjust generation or loads to accommodate the changes. This paper will discuss a supervisory control system designed to utilize PV forecasts to adjust generation to support stable operating conditions all day when a large PV array is integrated into the system. All analysis is based upon simulations that were done in advance of the deployment of this system to evaluate fault rates and diesel consumption under various system configurations.

## **1.1 Site Information**

This section will describe the current system at the micro-grid site prior to the introduction of photovoltaics. A partner company provided data for the mine site including:

1. Three months of load recordings
2. A single-line diagram that detailed the following:
  - a. System configuration prior to the introduction of PV
  - b. Electrical design
3. Diesel generator and PV array specifications

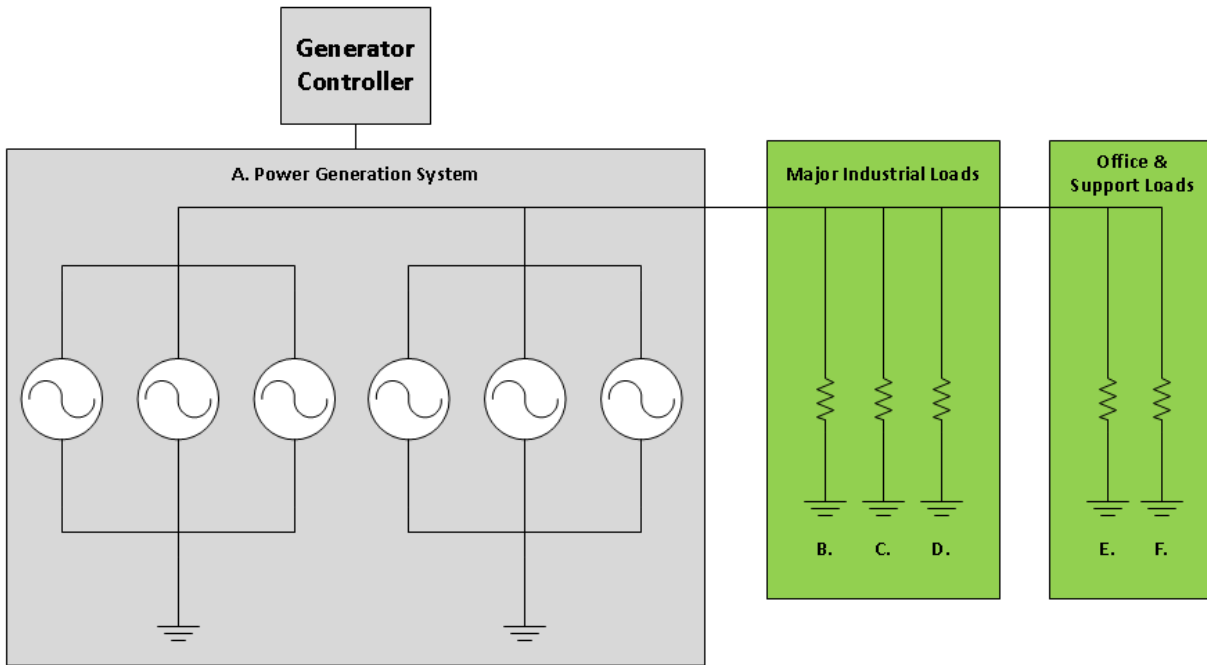


**Figure 1-1: Single-line diagram for Tanzania micro-grid**

Figure 1-1 shows a simplified single-line diagram for the Tanzania micro-grid. Six diesel-powered synchronous generator sets, combined in a single power plant (represented by item A), provide all electrical power to the facility. A generator set (abbreviated as genset) is defined as “an engine coupled with and driving an electrical generator”.<sup>1</sup>

The partner company indicated that the engine model was a Cummins QSK50 DQGAG, the specifications for which are shown in Table 1-1. Since the maximum load seen at the mine site is approximately 2.75 MW, 1-3 of the six gensets operate at any one time, providing redundancy should a unit fail.

<sup>1</sup> Engineer Educators, Inc., “Emergency and Standby Power Systems”, 2010. [Online]. Available: <https://www.engineereducators.com/docs/EmergencyAndStandbyPowerSystems.pdf>. [Accessed 30-Mar-2017].

**Table 1-1: Specifications for Cummins QSK50 DQGAG<sup>1</sup>**

Manufacturer	Cummins Inc.
Series	QSK50
Model	DQGAG
Prime Rating	1000 kW
Continuous Rating	1232 kW
Operating Frequency	50 Hz
Fuel Type	Diesel

A DEIF AGC-4 generation controller, modified by Aggreko for this application, controls the gensets. The DEIF control solution maintains uniform loading across all generators, provides start/stop control, round robin scheduling, synchronization, and other essential features necessary for generator control.

Power is distributed through an electrical system to two types of loads, shown in green. The major industrial loads (represented by B, C, and D) are the main power consumers at the site. These loads may consist of rock crushers, water pumps, screeners, and other mining equipment. In addition to the industrial loads, office and other miscellaneous support loads are also present (represented by E and F).

Three months of load data were collected from the micro-grid site via a partner company, and is shown in Figure 1-2. Load measurements were recorded once every minute. The maximum load recording was 2750 kW and the minimum load recording was 0 kW. Note that there was a gap in the recording from days 26.6 to 41.1, which is attributed to the failure of recording equipment.

---

<sup>1</sup> Cummins Power Generation Inc., “Generator Data Sheet”, D-3523b. [Revised June 2015].

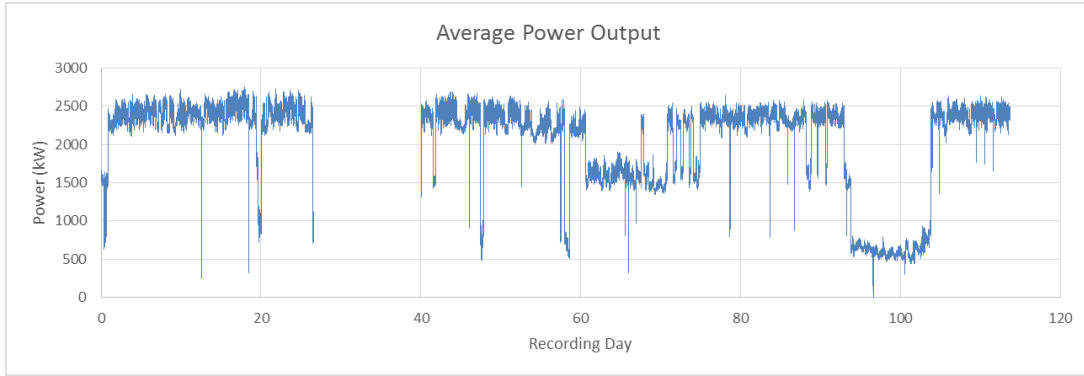


**Figure 1-2: Power output for the micro-grid for approx. 115 days**

While this paper will focus on a system to be deployed at a micro-grid based in Tanzania, this system can be implemented in any industrial micro-grid environment if given a single-line diagram, equipment specifications, and load recordings specific to the deployment site.

## 1.2 Generator Operation

Operation of the on-site generators and their control system play a critical role in the micro-grid's power system. This section will describe the operation of the diesel gensets powering the micro-grid facility. The first sub-sections will discuss load management for a multi-unit generator system, including load-following and load-sharing. Next, the criterion for stable generator operation will be described. By defining the conditions for stable operation of a generator, blackouts and damage to the equipment can be avoided and maintenance costs minimized. Following subsections will discuss the generator state machine used in the generator controller to ensure that the generators are operating under stable conditions. Final sub-sections will discuss fuel consumption of a diesel genset, and the formulas used to calculate the total diesel consumption of a generator.

## 1.2.1 Load Management

### 1.2.1.1 Load-Sharing

The generators in this system are configured so that the load is evenly dispatched amongst the total number of generators online,  $N_o$ . This is also known as “load sharing”. Equation 1-2 shows the calculation for the load that is dispatched to each generator,  $P$ , assuming no PV utilization.

#### Equation 1-2:

$$P = \frac{L}{N_o}$$

### 1.2.1.2 Load-Following

In this system, it is assumed that the generators operate in load-following mode, meaning that the power output of the generators is in balance with the load at all times. Therefore, all changes in load must be matched by immediate changes in generation.

## 1.2.2 Operating Range Definitions

To maximize the life of a generator and avoid equipment damage, it is important to keep the generators at a safe level of relative loading. The definition of relative load,  $p_a$ , is shown in Equation 1-3 where  $P_r$  is the continuous rating for a generator.

#### Equation 1-3:

$$p_a = \frac{P}{P_r}$$

Figure 1-3 illustrates the operating range definitions for the generators. The left side of the figure shows the relative power required to trigger various fault types. The right side of the figure shows the acceptable operating time before a fault is triggered. Generators can be underloaded,

but not in reverse power, for Max Underload Time. They can also be overloaded, within specified limits, for Max Overload Time. Additionally, fault definitions are outlined in Table 1-2.

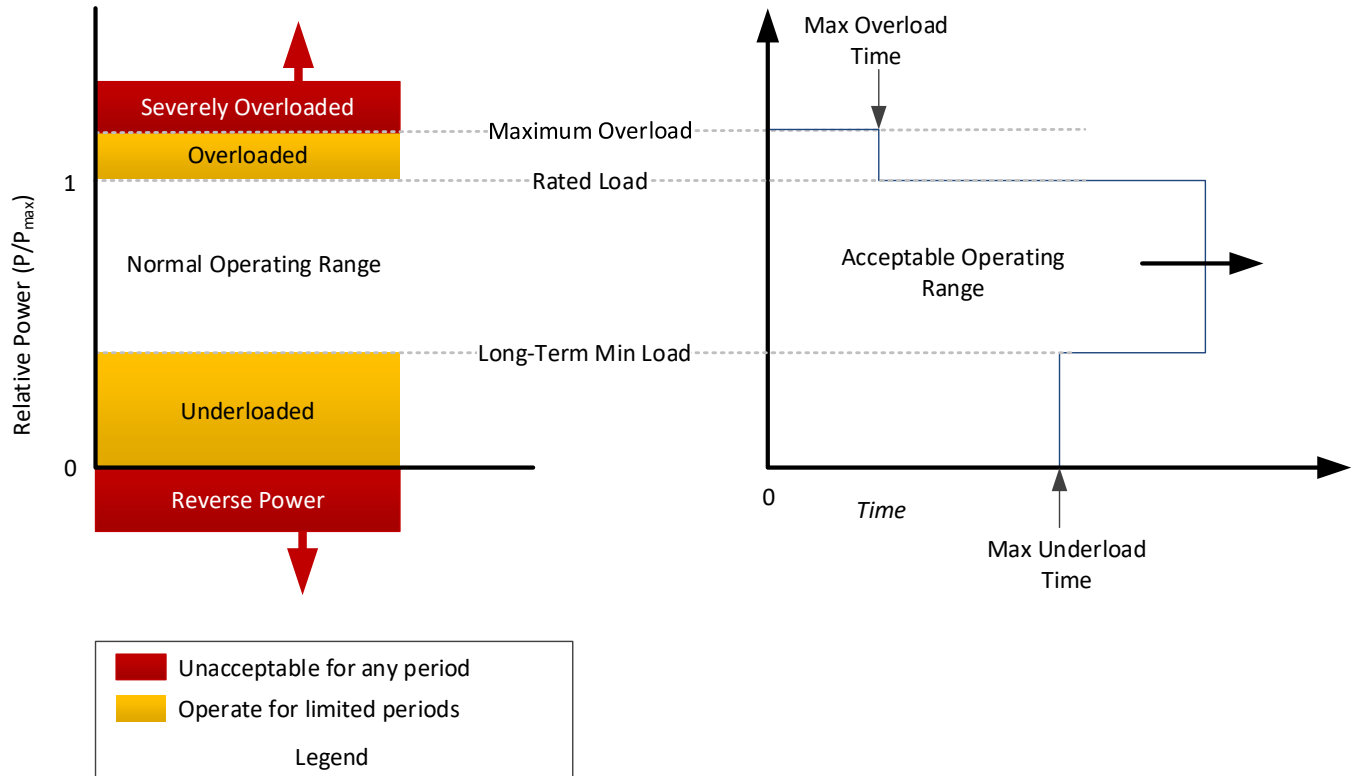


**Figure 1-3: Operating range definitions for the generators<sup>1</sup>**

**Table 1-2: Fault definitions**

Fault Type	Relative Power	Duration
Reverse Power	<0%	0 seconds
Underloaded	<29%	60 seconds
Overloaded	>100%	30 seconds
Severely Overloaded	>120%	0 seconds

<sup>1</sup>D. Zimmerle and J. Duggan, “Theory of Operation: High Penetration, Hybrid PV-Diesel Supervisory Control System Version V1”, Colorado State University, Fort Collins, Colorado, 2016.

The minimum recommended relative load for diesel generators is between 30-50%<sup>1</sup>. If a generator is operated below 30% relative loading, several maintenance issues arise such as wear and erosion. Operating below 0% relative loading is referred to as “reverse power” and may damage the generator or cause an over-speed condition. Since generator protection systems will typically disconnect the generator immediately if they sense reverse current, reverse power events are not allowed for any period of time. Alternatively, if a generator is overloaded ( $p_a > 100\%$ ) for an extended period, the generator may overheat and components may be damaged as a result. While gensets may operate in this mode for a period of time, sustained operation will cause a system failure. As a result, protection systems typically disconnect the generator if a set over- or under-load time is exceeded.

### *1.2.3 Generator State Machine*

A finite state machine is used to manage the genset at any point in time (i.e. stopped, starting, synchronizing, online, and cooling down). State transitions only occur when appropriate checks have been satisfied. These checks are used to ensure that the generator is in stable operation before switching to another state. A simplified state machine for the DEIF controller is shown in Figure 1-4.

---

<sup>1</sup> Fraunhofer Institute for Solar Energy Systems ISE “Technological and Economic Assessment of PV-Diesel Hybrid Solutions Versus Other Technologies”, 2013. [Online]. Available: <http://docplayer.net/21196728-Technological-and-economic-assessment-of-pv-diesel-hybrid-solutions-versus-other-technologies.html>. [Accessed 30-Mar-2017].

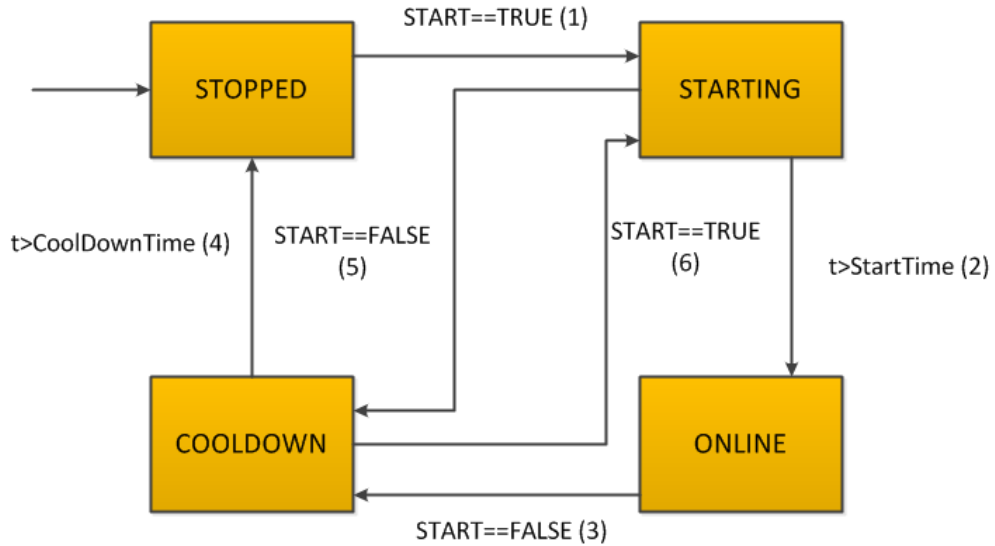


**Figure 1-4: Logic used in the generator controller**

The logic used in Figure 1-4 was validated using the DEIF utility software<sup>1</sup> and the Designer’s Reference Handbook (DRH) for the AGC-4 controller<sup>2</sup> and utilized in all simulations. Table 1-3 shows the sections in the DRH that correspond to the state transitions in Figure 1-4, as well as the ANSI device numbers the transitions are compliant with.<sup>3</sup>

**Table 1-3: References to states in DEIF documentation**

Transition No.	DRH Section(s)	ANSI Device No.(s)
1	3.8.5	2, 24
2	3.8.6, 3.8.7, 3.8.10	3, 6, 25
3	3.8.4	3, 5, 24
4	3.8.4	5
5	3.8.4	5
6	3.8.4	2,3

<sup>1</sup> DEIF, “Software-Power efficiency”, June 2015. [Online]. Available: <https://www.deif.com/software>. [Accessed Mar. 30, 2017].

<sup>2</sup> DEIF, “Designer’s Reference Handbook: Automatic Genset Controller AGC-4”, Document No. 4189340686K.

<sup>3</sup> Institute of Electrical and Electronics Engineers, “C37.2: IEEE Standard for Electrical Power System Device Function Numbers, Acronyms, and Contact Designations”, 2008.

Table 1-4 shows the checks that were done to validate each state. These checks included engine running status, ground breaker status (ground breaker positive on or off), auto start ready activated, and frequency/voltage within an acceptable tolerance. To ensure that the checks in Table 1-4 are being read from the DEIF controller properly, one can consult with the DEIF Modbus communication manual<sup>1</sup>. The ‘dgHzVOK’ check is compliant with ANSI device number 24, which states that a device must operate when a ratio of voltage to frequency is exceeded. This is also important because IEEE standard C37.106 warns that “Overexcitation exists whenever the per unit V/Hz exceeds the design limits of the equipment...Overexcitation of generators and transformers may result in the thermal damage to cores due to excessively high flux in the magnetic circuits....”.<sup>2</sup>

**Table 1-4: Classification of DEIF states**

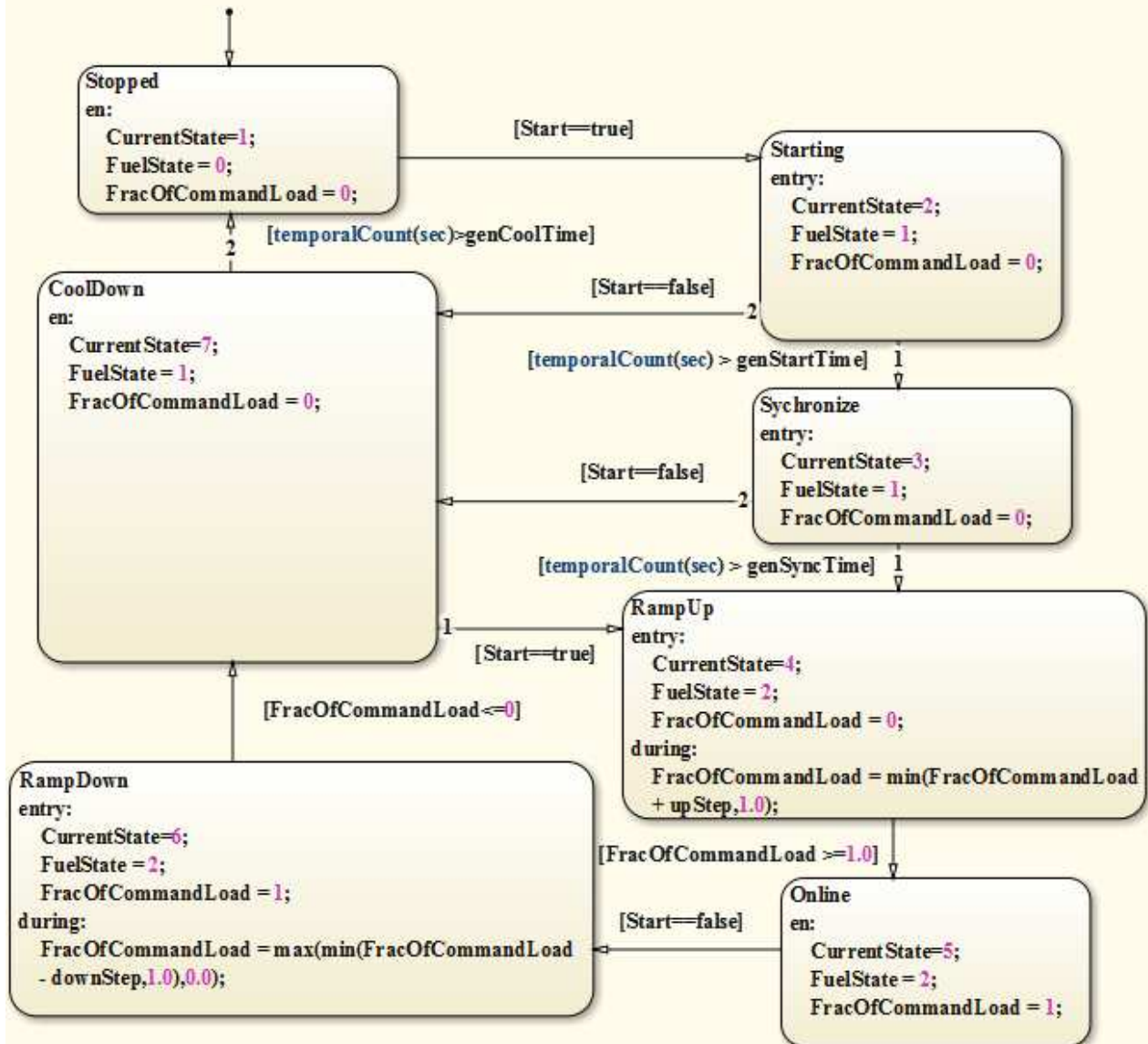
State	Engine Running	GB Pos.	Auto Start Ready	dgHzVOK
Stopped	No	Off	Yes	-
Starting	Yes	Off	-	No
Online	Yes	On	-	-
Cooldown	Yes	Off	-	Yes

Figure 1-5 shows the generator state machine that was used in simulations. Ramp up/down states were included to simulate the load ramp rates enforced by the genset controller. When emulations were done using the DEIF utility software, the results showed that generators were able to be fully loaded instantaneously. This is unrealistic because it would cause instability in the system in a real-world environment.

---

<sup>1</sup> DEIF, “Option H2 and H9 Modbus communication”, Document No. 4189340442V.

<sup>2</sup> Institute of Electrical and Electronics Engineers, “C37.106: IEEE Guide for Abnormal Frequency Protection for Power Generating Plants”, 2003.



**Figure 1-5: Generator state machine**

From Figure 1-5, it is observed that the total time it takes for a generator to transition to the 'ONLINE' state is composed of the start time, synchronization time, and the time it takes for a generator to ramp up. For simulations, it was estimated that this total time would be 240 seconds to account for false starts. Additionally, the generator state determines the amount of load a generator is able to support and the amount of fuel that is consumed. This will be discussed in further detail in the next section.

#### 1.2.4 Generator Fuel Consumption

To optimize diesel consumption for the micro-grid, one must first understand the fuel consumption trends of the gensets. The instantaneous fuel consumption for a diesel generator can be approximated by Equation 1-4. Additionally, the fuel consumption of a genset is dependent on the *FuelState* corresponding to the state machine in Figure 1-5.

**Equation 1-4:**

$$F_{inst} = \begin{cases} 0 & \text{if } FuelState = 0 \\ x_{idle} & \text{if } FuelState = 1 \\ p_a f_r x_{rel\ load} + x_{idle} & \text{if } FuelState = 2 \end{cases}$$

Where:

$F_{inst}$  is the instantaneous fuel consumption

$x_{rel\ load}$  is slope of the fuel consumption line as a fraction of relative load

$x_{idle}$  is the idle fuel consumption of a generator

$f_r$  is the fraction of load commanded to a generator, which increments up/down as the generator ramps up/down. This value will be one if the generator is online.

Fuel consumption of a generator is linear with relative load, as shown in Figure 1-6. The y-intercept represents the idle fuel consumption for a generator, or the amount of fuel consumed when the generators have no load on them. The slope represents additional fuel consumed due to the relative loading of the generators.

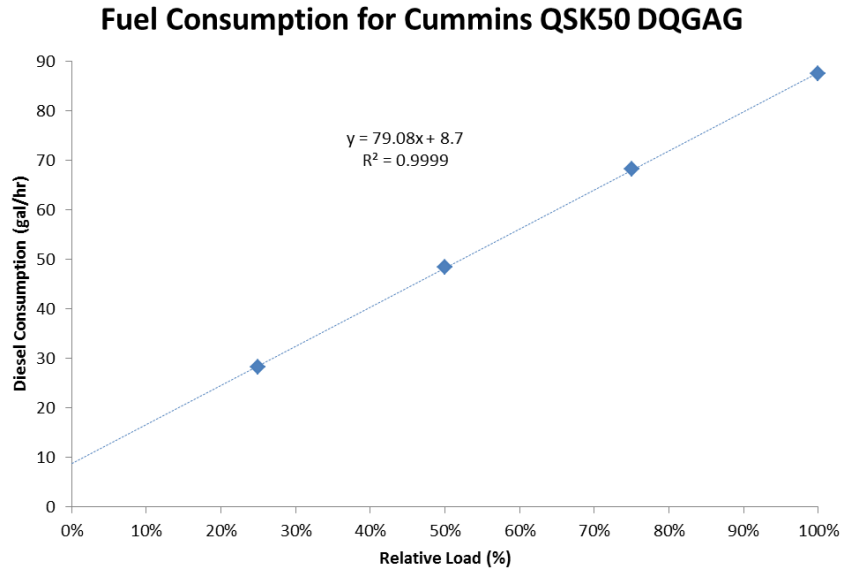


**Figure 1-6: Fuel consumption trend line for Cummins QSK50 DQGAG**

#### 1.2.4.1 Specific Fuel Consumption

Specific Fuel Consumption (SFC), defined in Equation 1-5, is a measure of efficiency that relates fuel input and power output of a generator. Figure 1-7 shows the specific fuel consumption of a Cummins QSK50 DQGAG. From this figure, it is evident that the generators are most efficient when they are at their highest relative load.

**Equation 1-5:**

$$SFC = \frac{F}{P_E}$$

Where:

*SFC* is the specific fuel consumption

$P_E$  is the power output of a generator

*F* is the fuel input

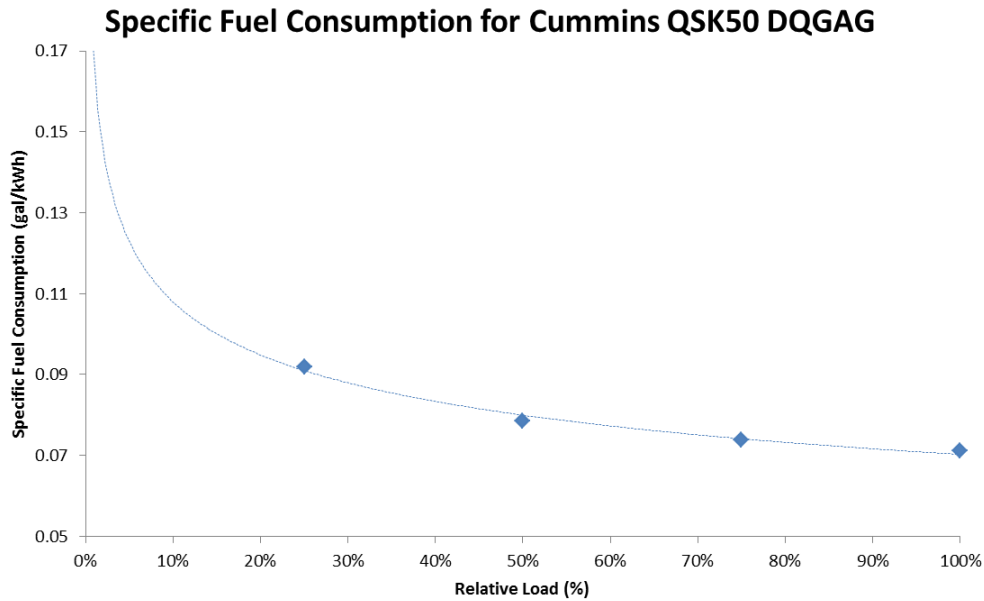


**Figure 1-7: Specific Fuel Consumption for Cummins QSK50 DQGAG**

### 1.3 Industrial Loading Patterns

Loads at the study site are industrial loads, which behave in a manner that is significantly different from the more familiar residential or commercial load profile. Residential loads are dominated by many small loads that switch on and off stochastically, but add to a predictable profile that varies by time of the day, weather conditions, and other factors. A typical residential load profile is shown in Figure 1-8. The load profile exhibits a base load pattern at night, through the morning and into the mid-day hours, driven by appliances that remain on at all hours (refrigerators, freezers, etc.) and the climate control system used to maintain a particular temperature in the residence. At the end of the day, the load increases due to a higher level of activity in most residences. Comparing Figure 1-8 to Figure 1-2, it is clear that residential/commercial load profiles are smoother than an industrial load profile.

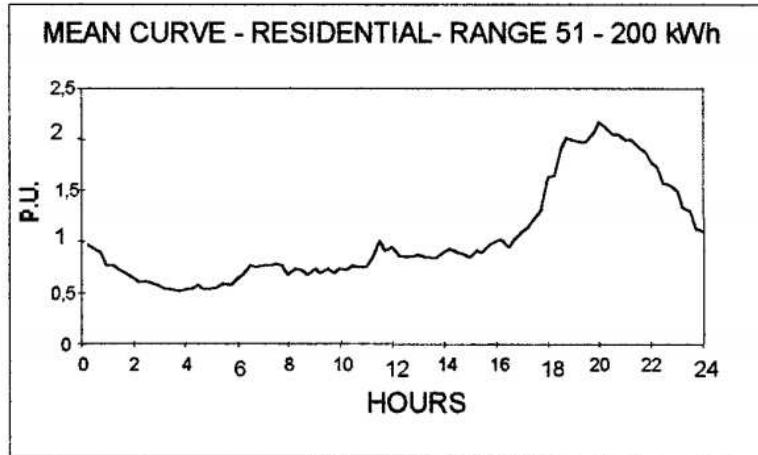


**Figure 1-8: Residential load profile for one day<sup>1</sup>**

It is important to note that a large portion of a residential load is the climate controls that are used to maintain a comfortable temperature for the inhabitants. This means that residential loads are heavily dependent on weather conditions which vary depending on time of year, cloud cover, and temperature. Figure 1-9 shows a histogram for a residential load profile that was assembled from one year of data.

---

<sup>1</sup> J. Jardini et al., "Daily load profiles for residential, commercial and industrial low voltage consumers," *IEEE Transactions on Power Delivery* *IEEE Trans. Power Delivery*, vol. 15, no. 1, Jan. 2000.

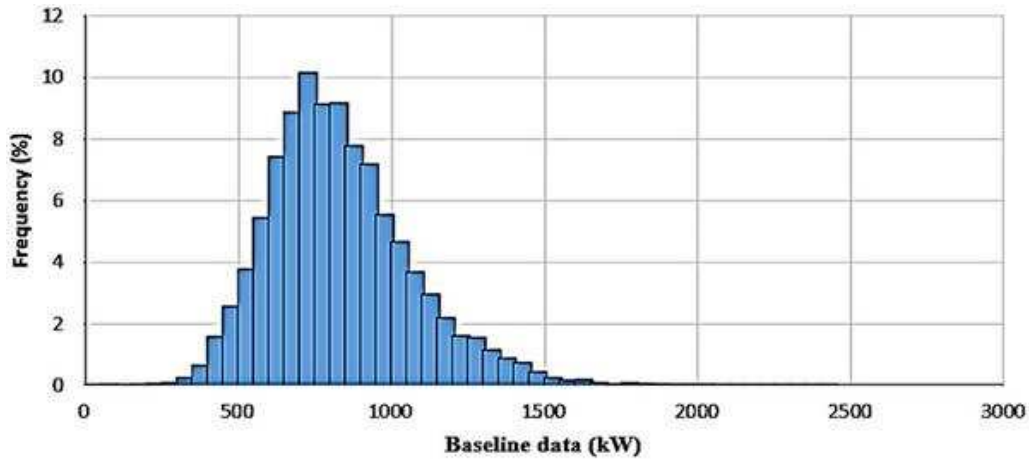


**Figure 1-9: Histogram for a residential load profile<sup>1</sup>**

In contrast to residential behavior, operations at industrial plants are not typically correlated with weather. The micro-grid in this study operates outdoors, and therefore there is no climate control system to be influenced by weather patterns. Further, industrial loads are often dominated by relatively few large loads, which are started and stopped depending upon needs of the operation, which often continues without interruption 24 hours per day. In the case of the Tanzania mine, large loads stayed online for days at a time and there was not a smooth transition from one load level to the next. This is shown in Figure 1-10.

---

<sup>1</sup> F. Diab et al., “An Environmentally-Friendly Tourist Village in Egypt Based on a Hybrid Renewable Energy System—Part Two: A Net Zero Energy Tourist Village,” *Energies*, vol. 8, no. 7, Oct. 2015.

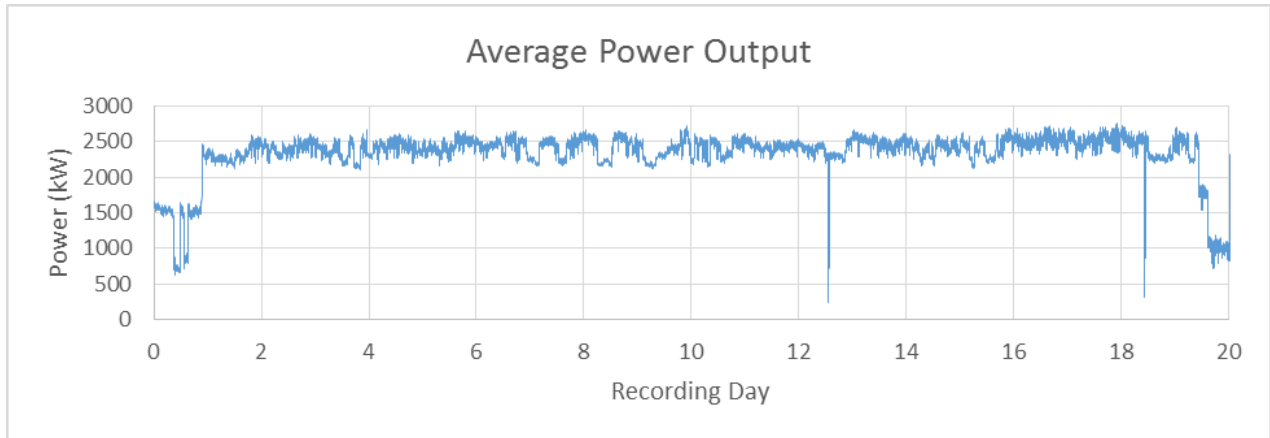


**Figure 1-10: Sample twenty-day load profile for the Tanzania mine**

Figure 1-11 shows a load histogram for 115 days of load data obtained from the micro-grid. From this histogram, it is evident that the load at the micro-grid typically operates around one of three load levels, with some level of variance within each load level. The residential load histogram in Figure 1-9 differs from the industrial load histogram in that there are no distinguishable higher-probability load levels and more fluctuation around the mode of the histogram.

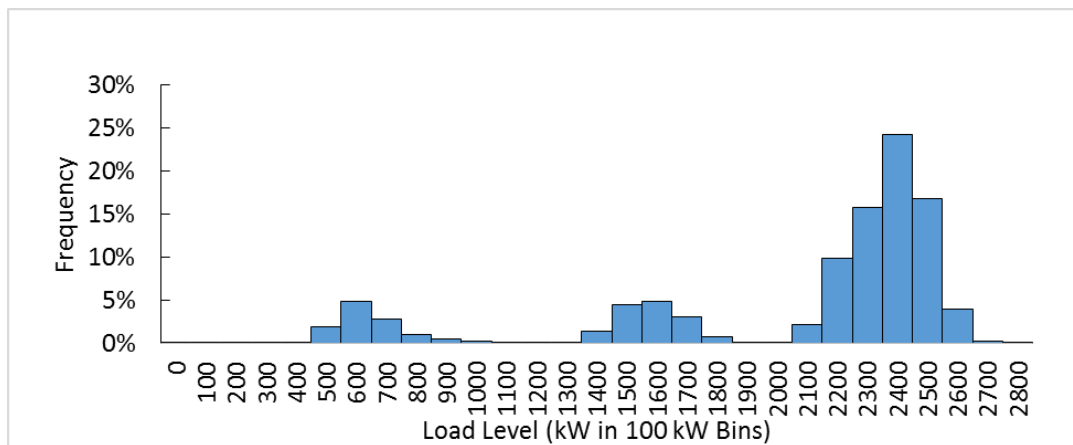


**Figure 1-11: Load histogram for the Tanzania mine**

Therefore, industrial loads typically operate for extended periods with only minor variations in load level, followed by fast transitions – often nearly instantaneous – from one load level to another, as large equipment is started or stopped. Genset controllers include special

functions to deal with these rapid transitions, including DEIF’s “heavy consumer” warning, which informs the genset controller that a large load is about to start.

#### **1.4 Micro-grid Definition**

For the purposes of this paper, it is important to have a clear understanding of the term “micro-grid”, as there are conflicting definitions in popular use. The US Department of Energy (US DOE) defines a micro-grid as “a group of interconnected loads and distributed energy resources (DER) with clearly defined electrical boundaries that acts as a single controllable entity with respect to the grid and can connect and disconnect from the grid to enable it to operate in both grid-connected or island mode.”<sup>1</sup> In this paper, we further restrict the definition of micro-grid to operate only in “island mode”, meaning that it functions independently from the consumer grid. Additionally, this system does not import or export any power to a public grid.

#### **1.5 Connection Standards**

There are two connection standards for connecting distributed generation to grid systems. The first standard to be discussed is IEEE standard 1547. This connection standard is of interest because it outlines connection standards for distributed energy resources under fault conditions and explains how to avoid operational conditions under common failure scenarios fails. The second connection standard to be discussed is IEEE standard 519-1992, which outlines thresholds for harmonics in a grid system.

---

<sup>1</sup> Microgrids at Berkeley Lab ,“Microgrid Definitions”, 2017. [Online]. Available: <https://building-microgrid.lbl.gov/microgrid-definitions>. [Accessed: 30-Mar-2017].

1.5.1 IEEE 1547: “Standard for Interconnecting Distributed Resources with Electric Power Systems”

IEEE standard 1547 outlines connection standards for Distributed Energy Resources (DER). A DER is defined as “a small-scale electric generator located next to and connected to the load being served either with or without an electric grid interconnection”<sup>1</sup>. Table 1-5 summarizes the series of interconnection standards that are contained within IEEE standard 1547.

**Table 1-5: Summary of IEEE standard 1547**

Standard	Description
P1547.1	Outlines the type, production, and commissioning tests that are required to validate the interconnection functions of a DER.
P1547.2	An application guide that offers alternate approaches for interconnecting DERs with electric power systems (EPSs).
P1547.3	Guide for information exchange, monitoring, and control for DERs.
P1547.4	Guide for design, operation, and integration of DER island systems with EPSs.

IEEE standard 1547 discusses the stability of a DER islanded system, which is influenced by the PV penetration for a system as the amount of PV penetration directly influences the frequency response of the entire grid.<sup>2</sup> In a public grid, it is assumed that PV penetration (defined in Equation 1-1:) is small relative to total load. The total spinning reserve in the system exceeds the power generation from the DER system by a very large amount, such that the amount of inertia in the system can be treated as “virtually infinite” ( $P \gg PV_a$ ). Considering that the frequency of the system is dominated by the contribution from large synchronous machines, changes in PV output are unlikely to affect the stability of the grid.

---

<sup>1</sup> Institute of Electrical and Electronics Engineers, “1547: IEEE Standard for Interconnecting Distributed Resources With the Electric Power System”, 2003.

<sup>2</sup> Institute of Electrical and Electronics Engineers, “1547.4: IEEE Guide for Design, Operation, and Integration of Distributed Resource Island Systems with Electric Power Systems”, 2011.

In a hybrid diesel-PV micro-grid, the PV power output is similar in magnitude to the power output of the gensets at high PV penetrations. This puts the frequency of the system at risk, as PV output may change rapidly due to cloud cover changes. Therefore, it is important to utilize inverters to control the output from the PV system in order to avoid damage to existing equipment in the system or loss of control that leads to a blackout.

IEEE standard 1547.1 lists several interconnection tests that are required to validate the integrity and functionality of a system. The functionality of the system is validated by performing tests to ensure that the DR responds to an abnormal voltage, abnormal frequency, and reverse power events by disconnecting itself from the Area EPS (defined as an EPS that serves local EPSs). The tests outlined in Table 1-6 describe the tests that are crucial for the validation of the system outlined in this paper.

**Table 1-6: Design tests outlined by IEEE standard 1547.1<sup>1</sup>**

Test No./Title	Description
5.2 Response to Abnormal Voltage 5.3 Response to Abnormal Frequency	These tests demonstrate that a DR interconnection system will cease to energize the Area EPS with respect to overvoltage conditions or an abnormal frequency.
5.7 Unintentional Islanding	This test ensures that a DR or its interconnection system will cease to energize the connection with the Area EPS when an unintentional island condition is present.
5.8 Reverse Power	This test validates the functionality of the reverse-power protection system. In addition, it recommends the use of a reverse or minimum power relay.

The tests in Table 1-6 must produce repeatable results that are reproducible independent of test site. By performing these tests, the integrity and functionality of the system are able to be validated. Therefore, component damage can be avoided, and thus the total system life maximized.

---

<sup>1</sup> Institute of Electrical and Electronics Engineers, “1547.1: IEEE Standard Conformance Test Procedures for Equipment Interconnecting Distributed Resources with Electric Power Systems”, 2015.

1.5.2 IEEE 519-2014: “IEEE Recommended Practice and Requirements for Harmonic Control in Electric Power Systems”

IEEE standard 519-1992 outlines the thresholds for harmonics in a grid system. Harmonics are of concern because they can cause excessive heating in equipment such as generators and capacitors. In addition, they can also lead to reduced torque in generators. These issues have the potential to reduce the life of the equipment at the micro-grid, and therefore must be managed.

Figure 1-12 outlines the current distortion limits for distribution systems.

**Current Distortion Limits for General Distribution Systems  
(120 V Through 69000 V)**

Maximum Harmonic Current Distortion in Percent of $I_L$						
Individual Harmonic Order (Odd Harmonics)						
$I_{sc}/I_L$	<11	$11 \leq h < 17$	$17 \leq h < 23$	$23 \leq h < 35$	$35 \leq h$	TDD
<20*	4.0	2.0	1.5	0.6	0.3	5.0
20<50	7.0	3.5	2.5	1.0	0.5	8.0
50<100	10.0	4.5	4.0	1.5	0.7	12.0
100<1000	12.0	5.5	5.0	2.0	1.0	15.0
>1000	15.0	7.0	6.0	2.5	1.4	20.0
Even harmonics are limited to 25% of the odd harmonic limits above.						
Current distortions that result in a dc offset, e.g. half-wave converters, are not allowed.						
* All power generation equipment is limited to these values of current distortion, regardless of actual $I_{sc}/I_L$ .						
Where						
$I_{sc}$	= maximum short-circuit current at PCC.					
$I_L$	= maximum demand load current (fundamental frequency component) at PCC.					
TDD	= Total demand distortion (RSS), harmonic current distortion in % of maximum demand load current (15 or 30 min demand).					
PCC	= Point of common coupling.					

**Figure 1-12: Current distortion limits from IEEE standard 519<sup>1</sup>**

Considering that IEEE standard 519 does not cover harmonic distortion for hybrid diesel-PV micro-grids, a study was performed by IEEE looked into the harmonic distortion in micro-grid systems that contained photovoltaic generators (PVGs) at PV penetration levels of 10%, 30%,

<sup>1</sup> T. Blooming and D. Carnovale, “Application of IEEE STD 519-1992 Harmonic Limits,” 2006 Annual Pulp and Paper Industry Technical Conference, 2006.

50%, and 90% in a nodal system up to the 31<sup>st</sup> harmonic<sup>1</sup>. The study found that at PV penetrations below 30%, the total harmonic distortion (THD) was within an acceptable range. At PV penetrations of 50% and 90%, the acceptable levels of harmonic distortion were exceeded. In this paper, it is assumed that a low pass filter in the inverters will eliminate high order harmonics. Therefore, harmonic distortion at high order harmonics is not of concern.

## 1.6 Integration of PV System Using Inverters

To successfully integrate a PV array at the micro-grid, the DC power output of the array must be converted to AC power using an inverter. The instantaneous PV penetration,  $\chi_{inst}$ , directly influences the current outputted by the inverters at any time. It is defined in Equation 1-6.

**Equation 1-6:**

$$\chi_{inst}(t) = \frac{PV_a(t)}{L(t)}$$

The current output by the inverters contributes to the frequency response of the entire system. Therefore, sharp changes up/down in PV output have the potential to introduce instability in the frequency of the system. To prevent this, the inverters limit the PV output by ramping it up via a current control loop. This ramp rate is limited to 15% of the rated array size per second. Note that the inverters cannot prevent the rate at which PV ramps down. An example of a current control loop is in Figure 1-13.

---

<sup>1</sup> M. Begovic et al., "Harmonic Distortion in Microgrids and Distribution Systems with Photovoltaic Generators," 2015 48th Hawaii International Conference on System Sciences, Waikoloa, Hawaii, 2015.

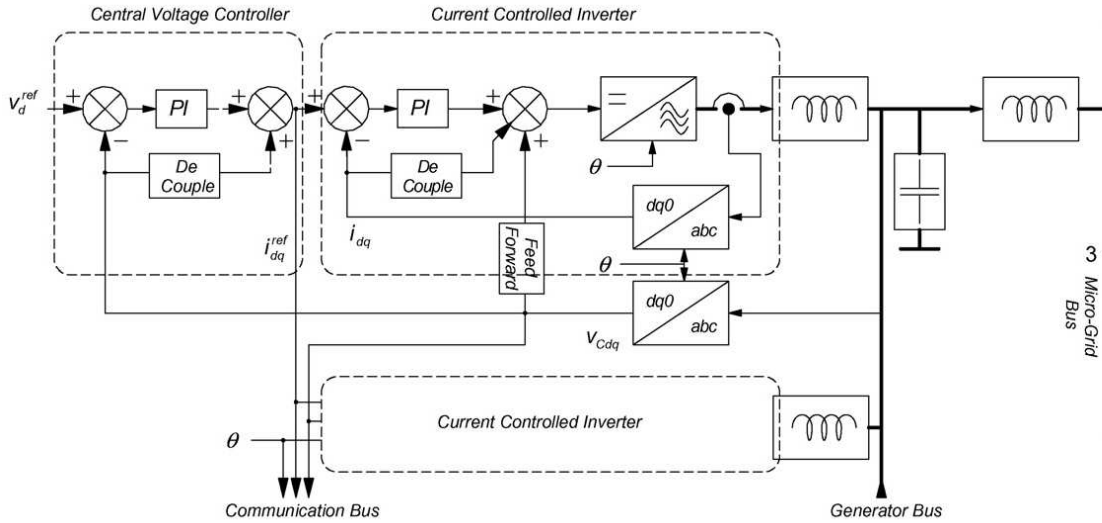


**Figure 1-13: Current control loop used in an inverter <sup>1</sup>**

In addition to controlling the rate at which PV can ramp up or down, the inverters also allow the user to set a maximum allowable PV output. This may be necessary in some instances to maintain generator operation within a stable range. The maximum allowable PV output will be discussed in section 1.8.2.

## 1.7 “Industry Standard” for PV Utilization

This section discusses the “industry standard” integration methods utilized to integrate PV into micro-grid systems. While no official standard exists for simplistic integration of PV into a micro-grid, several generation systems have implemented similar control methods to increase the amount of PV integrated into a stand-alone power system. The control solutions studied here will be compared to the industry standard method.

First, the industry standard controller estimates the PV output. This is calculated from the minimum PV output recorded in the last 900 seconds. The formula for the industry estimation of PV is shown in Equation 1-7.

<sup>1</sup> T. Green et al., “Control of inverter-based micro-grids,” *Electric Power Systems Research*, vol. 77, no. 9, 2007.

**Equation 1-7:**

$$PV_{est,ind} = f_c \min_{[t-900,t]} (PV_a)$$

Where:

$PV_{est,ind}$  is the industry standard estimate of PV output for the next control period

$f_c$  is the estimated fraction of PV output if clouds are detected

$\min_{[t-900,t]} (PV_a)$  represents selecting the minimum actual PV output over the preceding 900 seconds at any time t

Next, the controller calculates the forecasted load on the generators,  $L_{f,ind}$ . This calculation is shown in Equation 1-8.

**Equation 1-8:**

$$L_{f,ind} = \max_{[t-900,t]} (L) + R_a - PV_{est,ind}$$

Where:

$L_{f,ind}$  is the industry standard forecasted load on the generators

$\max_{[t-900,t]} (L)$  represents selecting the maximum load over preceding 900 seconds at any time t

$R_a$  is the current reserve on the generator system, which will be discussed in section 2.1.3

The industry controller then calculates the number of generators that should be online to support the forecasted load. This is denoted as  $N_{raw}$  and it is calculated using Equation 1-9.

**Equation 1-9:**

$$N_{raw} = \frac{L_{f,ind}}{P_g p_{max}}$$

Where:

$N_{raw}$  is the raw number of generators required online

$p_{max}$  is the maximum generator rating

Next, the industry uses a hysteresis to determine the number of generators that must be online. This is used to keep the number of generators stable if there is a rapid fluctuation in the PV forecast due to system noise or rapid cloud movement. An input to a relay is calculated using the raw number of generators online. This is shown in Equation 1-10.

**Equation 1-10:**

$$r_{in} = N_{raw} - N_{raw,r}$$

Where:

$r_{in}$  is the input to the relay

$N_{raw, r}$  is the raw number of generators required online rounded to the nearest integer

Next, the relay state is determined by the current state of the relay and the input to the relay. The state transitions for the relay block are outlined in Table 1-7, where  $r_{out}$  is the relay output and  $W$  is the width of the dead band.

**Table 1-7: State transition table for relay block**

Original State	$r_{in} < -W$	$-W < r_{in} < W$	$r_{in} > W$
State=0 (Off)	State=0, $r_{out} = -W$	State=0, $r_{out} = -W$	State=1, $r_{out} = W$
State=1 (On)	State=0, $r_{out} = -W$	State=1, $r_{out} = W$	State=1, $r_{out} = W$

In summary, the relay block implements a hysteresis. An illustration of a hysteresis is shown in Figure 1-14.

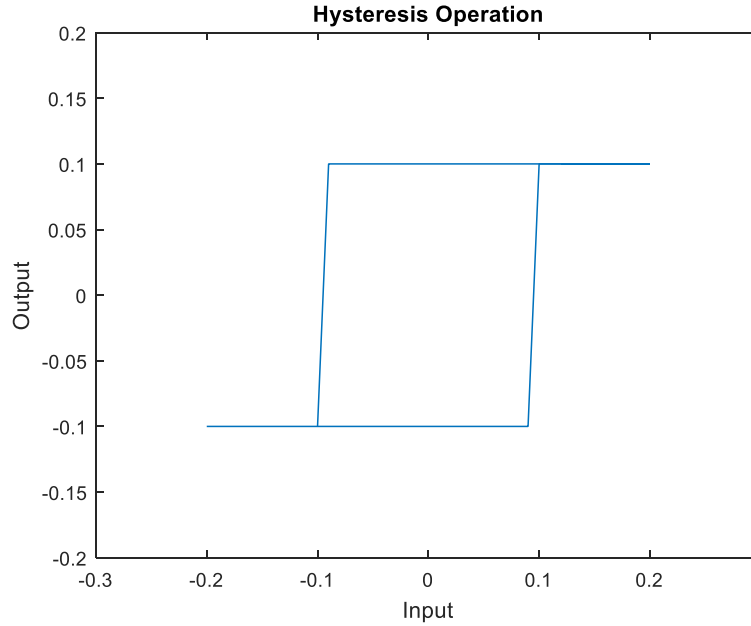


**Figure 1-14: Hysteresis behavior**

During daytime hours (from sunrise to sunset) when PV output is usable, the relay block is then used to calculate the required number of generators online. During all other hours, the forecasted number of generators is calculated as the raw number of generators required rounded up to the nearest whole integer. This is shown in Equation 1-11.

**Equation 1-11:**

$$N_{f,ind} = \begin{cases} \max(1, \text{ceil}(N_{raw,r} + r_{out})) & \text{if } H_a \in [H_{start}, H_{end}] \\ \text{ceil}(N_{raw}) & \text{if } H_a \notin [H_{start}, H_{end}] \end{cases}$$

Where:

$N_{f,ind}$  is the minimum number of generators the industry controller commands online

$H_{start}$  is the hour of the day when the industry controller starts. This is a fixed value used to indicate sunrise.

$H_a$  is the current hour of the day

$H_{end}$  is the hour of the day when the industry controller turns off. This is a fixed value used to indicate sunset.

Last, the industry standard calculates the maximum allowable PV output, which is the amount of PV that would keep the generators currently online at their minimum relative loading. This calculation is shown in Equation 1-12.

**Equation 1-12:**

$$PV_{max,ind} = L - p_{min}N_oP_g$$

$PV_{max,ind}$  is the maximum allowable PV output calculated by the industry controller

$p_{min}$  is the minimum relative loading for a generator

## **1.8 Planned System Configuration**

A planned system configuration is shown in Figure 1-15. This system consists of three sets of loads to simulate the “load islands” shown in Figure 2-15, multiple diesel generators that managed by a generator controller, a supervisory control that commands settings to the inverter and the generator controller, and a forecasting system.

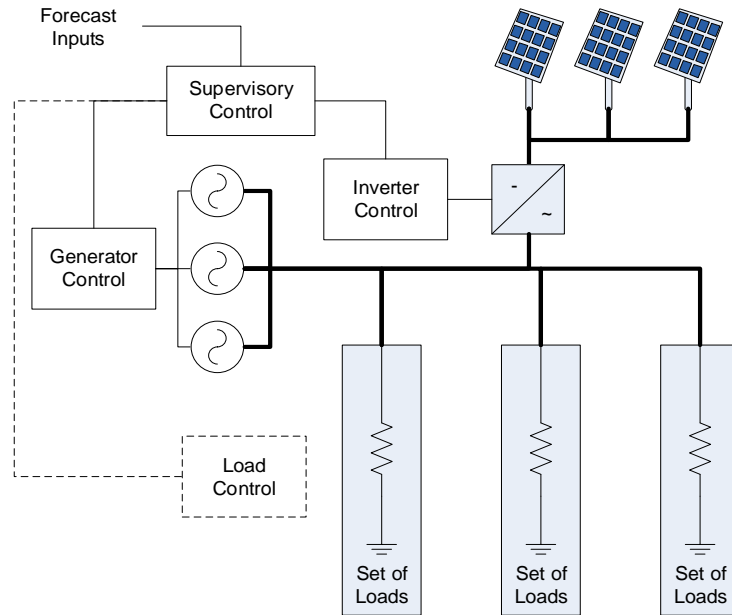


**Figure 1-15: Set-up of the hybrid diesel-PV micro-grid**

The inputs to the supervisory controller are the forecasted PV output, reserve, and the total load. The goal of this controller is to keep the generators in a stable operating range at all times. To accomplish this, it commands two outputs:

1. Minimum number of generators online
2. Maximum allowable PV output

### 1.8.1 Calculation of the Minimum Generators Online

To determine the minimum number of generators online, the supervisory controller must first estimate the load on the generators. This calculation is shown in Equation 1-13.

**Equation 1-13:**

$$L_f = L + R_a - PV_{est}$$

Where:

$L_f$  is the forecasted load on the generators

$PV_{est}$  is the estimated PV output (see section 2.1.4 for more detail)

Once the controller has estimated the load on the generator system, it can determine the minimum number of generators to command online,  $N_f$ . This is dependent on the continuous rating for one generator and the maximum relative loading for a generator. The calculation of the minimum number of generators online is shown in Equation 1-14.

**Equation 1-14:**

$$N_f = \text{ceil}\left(\frac{L_f}{P_r p_{max}}\right)$$

### 1.8.2 Calculation of Maximum PV Output

To calculate the maximum PV output, the controller first calculates the amount of PV that would be utilized under the assumption that the generators are loaded at their minimum and maximum relative load levels,  $p_{min}$  and  $p_{max}$ . Equation 1-15 shows the minimum amount of PV that could be utilized under the assumption that the generators are operating at their maximum relative loading,  $PV_{min,p_{max}}$ . Equation 1-16 defines the maximum amount of PV that could be utilized under the assumption that the generators are operating at their minimum relative loading,  $PV_{max,p_{min}}$ .

**Equation 1-15:**

$$PV_{min,p_{max}} = L - p_{max} N_o P_r$$

**Equation 1-16:**

$$PV_{max,p_{min}} = L - p_{min} N_o P_r$$

Next, the controller calculates the maximum amount that the PV can ramp up given the current number of generators online and the current PV online. Note that this value cannot exceed

$PV_{max,p_{min}}$ , which is the maximum amount of PV that can be kept online to keep the generators loaded at their minimum relative loading. This is shown in Equation 1-17. In addition, it is illustrated in Figure 1-16.

**Equation 1-17:**

$$PV_{max,up} = \min(PV_a + fN_oP_r, PV_{max,p_{min}})$$

Where:

$PV_{max,up}$  is the maximum PV output, assuming that PV increases

$f$  is a fraction that specifies the allowable ramp rate of PV after curtailment

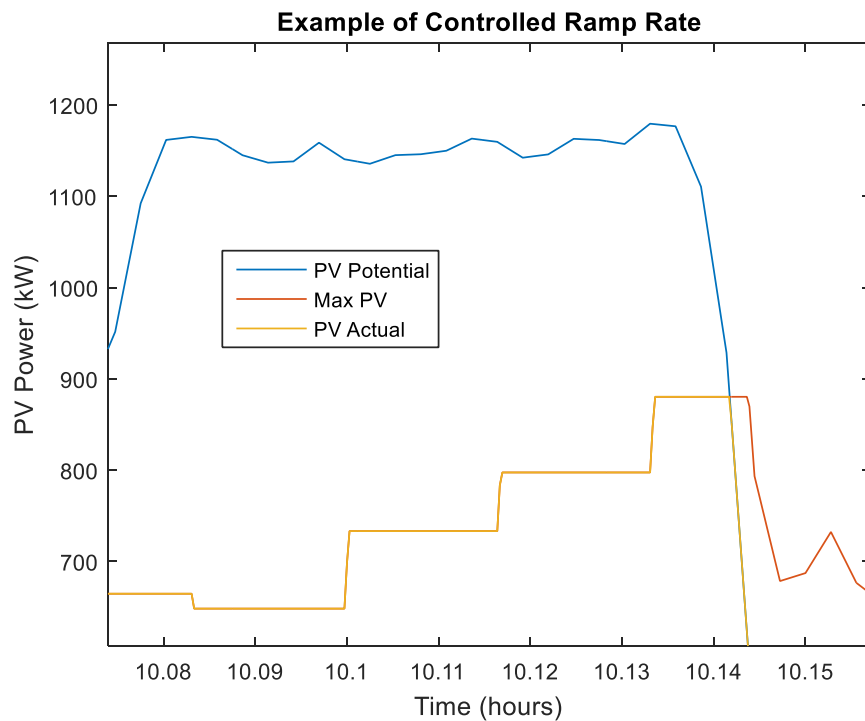


**Figure 1-16: Controlled PV ramp using supervisory controller**

Steps in PV output (orange line) represent the inverters tracking a maximum output command set by the controller. Ramp rate limitations on these setpoints causes the total PV output to be less than potential output, and in the case shown, PV does not ramp to maximum potential before another cloud causes a significant drop in potential PV output.

Lastly, the controller finalizes the calculation of the maximum PV output,  $PV_{max}$ , as shown in Equation 1-18. If the maximum PV in the upwards direction exceeds the minimum amount of PV that could be utilized, it is safe to set the maximum allowable PV output to  $PV_{max,up}$ .

**Equation 1-18:**

$$PV_{max} = \max(PV_{max,up}, PV_{min,p_{max}})$$

## **1.9 Existing Cloud Tracking Methods and Limitations**

In Equation 1-13, it is observed that the estimated PV output directly influences the forecasted load on the generator system. Therefore, it is crucial to identify PV transients as early as possible to allow time for the diesel generators to start or stop gensets to handle the PV transient. For the controls system discussed in this paper, a forecast window of 240 seconds (4 minutes) will be necessary to give the gensets adequate time to start. If the forecast window exceeded this length, the generators are at risk to become overloaded. By identifying PV transients 240+ seconds in advance, the gensets are prepared to carry the additional load when the PV transient occurs.

Additionally, one must consider the required spatial resolution for a cloud tracking system. It is ideal to have a horizontal spatial field of view <5 km, as it is assumed that the sky area that influence PV output will be no larger than this. Next, one must understand why current cloud tracking methods are insufficient for micro-grid control. This section will outline previous work that has been done to forecast cloud cover and irradiance.

### *1.9.1 Intra-week forecasts*

Numerical Weather Prediction (NWP) is the method by which current weather observations are used to forecast future meteorological conditions such as temperature, precipitation, and cloud cover through the means of mathematical models and computer

simulations<sup>1</sup>. Traditionally, NWP models have been used to forecast cloud cover anywhere from 1-7 days in advance. Time horizons for various NWP forecasts are shown in Figure 1-17.

	Forecast models – the number in () corresponds to the descriptive number in the text	Time horizon (days)
<i>Europe</i>		
Germany	ECMWF (2)	3
	WRF-Metcotest (3)	3
	SKIRON-CENER (6)	3
	BLUE FORECAST (9)	2
Switzerland	ECMWF (2)	3
	WRF-Meteotest (3)	3
	BLUE FORECAST (9)	3
Austria	ECMWF (2)	3
	WRF-Meteotest (3)	3
	CENER (6)	3
	BLUE FORECAST (9)	2
Spain	BLUESKY-Meteorologists (10)	2
	ECMWF (2)	3
	WRF-UJAEN (3)	3
	CENER (6)	3
	HIRLAM (7)	2
	BLUE FORECAST (9)	3
<i>USA</i>		
USA	GEM (1)	2
	ECMWF (2)	3
	WRF-ASRC(3)	2
	WRF-AWS <sup>a</sup> (3)	2
	MASS <sup>a</sup> (4)	2
	ARPS <sup>a</sup> (5)	2
	NDFD (8)	7
<i>Canada</i>		
Canada	GEM (1)	2
	ECMWF (2)	2
	WRF-ASRC (3)	2

<sup>a</sup> Models run both with and without MOS.

**Figure 1-17: Time horizons for various NWP models<sup>2</sup>**

Table 1-8 shows the spatial resolutions for the corresponding forecasts shown in Figure 1-17. These forecasts are problematic because their spatial resolutions are too large ( $\geq 5$  km), i.e. they cannot forecast the exact position of a cloud at the time of the forecast. However, they are sufficient for forecasting general weather trends.

<sup>1</sup>National Oceanic and Atmospheric Administration, “Numerical Weather Prediction”, 2017. [Online]. Available: <https://www.ncdc.noaa.gov/data-access/model-data/model-datasets/numerical-weather-prediction> [Accessed: 08-Jan-2017]

<sup>2</sup>R. Perez et al., “Comparison of numerical weather prediction solar irradiance forecasts in the US, Canada and Europe”, *Solar Energy*, vol. 94, 2013.

**Table 1-8: Spatial Resolutions for various NWP forecasts**

Model	Spatial Resolution
Global Environmental Multiscale (GEM)	~15 km
European Centre for Med. Range Weather Forecasts (ECMWF)	25 km
Weather Research and Forecasting (WRF) Model	5 km
Mesoscale Atmospheric Simulation System (MASS)	5 km
Advanced Multiscale Regional Prediction System (ARPS)	5 km
Centro Nacional De Energías Renovables (CENER)	0.1°x0.1°
High Resolution Limited Area Model (HIRLAM)	20 km
US National Digital Forecast Database (NDFD)	~5 km
BLUE Forecast (based on GFS predictions from NCEP)	1°x1°, 0.5°x0.5°
BLUESKY	Varies by location

### 1.9.2 Intra-day forecasts

A 2007 study evaluated the NDFD, ECMWF, WRF models for various sites. The metrics that were used to compare the forecasts included Mean Bias Error (MBE), Root Mean Squared Error (RMSE), and uncertainty. ECMWF Version 2 was found to have the lowest RMSE. ECMWF Version 2 also yielded the lowest discrepancies when Kolmogorov-Smirnov Tests compared statistical distributions of Global Horizontal Irradiance (GHI) outputs from the forecasts to satellite and ground data<sup>1</sup>. The study concluded that the ECMWF Version 2 model performed best for 3-hour-ahead forecasts. A 2010 study concluded that satellite models yield favorable results in comparison to NWP models<sup>2</sup>.

### 1.9.3 Intra-hour forecasts

A 1999 study used a methodology that calculated cloud velocimetry from satellite images and found that solar radiation could be forecasted for time horizons ranging from 30 minutes to 2

---

<sup>1</sup>J. Redmund et al., “Comparison of Solar Radiation Forecasts for the USA”, The University of Albany, Albany, New York, 2007.

<sup>2</sup>R. Perez et al., “Validation of short and medium term operational solar radiation forecasts in the US”, *Solar Energy*, vol. 84, 2010.

hours using this methodology with a spatial resolution of 2.5 km x 2.5 km.<sup>1</sup> In 2013, a study evaluated the results of the analysis of processed satellite images with Artificial Neural Networks (ANNs) for forecast periods ranging from 30 min to 2 hours ahead with a spatial resolution of 1 km. This study was compared to results from the 1999 study and found improvements of 5-19% for 30-min ahead forecasts<sup>2</sup>.

Most recently, sky-imaging technologies have been used to forecast Direct Normal Irradiance (DNI). In 2011, a Total Sky Imager (TSI) was developed to improve upon sky-imaging technologies. The methodology used in this study was the identification of cloud pixels and the computation of a velocity vector for various cloud pixels. This system is effective for forecasting cloud cover up to 3 minutes ahead.<sup>3</sup> Although this did improve the time horizon and spatial resolution for irradiance forecasting, this system was costly and may not be practical for large-scale implementation. In addition, the time horizon of the forecast outputted by sky imagers may extend up to 30 minutes for high clouds.<sup>4</sup>

To summarize the above cloud tracking methods, numerical weather prediction models are sufficient for general day-to-day weather forecasts. Satellite image processing combined with cloud velocimetry provides improved short term forecasts, but does not forecast for time horizons of less than 30 minutes. However, the spatial resolution for satellite image processing is too large

---

<sup>1</sup>A. Hammer et al., "Short-Term Forecasting of Solar Radiation: A Statistical Approach Using Satellite Data", *Solar Energy*, vol. 67, 1999.

<sup>2</sup>R. Marquez et al., "Hybrid solar forecasting method uses satellite imaging and ground telemetry as inputs to ANNs," *Solar Energy*, vol. 92, 2013.

<sup>3</sup>R. Marquez and C. F. Coimbra, "Intra-hour DNI forecasting based on cloud tracking image analysis," *Solar Energy*, vol. 91, 2013.

<sup>4</sup>S. Pelland and J. Remund, "Photovoltaic and Solar Forecasting: State of the Art", *International Energy Agency Photovoltaic Power Systems Programme*, Oct. 2013.

(i.e. the resolution is not specific enough for a micro-grid location containing a single PV array). Lastly, sky-imaging did improve upon the time horizon for cloud forecasting, but the time horizon varies, depending on the height of the cloud.

As stated previously, a forecast window of 240 seconds is required to give the gensets adequate time to start. If the forecast window fails to meet this length, the generators are at risk to become overloaded. By identifying PV transients 240+ seconds in advance, the gensets are prepared to carry the additional load when the PV transient occurs. Additionally, it is important to consider that each time a cloud is detected, it directly affects the calculation of the minimum number of generators online (see section 1.8.1), and therefore also impacts the total diesel consumption. Therefore, it is desirable to have cloud detections as close to the 240 second forecast window.

### **1.10 Problem Statement**

Currently, one of the main problems with deploying large solar arrays to micro-grids is that there is a very high likelihood of faults without a forecasting system at high PV penetrations. This is due to the fact that PV can drop as much as 80% within a few seconds as clouds come between the sun and an array, causing a sudden drop in PV output. Due to the high likelihood of faults without a forecasting system, micro-grid site owners may hesitate to invest in large amounts of solar to avoid jeopardizing the integrity and functionality of their current system.

One of the most frequently observed faults in a hybrid PV-diesel micro-grid is overloading of the generators. The problem here is simple: the grid operates under stable conditions until a cloud shades the array. When the cloud has covered the array, the PV output begins to drop and the net power required from the generators increases, thus causing them to become overloaded. The risk of encountering an overloading event increases at large array sizes due to the fact that

more load is carried by the PV system, and thus the increase in the net power required from the gensets becomes larger when a cloud shades the array. Figure 1-18 illustrates an example of overloading event in a system with an array size of 1500 kW.

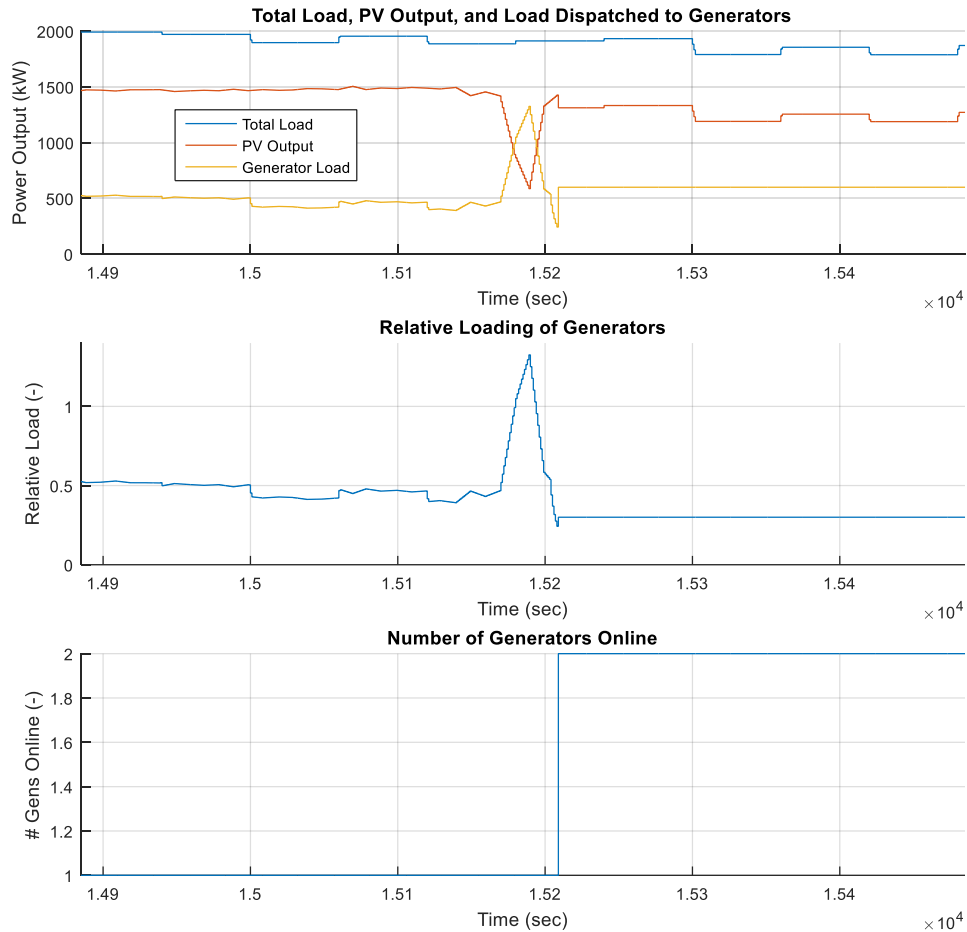


**Figure 1-18: Example of an overloading event**

As observed in Figure 1-18, the relative loading of the gensets exceeds the threshold defined in Table 1-2 when the PV output decreases. Diesel engines driving synchronous generators have limited capacity to absorb power during an overloading event. In a severe case, such as pictured in Figure 1-18, the system will begin to shut down generation units to protect the generators from overheating and to protect against component failure. In many cases, the sudden

shut-down of one or more generation units would likely cause a system blackout. This can be avoided if rapid changes in PV output can be forecasted, and generators can be started or stopped, or PV output curtailed, to maintain safe operating conditions. The goal of the PV forecasting system and the supervisory control studied here is to identify and properly react to changes in PV output. This paper will investigate how to configure the supervisory control system to minimize diesel fuel consumption for a given PV system size, while reducing PV-transient induced faults to an acceptably low level.

## 2 METHODS

The following sections will outline the functions of the supervisory controller, the forecast inputs to the supervisory controller, and the generator controls that are of concern for this system. Additionally, load forecasting using a Markov Transition Matrix (MTM) and reserve calculations will also be discussed.

### 2.1 Forecast Inputs to the Supervisory Controller

The following sections will go over inputs that are forecasted and sent to the supervisory controller. These include a PV forecast, a reserve calculation, and a load forecast.

### 2.2 System Overview

An overview of the controller operation is shown in Figure 2-1. The green blocks indicate the measurements that are readily available to the controller, which are the measured load and PV output. The controller assumes that these measurements do not have a substantial delay in comparison to the time step of the controller (no longer than one second). The blocks shown in blue indicate the control subsystems. The generator controller and inverters give feedback to the supervisory controller such as the current number of generators online and the current PV output.

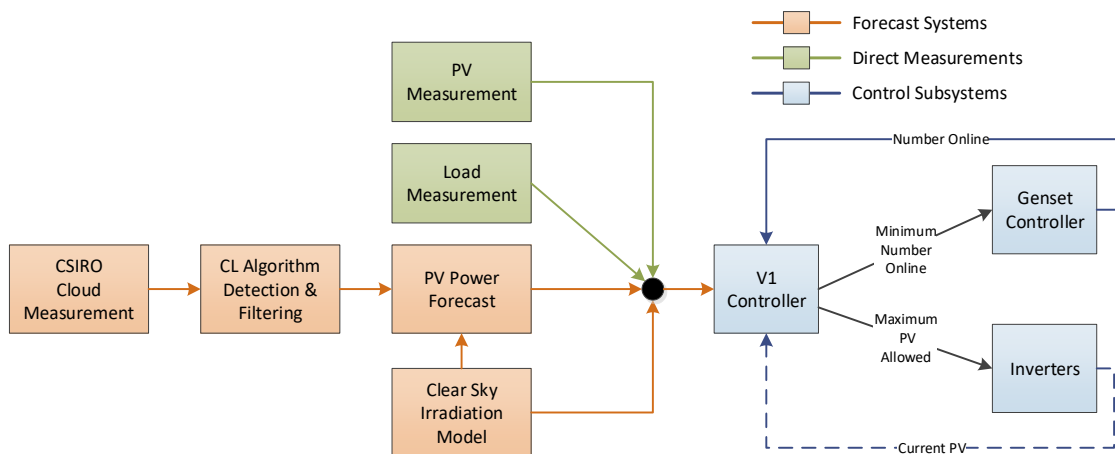


**Figure 2-1: Overview of the controller operation**

### 2.2.1 PV Forecasting System

The next sections will detail the calculation of forecasted PV. The PV forecasting system consists of four subsystems and is shown in orange in Figure 2-1:

1. A system to identify clouds was developed in collaboration with an Australian national lab known as the Commonwealth Scientific and Industrial Research Organization (CSIRO). This will be discussed in further detail in section 2.2.1.1.
2. Clear sky PV forecasts were estimated using the Sandia PVL Library, which will be discussed in further detail in section 2.2.1.2.
3. Clouds that may cause a drop in irradiance are identified using the “CL Algorithm” and filtered using the jitter filter, to be outlined in section 2.1.1.3.
4. Using the data from (2) and (3), the controller estimates the PV power for the next period.

Based on the output from step (4), the controller commands the maximum allowable PV output from the inverters and the minimum number of generators online. These calculations were previously discussed in section 1.8.

#### 2.2.1.1 Identifying Clouds Using CSIRO Software

To forecast PV output, a cloud identification and tracking system was created in collaboration with an Australian lab known as the Commonwealth Scientific and Industrial Research Organization (CSIRO). Images were collected from a low-cost security camera fitted with a 180° fish-eye lens to view a large area of the sky. Image processing steps are outlined in Figure 2-2.

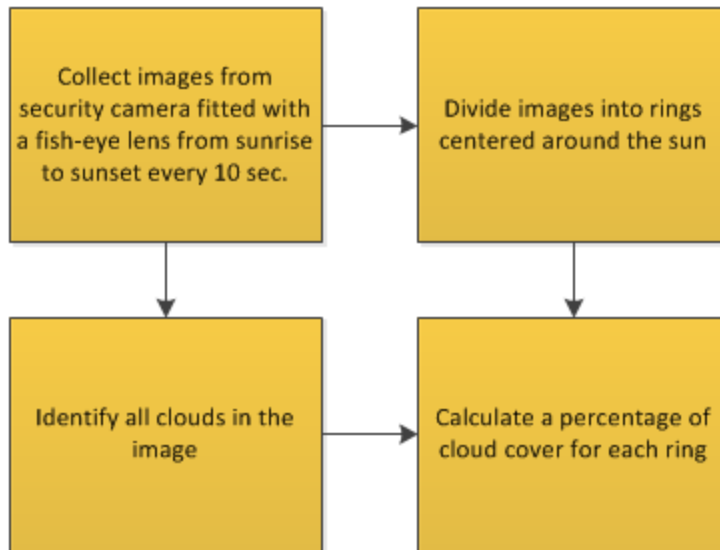


**Figure 2-2: Outline of image processing procedure**

Images are divided up into 16 concentric rings centered on the current position of the sun. A percentage of cloud cover was calculated for each ring. An example of a processed image is shown in Figure 2-3. The portions of the processed image shown in pink correspond to cloud detections.

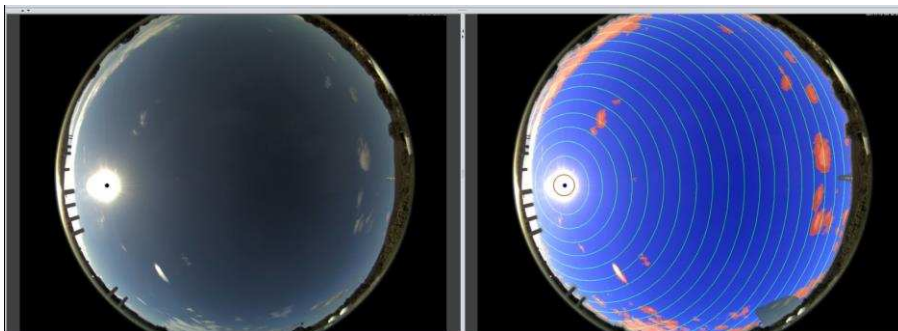


**Figure 2-3: Processed image with rings centered on the sun**

The cloud identification system updates every 10 seconds (frequency of .1 Hz). At each iteration, it provides a fraction of cloud cover in each ring. Note that it does not provide a forecast, but rather an analysis of the sky as it currently exists. The controller’s processing of this analyzed image produces the actual forecast of whether a cloud is imminent.

### 2.2.1.2 “Clear Sky Irradiance” Calculation Using Sandia Model

Clear Sky irradiance can be approximated using the Sandia PV LIB<sup>1</sup>, which forecasts irradiance under the assumption that there is no cloud cover. The inputs to the Sandia model and their definitions are shown in Table 2-1.

**Table 2-1: Inputs to the Sandia Model**

Input	Abbreviation	Description
Date/Day of Year	DOY	Time of year, given in Universal Coordinated Time (UTC), which is the mean solar time at 0° longitude.
Timestamp	N/A	Time of day, given in HH:MM:SS
Latitude	$\phi$	Geographic coordinate indicating the north-south position of a point on the Earth's surface
Longitude	$\lambda$	Geographic coordinate indicating the east-west position of a point on the Earth's surface
Elevation	N/A	Height of a geographic location relative to sea level
Turbidity	T	Cloudiness of a fluid due to large numbers of individual particles that are generally invisible to the naked eye
Albedo	A	Fraction of light that is reflected by a surface
Angle of Surface Tilt	$\beta$	Tilt angle of a PV module, relative to the horizontal
Azimuth Angle	$\alpha$	East-west orientation of an array

Figure 2-4 illustrates the angle of surface tilt and azimuth angle for an array. The azimuth angle measures the angle of an object around the horizon. Note that the azimuth angle of the array in Figure 2-4 is 180°, as this array faces south and the azimuth angle is measured from the north. The angle of tilt indicates how the array is tilted relative to the Earth’s surface. It is important to note that this angle has a major impact on the amount of irradiation that is incident on the array.

---

<sup>1</sup>Sandia National Labs, “Global Horizontal Irradiance Clear Sky Models: Implementation and Analysis”, Mar. 2009.

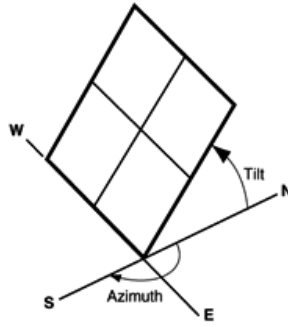


**Figure 2-4: Tilt and azimuth angles for a south facing array<sup>1</sup>**

The flow chart in Figure 2-5 shows the steps to calculate the total irradiance in the Sandia model. Descriptions of the variables used in the calculation of total irradiance are outlined in Table 2-2. The total irradiance is a sum of the diffuse sky irradiance, ground diffuse irradiance, and black body irradiance.

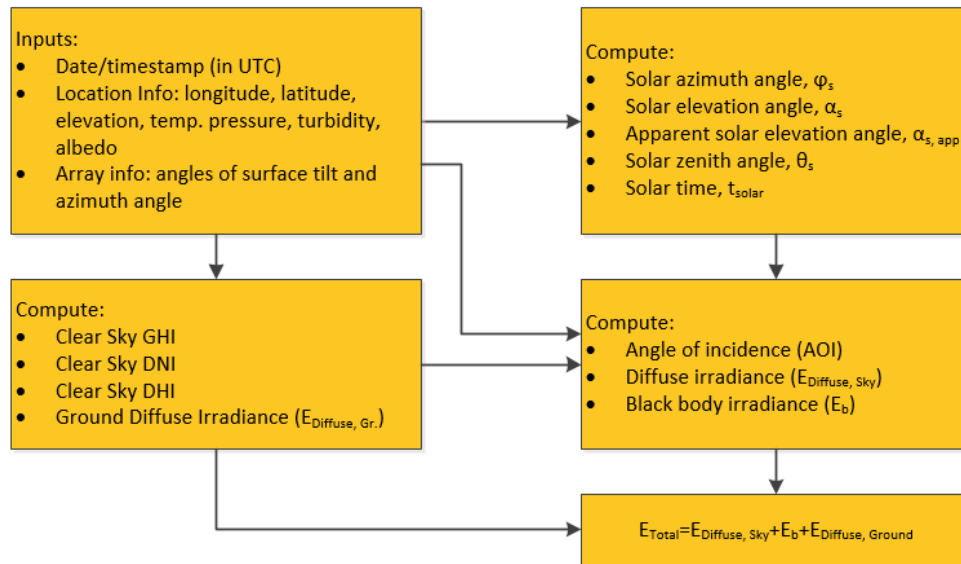


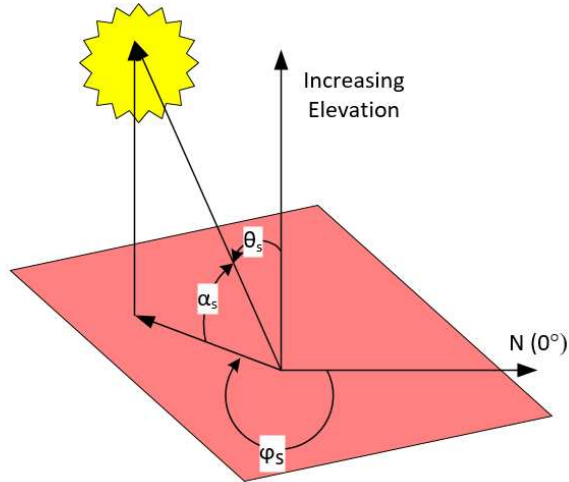
**Figure 2-5: Flowchart outlining calculation of total irradiance**

<sup>1</sup>National Renewable Energy Laboratory Renewable Resource Data Center, “Changing System Parameters” [Online]. Available: <http://rredc.nrel.gov/solar/calculators/pvwatts/system.html>. [Accessed: 08-Jul-2016].

**Table 2-2: Definitions of variables used in Figure 2-5**

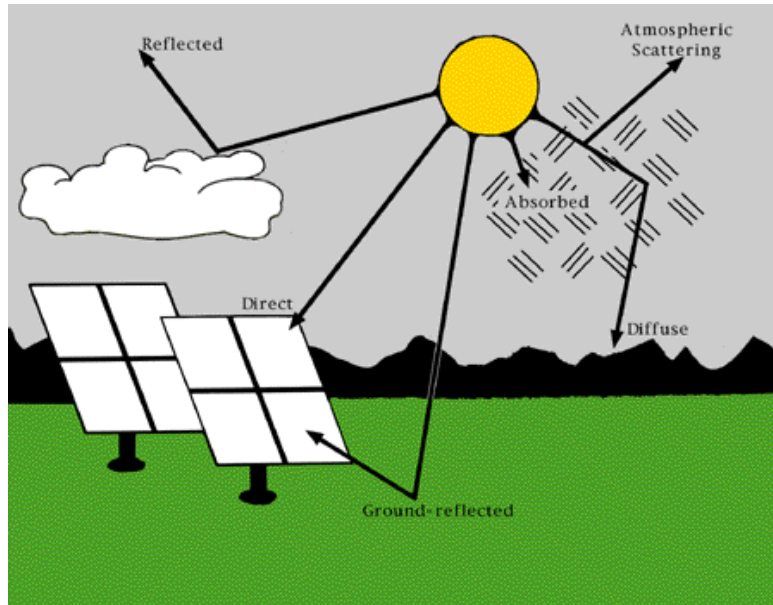
Variable	Symbol	Description
Solar Azimuth Angle	$\phi_s$	Azimuth angle of the sun
Solar Elevation Angle	$\alpha_s$	Angular height of the sun in the sky as measured from the horizontal
Solar Zenith Angle	$\theta_s$	Angle between the sun and the vertical
Apparent Solar Elevation Angle	$\alpha_{s, app}$	Solar apparent elevation angle, with refraction included in measurement
Solar Time	$t_{solar}$	Time of day, based on the rotation of the earth with respect to the sun
Clear Sky Direct Normal Irradiance	$DNI_{CS}$	Amount of irradiance received by a surface that is always held normal to the rays that come in a straight line from the direct of the sun
Clear Sky Diffuse Horizontal Irradiance	$DHI_{CS}$	Amount of scattered irradiance received by a horizontal surface
Clear Sky Global Horizontal Irradiance	$GHI_{CS}$	Sum of DNI and DHI
Ground Diffuse Irradiance	$E_{diffuse, Gr.}$	Amount of irradiance that is reflected from the ground
Angle of Incidence	AOI	Angle that an incident ray makes with a perpendicular surface at the point of incidence
Sky Diffuse Irradiance	$E_{diffuse, Sky}$	Amount of irradiance that reaches the Earth's surface after scatter of the direct beam

Figure 2-6 illustrates the solar azimuth angle ( $\phi_s$ ), solar elevation angle ( $\alpha_s$ ), and the solar zenith angle ( $\theta_s$ ). The solar azimuth angle indicates in which direction the sun is. The solar elevation angle is an indicator of the sun's height and is measured from the horizon to the center of the sun. The solar zenith angle measures the angle from the zenith to the center of the sun.



**Figure 2-6: Solar azimuth, zenith, and elevation angles**

Figure 2-7 illustrates direct irradiance, ground-reflected irradiance, reflected irradiance, absorbed irradiance, and direct irradiance. Diffuse irradiance is irradiation that reaches a surface after being scattered and absorbed by molecules in the atmosphere. Ground reflected irradiance is irradiance that has been reflected after coming in contact with the ground. Direct irradiance is the amount of irradiance a surface receives from the direction of the sun. Lastly, this figure shows that irradiance can be reflected from clouds in some cases.



**Figure 2-7: Illustration of various types of irradiance<sup>1</sup>**

It is important to note that some portions of the Sandia PVL LIB were not utilized. This model was not used to calculate inverter losses, parameters for the electrical circuits of the PV modules, or the power output for the PV array.

For simulation purposes, the portion of the Sandia PVL LIB implemented of this study produced PV forecasts that had on average -3.56% error when compared to the actual PV output recorded in Canberra, Australia for a 1.56 kW array. Figure 2-8 show a distribution of the forecast error for the PV forecasts outputted from the Sandia PVL Library. This illustration shows that the clear sky PV estimate often exceeds the actual PV output due to the fact that the Sandia PVL LIB estimates PV output under clear sky conditions (i.e. no cloud cover).

---

<sup>1</sup>National Renewable Energy Laboratory Renewable Resource Data Center, “Shining On”, [Online]. Available: <http://rredc.nrel.gov/solar/pubs/shining/chap4.html#fig3>. [Accessed: 08-Jul-2016].

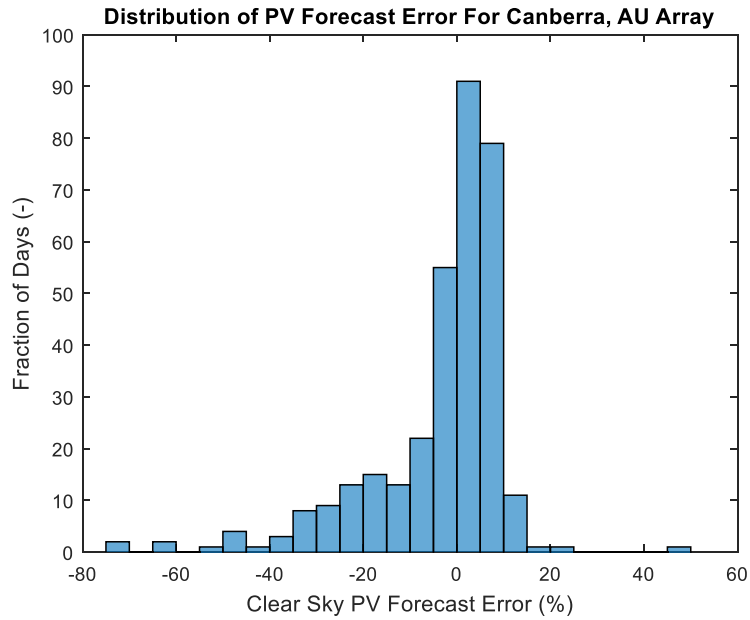


**Figure 2-8: Clear Sky PV Forecast Error for Canberra array**

In some cases, the Clear Sky PV estimate is exceeded to “white cloud edges” which cause sunlight to reflect from the clouds and amplify the irradiance observed by the pyranometer, a device used to measure irradiance<sup>1</sup>. These events are typically short-lived. The amplified irradiance effect is illustrated in Figure 2-9.

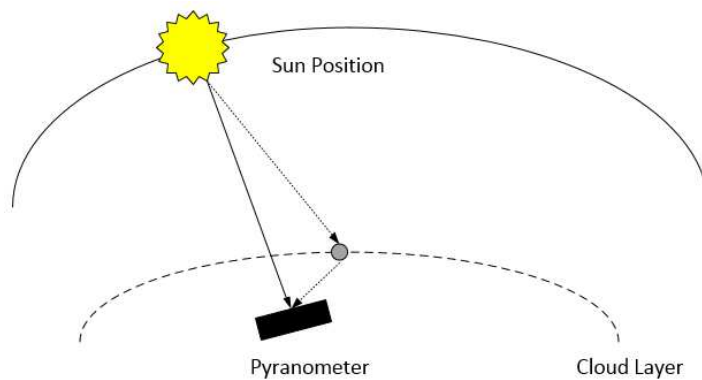


**Figure 2-9: Illustration of cloud edge effect**

<sup>1</sup>M. Almeida et al., “Extreme overirradiance in São Paulo, Brazil”, *Solar Energy*, vol. 110, 2014.

An example of an image with white cloud edges is shown in Figure 2-10. Figure 2-11 shows a plot which illustrates the amplified irradiation caused by the white cloud edges in Figure 2-10.



**Figure 2-10: Sample image with white cloud edges due to refraction**

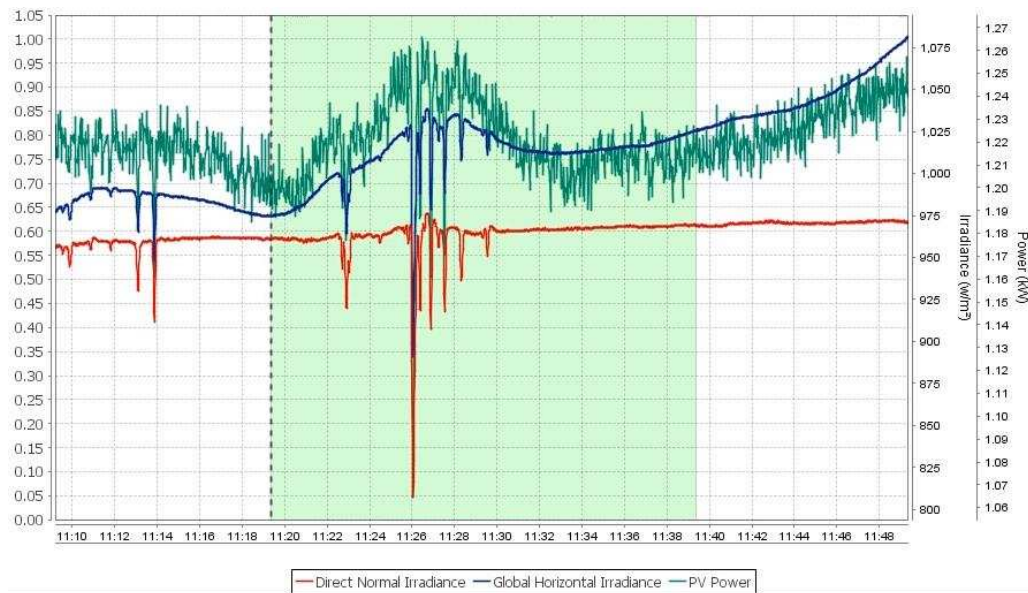


**Figure 2-11: Amplified irradiation due to white cloud edges**

Since the Sandia PVL LIB assumes no cloud cover, if clouds are present the calculated clear sky irradiation must be modified by some estimate of the irradiation that will be blocked by the cloud. Therefore, cloud cover will need to be examined and the effect on irradiance analyzed.

### 2.2.1.3 CL Algorithm

The PV forecasting system is shown in Figure 2-12. Cloud measurements provided by CSIRO software (A) are given as a fraction of the sky covered with clouds in each of the 16 rings surrounding the current sun position. These measurements are compared to a set of thresholds (B) and if any cloud fraction exceeds a threshold, it is flagged as a cloud detect. Thresholds for the first ring are set high due to flare near the sun. A jitter filter (C) is used to filter the cloud detections. This will be discussed in section 2.2.1.3.1. Next, the controller takes inputs from the Sandia model (D) and the actual PV output as measured by the inverters (F) to calculate the maximum allowable PV output.

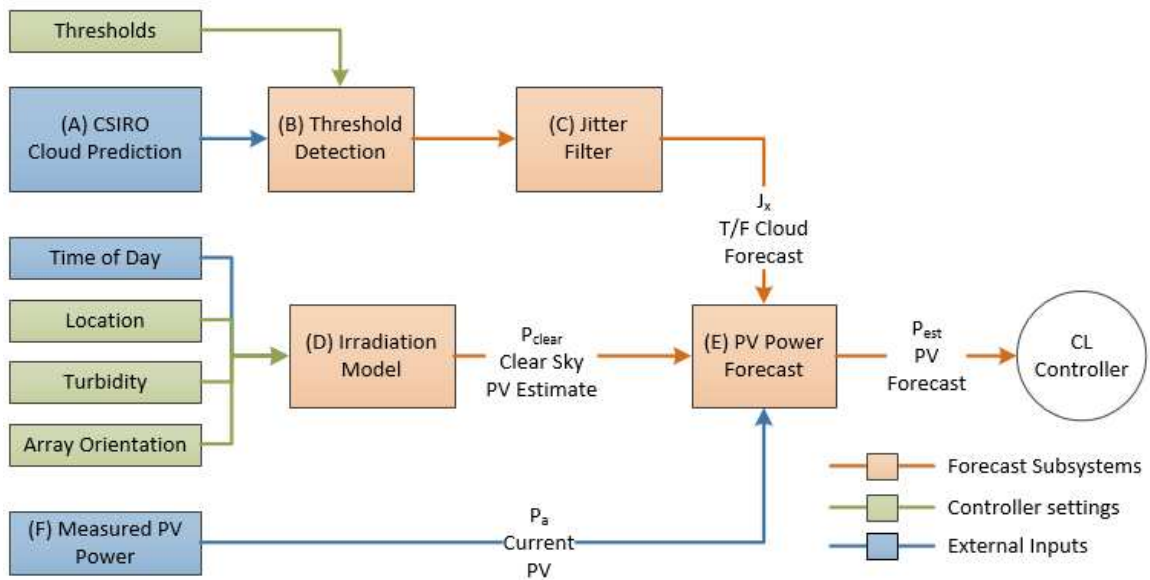


**Figure 2-12: PV forecasting subsystem**

#### 2.2.1.3.1 Jitter Filter

Detections are filtered using the jitter filter, shown as a state machine in Figure 2-13. If a cloud is detected more than  $K_t$  consecutive periods, the filter outputs a cloudy state ( $J_x = 1$ ). The

filter only returns to a “no clouds” state ( $J_x = 0$ ) when no clouds have been detected for longer than  $K_m$  seconds. The output of the filter is a true/false indicator of cloud cover.

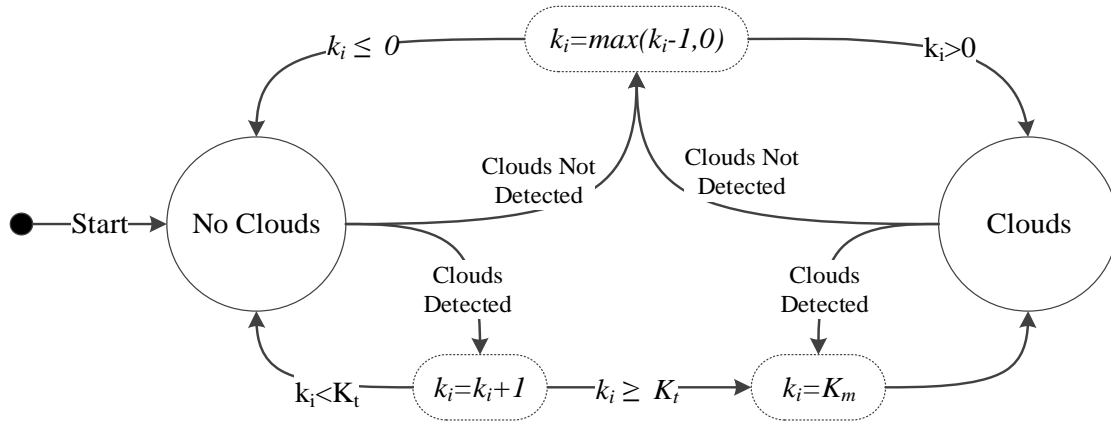


**Figure 2-13: Jitter filter configuration**

The PV forecast, labeled as (E) in Figure 2-12, is calculated using Equation 2-1 and

Equation 2-2.

**Equation 2-1:**

$$f_x = \begin{cases} 1 & \text{if } J_x = 0 \\ f_c & \text{if } J_x = 1 \end{cases}$$

**Equation 2-2:**

$$PV_{est} = \max(PV_a, f_x PV_{clear})$$

Where:

$f_x$  is the fraction of cloudiness outputted by the jitter filter

$J_x$  is the cloudiness state outputted by the jitter filter

$PV_{clear}$  is the PV clear sky estimate

By using the max() computation in Equation 2-2, the equation covers the cases where the PV output exceeds the clear sky estimate. This could happen due to enhancements in PV output as a result of white cloud edges around mid-day or as a result of an inaccurate clear sky PV estimate.

### 2.2.1.3.2 CL State Machine

On every execution of the CL controller, the maximum PV output and the minimum number of generators online are calculated from PV forecast information, the forecasted load, PV output reported by the inverters, and the number of generators online. The controller then forecasts the relative loading of the generators to evaluate if they will be operating under stable conditions, as shown in Equation 2-3.

**Equation 2-3:**

$$p_{a,f} = \frac{L_f - PV_{est}}{P_r N_f}$$

Figure 2-14 shows the state machine within the CL controller. At each time step, the state machine iterates until a stable end state has been reached. Multiple state transitions can occur within a single time step, with a maximum of five iterations on any execution.

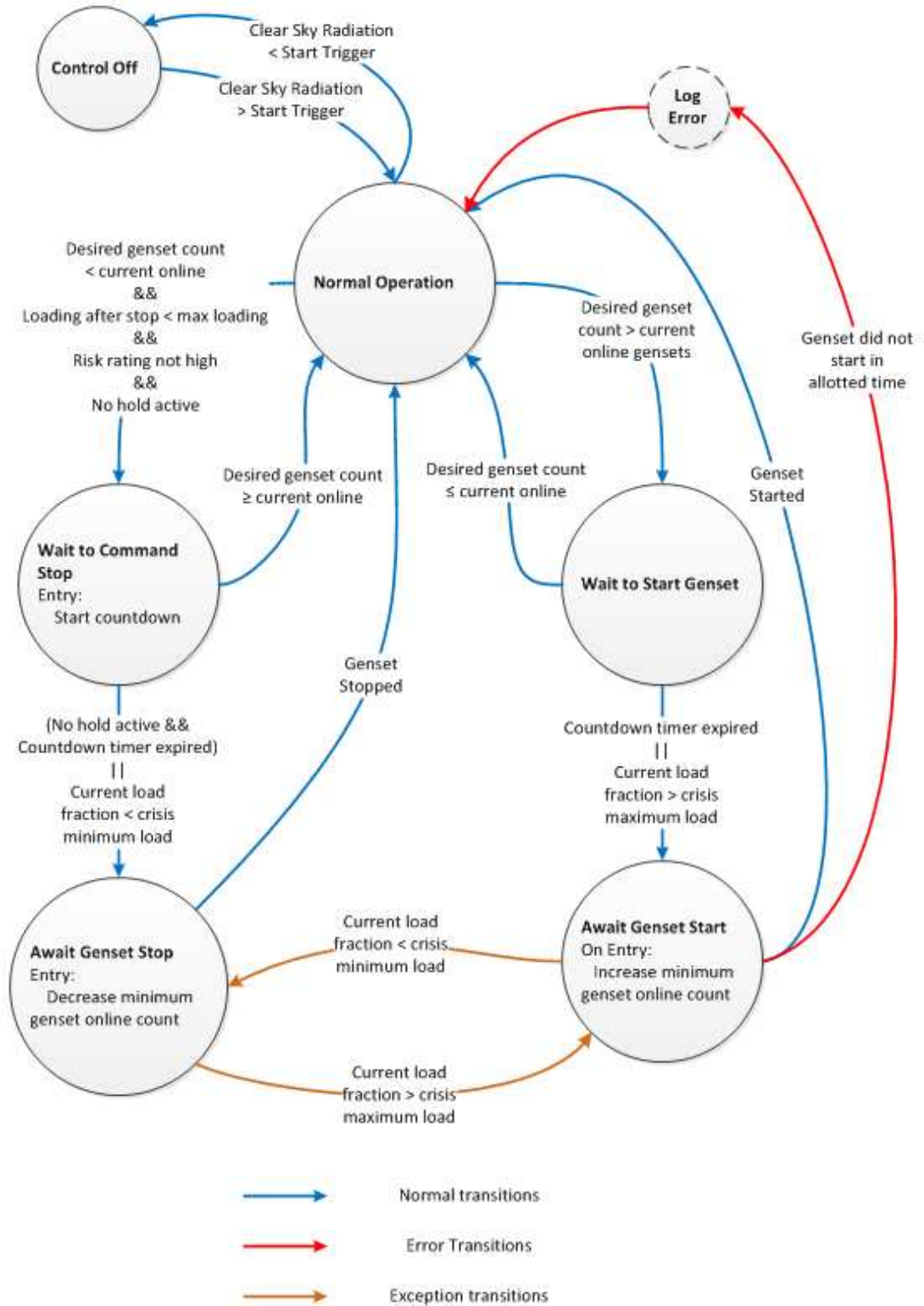


Figure 2-14: The CL ("Chicken Little") controller state machine

The controller only operates when the estimated clear sky irradiation increases above or below a specified starting threshold (i.e. during daytime hours).

During steady-state (normal) operation, there are no changes made to the minimum number of generators commanded online. If the minimum number of generators online does not match the number of generators online (i.e. a generator start or stop is occurring), the controller must wait until the number of generators online reported by the generator system matches the minimum number of generators online. This confirms that a command has been executed. The only exception to this is if the controller observes that the current generator relative loading is below/above the generator minimum/maximum relative loading levels while a command is being executed, in which case the controller modifies the minimum number of generators online and waits to confirm that the number of generators online equals the number it has commanded online.

### *2.2.2 Load Forecasting Using a Markov Transition Matrix*

This system was designed based on several months of load information and irradiance records for the Tanzania site. The average power output for this site for approximately 115 days is shown in Figure 1-2. There are a couple of observations that should be noted from this load profile. First, the load tends to fluctuate around the same level for long periods of time. This is called “load segmenting” and the load appears to be fluctuating by different amounts in each “load segment”. However, it’s very hard to tell the frequency of this fluctuation from Figure 1-2. A Markov Chain will be used to represent the load transitions in Figure 1-2. Markov Chains are used to represent stochastic processes where a future value depends on the current value, but are independent of past values. To simplify the Markov Chain, a Markov Transition Matrix (MTM) will be used. The MTM will be utilized to predict the transition probability to/from a given load level in the next 60 seconds.

The transition matrix,  $T$ , is divided into several load bins and has a size of  $N \times N$ , where  $N$  is the total number of bins. The value contained in each load bin indicates the probability of transitioning from a load level between  $L_1$  and  $L_2$  to another load level between  $L_3$  and  $L_4$ . The number of bins is dependent on the bin size,  $\Delta L$ , and the maximum load observed in the load profile,  $L_{max}$ . The calculation of the total number of load bins is shown in Equation 2-4. Equation 2-5 shows how to calculate the transition probabilities an MTM.

**Equation 2-4:**

$$N = \frac{L_{max}}{\Delta L} \text{ where } \Delta L = L_2 - L_1$$

**Equation 2-5:**

$$p_{i,j} = P(X_{m+1} = L_j | X_m = L_i)$$

In Equation 2-5,  $p_{i,j}$  is the probability that the next load at the next time step,  $X_{m+1}$ , will equal another load level,  $L_j$ , given that the current load level, at time  $X_m$ , equals  $L_i$  where  $i$  and  $j$  correspond to the rows and columns in the transition matrix.

MTMs are useful in fault analysis to ensure that the loads that are being tested in the simulations realistic for the particular micro-grid this system will be deployed to. The MTM for the Tanzania micro-grid is shown in Figure 2-15. The columns represent the current load and the rows represent the load at the next time step.

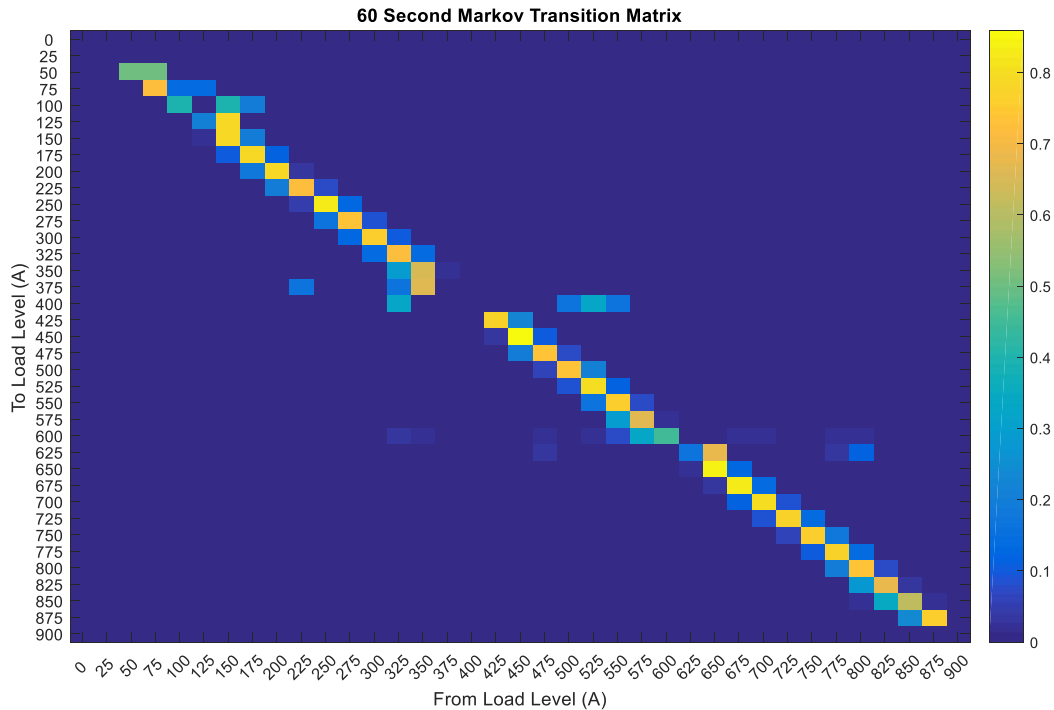


**Figure 2-15: Markov Transition Matrix for Tanzania data**

The MTM in Figure 2-15 is color-coded to show the most likely load transitions. Yellow blocks are the most probable transitions and blue blocks are the least probable transitions. Probability peaks seen in Figure 1-2 are easily observable as high probability “islands” along the diagonal of the MTM. Additionally, the straight yellow diagonal bins indicate that if the mine is at a particular load level, it is more likely to stay at that load level 60 seconds later. The MTM also allows you to get more detailed information about the “load islands”. For example, at load levels from 175-300A, there is little fluctuation in load from minute-to-minute. The load is relatively stable with a less than 20% probability that a transition of  $\pm 75A$  will occur in the next minute.

### 2.2.3 Reserve Calculation

A reserve is utilized to account for small, random, variations in load seen by the gensets. Reserve is important because it ensures that sufficient generation is online to pick up load if

necessary. Maximum current transients were measured from the given load data using the MTM analysis previously discussed in section 2.2.2. Equation 2-6 defines a normalized current and Equation 2-7 defines the normalized current transient.

**Equation 2-6:**

$$\phi = \frac{I}{I_{max}}$$

Where:

$\phi$  is the normalized current

$I$  is the current

$I_{max}$  is the maximum current observed in the load data

**Equation 2-7:**

$$\psi = \frac{\Delta I}{I_{max}}$$

Where:

$\psi$  is the normalized current transient

$\Delta I$  is the change in current

The normalized current transients and power transients are plotted in Figure 2-16a and Figure 2-16b. From this data, it is evident that “up” transients are smaller at higher load levels. A model for the maximum transient was created and it is defined by Equation 2-8 where  $\phi_b$  is the breakpoint between a constant value and the sloping line. The value of  $\phi_b$  was found to be 0.25.

**Equation 2-8:**

$$\psi_{max} = 1.15 \begin{cases} \phi \leq \phi_b: & 1.0 \\ \phi > \phi_b & \frac{1 - \phi}{1 - \phi_b} \end{cases}$$

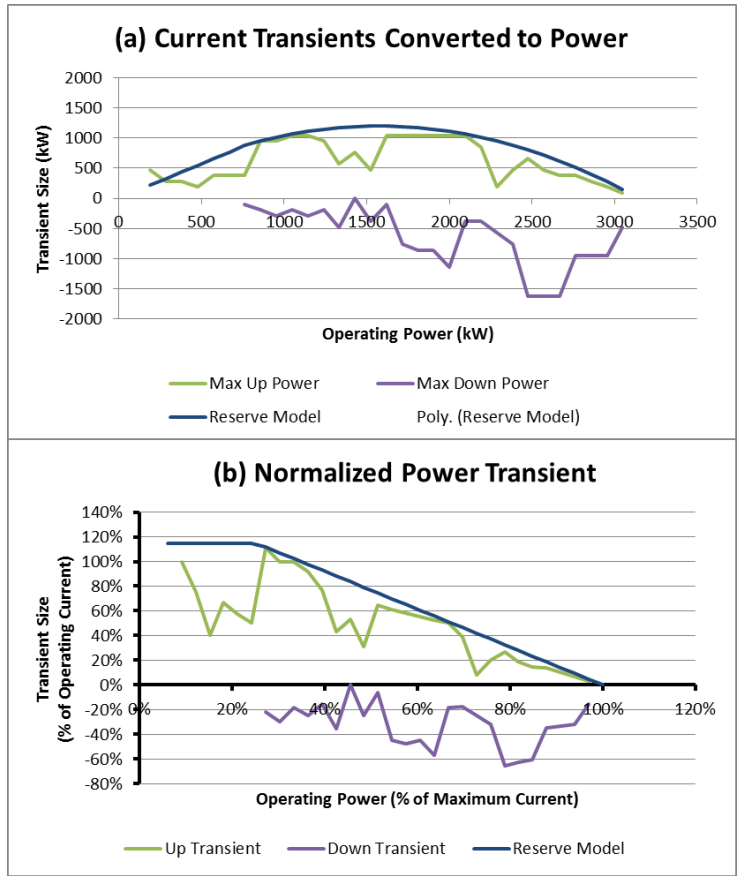


**Figure 2-16: Maximum Power Transients**

Given the current power output (or measured current), the reserve model can be used to calculate reserve levels for the controller. The reserve will be compared to the current online reserves to decide if a generator will need to be started.

### 2.3 Generator Controls

A system of generators is controlled by a central generator controller. The purpose of the generator controller is to protect the generators from damage due to faults (see fault definitions in section 1.2.2), and to balance load, track maintenance, and similar management tasks. In this type of micro-grid, the generator controller is operating in “island mode” meaning that it is not importing power from external sources such as a public grid. The main functions of the generator

controller that will be evaluated in this section are: (1) Executing start commands and (2) Maintaining reserve settings (3) Shutdown generators if fault conditions in section 1.2.2 are met.

The generator controller balances the current net load (total load minus the amount of load being satisfied by PV generation) amongst the diesel generators and starts/stops the generators if necessary. It is important to note that the generator controller must also maintain the minimum number of generators online specified by the supervisory controller. If the minimum number of generators online is reduced, the generator controller may hold a generator online depending on the amount of reserve that is currently available in the generator system.

The load management functions described in the following sections are dependent on the net load on the generators,  $P_{net}$ , which is defined in Equation 2-9.

**Equation 2-9:**

$$P_{net} = L + R_a - PV_a$$

The net load on the generators results in an amount of unused generation capacity on the current number of generators online. This is referred to as available. It is denoted by  $P_{avail}$  and defined in Equation 2-10.

**Equation 2-10:**

$$P_{avail} = N_o P_r - P_{net}$$

*2.3.1 'Min Num On' Parameter*

The 'Min Num On' parameter maintains a minimum number of generators online This is useful because it can prepare the system for a forecasted drop in PV output by starting a generator in advance of the PV transient. In addition, the 'Min Num On' parameter can often respond before load-dependent start would command a generator online, as the load-dependent start subsystem only utilizes the current instantaneous power and load, and is not aware of forecasted changes in PV generation.

### 2.3.2 *Load-Dependent Start*

The load dependent start setting forces a generator to synchronize if the power available remains low for an extended period of time. Additionally, this parameter is only used when the ‘MinNumOn’ parameter has not yet commanded a generator to start. This is described in further detail in section 6.1.

#### 2.3.2.1 *‘Non-Connected Gens’ Parameter*

The ‘Non-Connected Gens’ parameter is only utilized after ‘Load Dependent Start’ has triggered a ‘START’ command. If a generator has not yet transitioned to ‘ONLINE’ and the power available falls within the acceptable range for an extended period of time, this parameter will stop the generator from synchronizing (generator transitions to ‘COOLDOWN’, (see generator state machine in Figure 1-5). This can happen if there is a load drop shortly after a ‘START’ command has been sent. The requirements for this parameter to activate are defined in section 6.1.1.

### 2.3.3 *Load-Dependent Stop*

The load-dependent stop function checks to see if the relative loading and power available on the generators will be an acceptable range if a generator is taken offline. Too much spinning reserve on the generators will mean that the micro-grid is burning more diesel than necessary. This is described in further detail in section 6.1.2.

Figure 2-17 shows a state machine which shows how the load dependent start/stop parameters function with the ‘MinNumOn’ parameter and the ‘NonConnGens’ parameter.

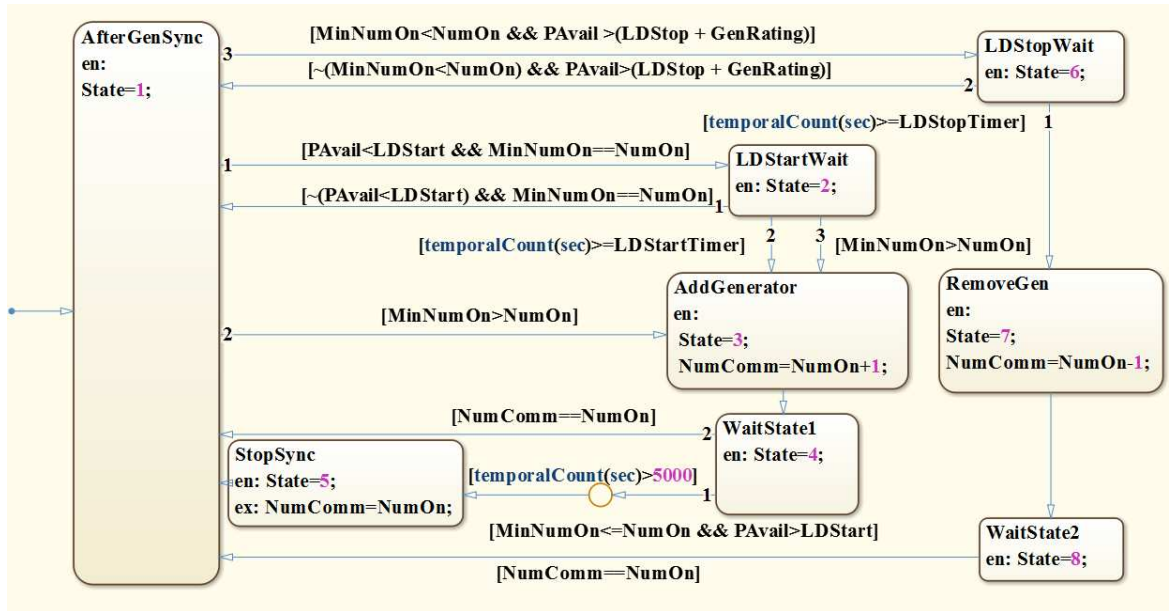


**Figure 2-17: State machine for the generator load controller**

### 2.3.4 Fault Protection Methods

#### 2.3.4.1 Reverse Power

The DEIF controllers have two configurable parameters to protect the generators from reverse power. For example, if  $p_a < p_{a,r_1}$  for  $X_1$  seconds a fault would be triggered and if  $p_a < p_{a,r_2}$  for  $X_2$  seconds a fault would also be triggered).

#### 2.3.4.2 Overload Protection

The DEIF controllers have five configurable parameters for overload protection. If  $p_a > p_{a,o_1}$  for  $X_1$  seconds a fault would occur. A fault could also be triggered if  $p_{a,o_n}$  for  $X_n$  seconds where  $n$  is the overload protection parameter that coincides with the first through fifth layers of overload protection.

## 2.4 Optimization Techniques

The following sections will describe the methodology that was used to accomplish a reduction in diesel fuel consumption along with a reduction in the PV energy discarded. Simulations were performed to model the system shown in Figure 2-1. Additionally, diagnostic information was collected. This included:

1. Total PV discarded,  $PV_d$  (shown in Equation 2-11)
2. Total diesel consumption,  $F_{total}$  (see Equation 2-12)
3. Number of faults

### Equation 2-11:

$$PV_d = PV_a - PV_{max}$$

### Equation 2-12:

$$F_{total} = N_o \int_0^{t_e} F_{inst} dt$$

Simulation parameters were then modified to reduce the total diesel consumption, while minimizing the number of faults so that the integrity of the system would not be compromised. Overall, the goal of the simulations is to show that large array sizes can be utilized without compromising the integrity of the generator system.

### 2.4.1 Improvement of PV Forecast Based on Number of Rings

In early simulations, it was assumed that the first six concentric rings around the sun would be necessary to compile a PV forecast. However, it was noted that at large array sizes (>1000kW), there were high fault rates in comparison to small array sizes. After further investigation of the faults, it was determined that the majority of them were due to generator overloading as a result of an inaccurate PV forecast (i.e. the PV forecast was not forecasting all of the drops in irradiance).

This problem could have been resolved by adding more reserve to the generator subsystem to ensure that more generators would remain online, and thus the gensets would remain in stable operation. However, the consequences of this solution would be tighter restrictions on the maximum allowable PV output (see Equation 1-17 and 1-18) and increased diesel fuel consumption (see Equation 2-12). Therefore, the methodology going forward needed to concentrate on improving the CL prediction.

One of the options to improve the CL prediction was to increase the Jitter Filter hold time. This would extend the period for which the forecast PV output would be reduced. However, it was concluded that this would not be an ideal approach because it would extend the period of the reduced forecast for every cloud detection, which would have been unnecessary if there were no fault occurring at that particular time in the simulation. Additionally, increasing the hold time would increase diesel fuel consumption for every cloud detection which is not desirable.

Prior to performing simulations, a search of settings was done to find the best settings. From these results, it was determined that the thresholds should be [.5 .1 .1 .1 .1 .1]. In early simulations, only 6 rings were utilized to formulate the PV forecast. In later simulations, it was decided that simulations should be done to look at results for 6, 8, and 10 rings to determine if utilizing more rings in the forecast would improve the PV forecast. By doing this, the fault rate could be reduced with minimal impact on diesel fuel consumption.

#### *2.4.1.1 Monte Carlo Method*

The Monte Carlo method was used to determine the statistical probability of the number of faults, total diesel consumption, and energy discarded for a single operational year. One thousand randomly assembled years were assembled to use for probability analysis. The procedure to assemble a year is shown in Figure 2-18.

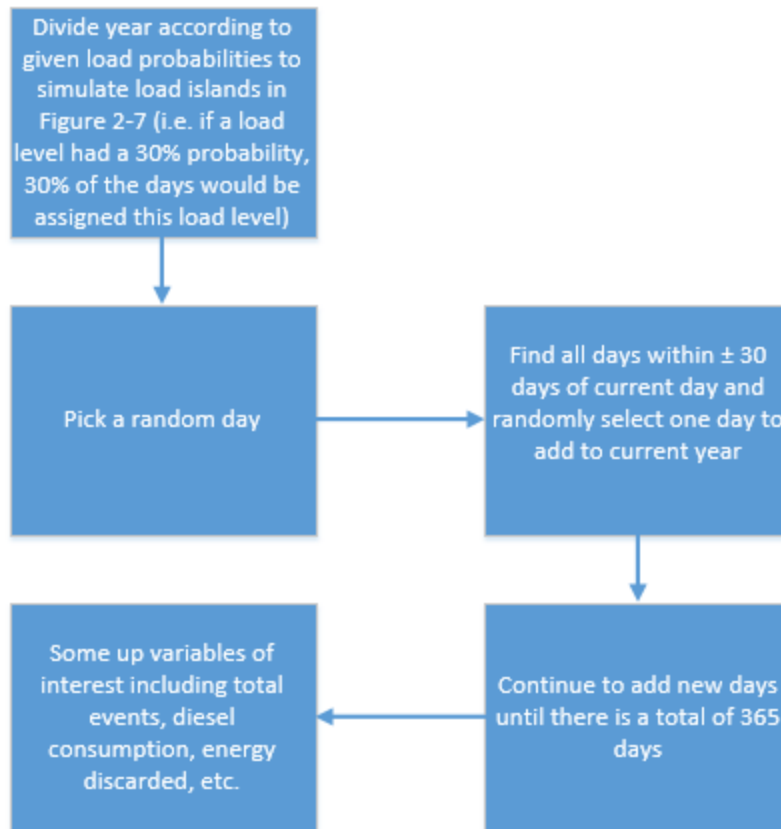


**Figure 2-18: Procedure to compile a random year**

From the load data given in Figure 1-11 and the MTM shown in Figure 2-15, it can be estimated that there are fractions of the year where the micro-grid is operating around a particular load level. These can be estimated by a general probability for each of the three “load islands” in the MTM. Thus, the number of days per year where the micro-grid is operating around at each load island can also be determined.

To assemble a single year, an array size must be selected and a random day must be chosen. It is assumed that you start at the first load island. Next, a random day within  $\pm 30$  calendar days is selected where the same load level and PV array was simulated. This is continued until the structure has enough days for the first load island. It is then repeated to compile the data for the

second and third load island. Lastly, the number of faults, total annual diesel consumption, and total annual energy discarded is summed for the current year. This process is repeated until there a total of 1000 years. With this data, histograms can be created to illustrate the impact of the number of rings on diesel consumption, fault occurrence, and PV utilization.

*2.4.2 Use of Smaller Generators to Reduce Fuel Consumption*

Another option that was evaluated was to decrease fuel consumption was the use of smaller generators. With the micro-grid being limited to adding generation in 1 MW intervals, it is difficult to turn off a generator, which is what ultimately drives fuel consumption down. The use of smaller generators will allow for increased PV utilization, as the calculation of the maximum PV output is directly influenced by the generator size (see Equation 1-16). Table 2-3 compares the specifications of a 400 kW generator (Cummins QSK15) to the original 1 MW generator (Cummins QSK15) on site at the micro-grid<sup>1</sup>.

**Table 2-3: Specifications for Cummins QSK50 DQGAG and QSK15 DFEK**

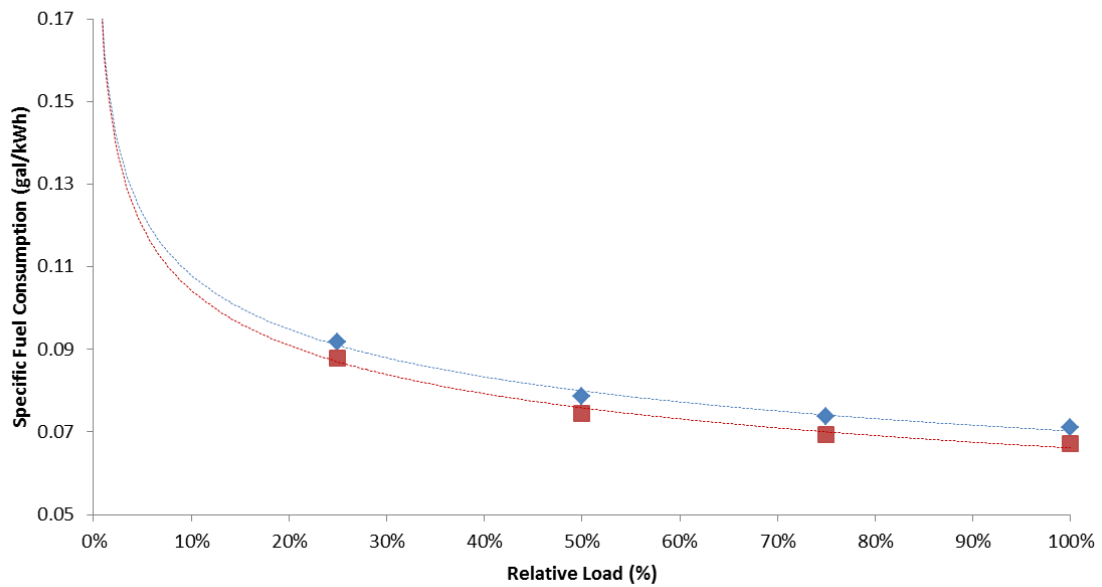
Manufacturer	Cummins Inc.	Cummins Inc.
Series	QSK50	QSK15
Model	DQGAG	DFEK
Prime Rating	1000 kW	400kW
Operating Frequency	50 Hz	50 Hz
Fuel Type	Diesel	Diesel

Figure 2-19 shows the specific fuel consumption for the Cummins QSK15 DFEK and QSK50 DQGAG generators scaled to their rated load levels.

---

<sup>1</sup> Cummins Power Generation Inc., “Generator Data Sheet”, D-3404a. [Revised October 2010].

### Specific Fuel Consumption for Cummins QSK50 DQGAG and Cummins QSK15 DFEK



**Figure 2-19: Specific fuel consumption for Cummins DQGAG and DFEK**

From Figure 2-19, it is evident that the specific fuel consumption for the DFEK is less than that of the DQGAG at all levels of relative loading. This means that the DFEK generator is able to burn less fuel per kWh of energy demanded at all times. On average, the specific fuel consumption of the DFEK is 5.22% less than that of the DQGAG. Therefore, in addition to having the ability to save fuel by turning generators off in smaller increments, the DFEK burns less fuel because it is more fuel efficient.

### 3 RESULTS AND DISCUSSION

#### 3.1 Modification of PV Forecasting Settings

Results with six, eight, and ten rings were examined to evaluate if the number of faults could be reduced by increasing the number of rings. Fault definitions were previously outlined in Table 1-2. The thresholds for the added rings was set to 0.1. This threshold was chosen for consistency purposes because all of the other rings were previously thresholds of 0.1, except for the ring closest to the sun which had a threshold of 0.5 to account for flare due to the sun. This threshold was deemed appropriate by use of a genetic algorithm. In addition to examining the number of faults for various ring numbers, fuel consumption was also examined.

Figure 3-1 through Figure 3-6 show the fault histograms for PV values ranging from 500 kW to 2500 kW for one thousand random years. The y-axis represents the fraction of the year with the corresponding number of faults on the x-axis. From these histograms, it is observed that increasing the number of rings reduces the number of faults at all array sizes.

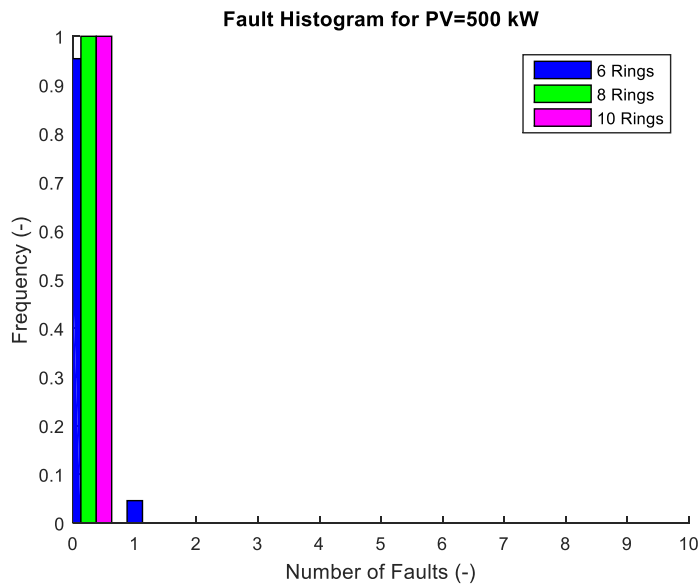


**Figure 3-1: Fault histogram for PV=500 kW**

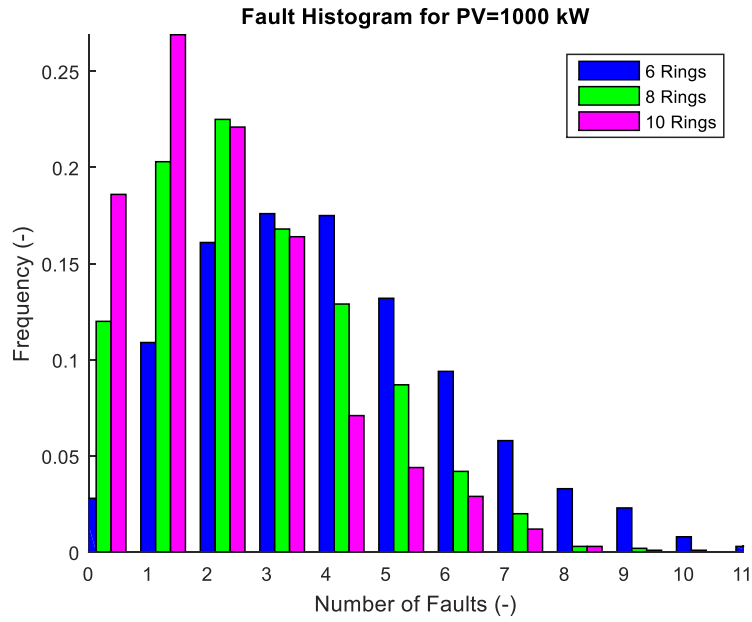


**Figure 3-2: Fault histogram for PV=1000 kW**

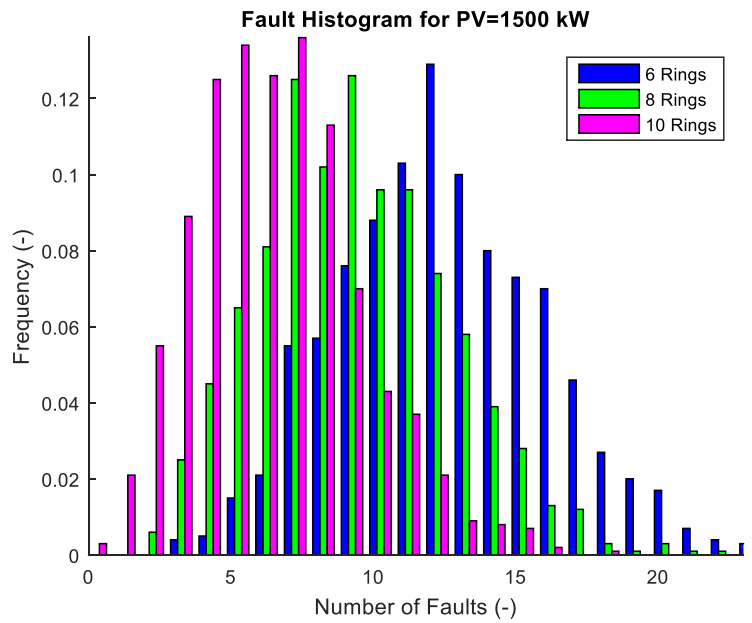


**Figure 3-3: Fault histogram for PV=1500 kW**

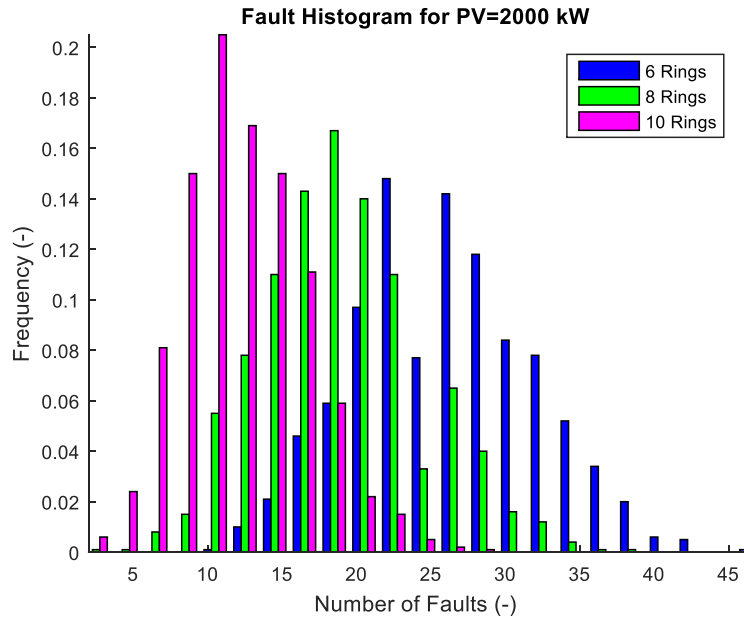


**Figure 3-4: Fault histogram for PV=2000 kW**

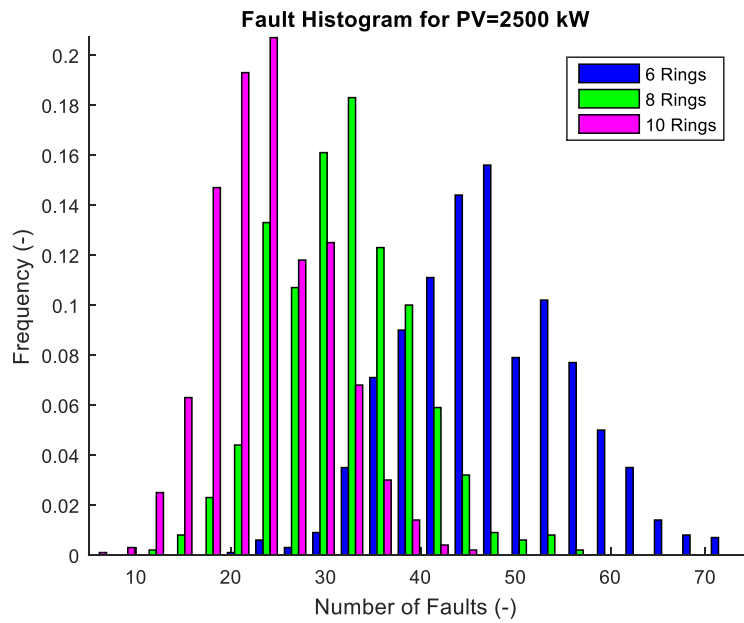


**Figure 3-5: Fault histogram for PV=2500 kW**

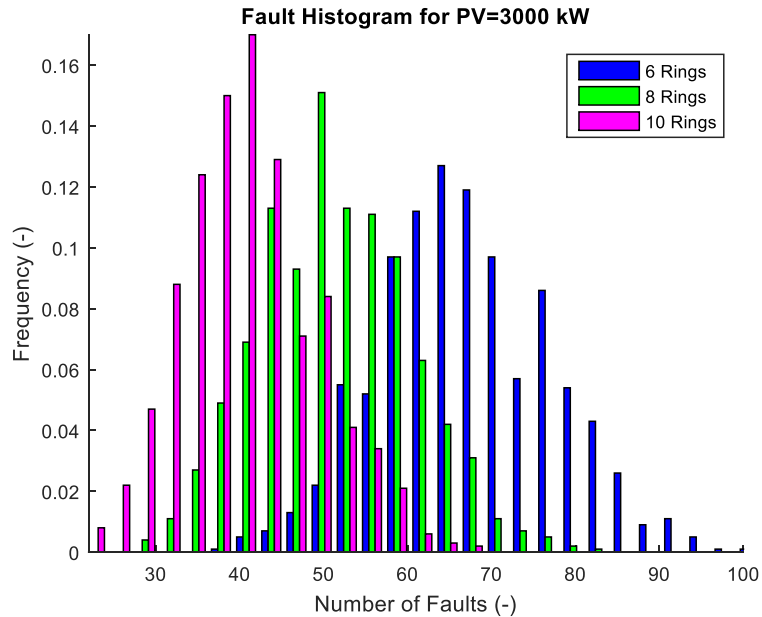


**Figure 3-6: Fault histogram for PV=3000 kW**

At small array sizes ( $< 1000kW$ ), the number of faults seen by the system is low if six rings are utilized. This is attributed to the fact that the generator system is satisfying the majority of the load and therefore, the effects of PV transients are minimized. Additionally, these faults are eliminated by increasing to eight or ten rings. At larger array sizes ( $\geq 1000kW$ ), the system is at higher risk for faults. The frequency of faults the system experiences is a direct result of any transients in the net power required from the gensets (see Equation 2-9), as this directly impacts their relative loading. When a cloud shades the PV array, the rapid reduction in PV output causes the net power required from the gensets to increase. Therefore, the gensets have the potential to become overloaded. At large array sizes ( $\geq 1000kW$ ), the generators are at a higher risk of becoming overloaded because the instantaneous increase in net power demanded from the gensets is higher.

Next, it was decided that the distributions in Figure 3-1 to Figure 3-6 should be compared to find out how similar they are, i.e. if statistical analysis will show there is benefit to adding more

rings. Two-sided Kolmogrov-Smirnov (KS) tests were used to evaluate if the “null hypothesis” was accepted or rejected at the 5% significance level. The “null hypothesis” states that there is no statistical relationship between two distributions. A KS test that returns a value of zero indicates that there is no statistical difference between the distributions and a KS test that returns a value of one indicates that there is a difference between the distributions at the 5% significance level. Results of the KS tests comparing the distributions for the total number of faults with 6, 8, and 10 rings are shown in Table 3-1.

**Table 3-1: Results for KS Tests comparing fault distributions**

Array Size (kW)	h value	
	6 to 8 Ring Comparison	8 to 10 Ring Comparison
500	0	0
1000	1	1
1500	1	1
2000	1	1
2500	1	1

From the results of the Kolmogrov-Smirnov tests shown in Table 3-1, it is clear that the fault distributions are statistically different for array sizes  $\geq 1000kW$ . At 500kW, the distributions are statistically similar because there are no distributions to compare when 8 or 10 rings are utilized (Figure 3-1 shows that there are zero faults for 8 and 10 rings when a 500 kW array is selected).

Figure 3-7 compares the occurrence of faults for array sizes ranging from 500-3000 kW. As the array size increases, the occurrence of faults also increases. However, increasing the number of rings in the system greatly reduces the occurrence of the faults.

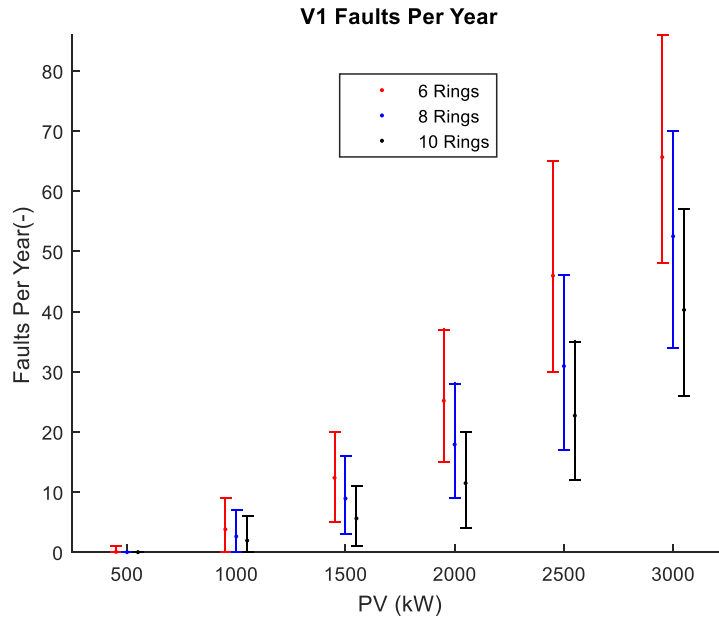


**Figure 3-7: Comparison of fault occurrence for all array sizes**

It is assumed that a micro-grid operator may be willing to tolerate some number of faults during an operational year in exchange for a reduction in fuel consumption. If it is assumed that one fault per month, or 12 faults per year, is acceptable, then it is possible to analyze the practical impact of considering more rings.

PV penetration, as defined by Equation 1-1, increases with increasing PV array sizes, as shown in Table 3-2. Additionally, Table 3-2 shows the mean values and confidence intervals for annual fault counts and diesel consumption. Upper and lower bounds for the confidence intervals were calculated using Equation 3-1 and Equation 3-2.

**Table 3-2: Mean annual values for PV penetration, fault count, and daytime diesel consumption for 6, 8, and 10 rings across all array sizes**

Array Size (kW)	No. Rings	PV Penetration			Fault Count			Diesel Consumption (Thousands of gallons)		
		Avg	CI <sub>min</sub>	CI <sub>max</sub>	Avg	CI <sub>min</sub>	CI <sub>max</sub>	Avg	CI <sub>min</sub>	CI <sub>max</sub>
500	6	8.3%	8.0%	8.5%	0	0	1	811	807	814
	8	8.3%	8.0%	8.6%	0	0	0	809	806	813
	10	8.3%	8.0%	8.6%	0	0	0	809	806	812
1000	6	16.5%	16.0%	17.1%	4	0	9	749	744	754
	8	16.6%	16.0%	17.1%	3	0	7	748	743	753
	10	16.6%	16.0%	17.1%	2	0	6	748	743	753
1500	6	24.3%	23.5%	25.1%	12	6	20	688	681	695
	8	24.3%	23.5%	25.1%	9	3	16	687	681	694
	10	24.3%	23.5%	25.2%	6	2	13	688	681	694
2000	6	30.9%	29.8%	31.9%	25	15	37	638	629	647
	8	30.8%	29.8%	31.8%	19	9	29	638	629	646
	10	30.8%	29.8%	31.9%	12	5	21	638	629	646
2500	6	35.9%	34.6%	37.0%	46	31	64	597	587	608
	8	35.7%	34.5%	36.9%	31	19	45	598	588	609
	10	35.6%	34.5%	36.8%	24	13	36	599	589	608
3000	6	39.2%	37.9%	40.4%	66	47	86	571	560	581
	8	39.0%	37.7%	40.2%	51	35	69	571	561	583
	10	38.9%	37.7%	40.1%	41	27	58	573	562	583

**Equation 3-1:**

$$CI_{min} = Z_{\frac{\alpha}{2}}$$

**Equation 3-2:**

$$CI_{max} = Z_{1-\frac{\alpha}{2}}$$

Where:

$CI_{min}$  is the minimum value of the confidence interval

$CI_{max}$  is the maximum value of the confidence interval

$Z$  is the array containing all samples sorted from smallest to largest

$\alpha$  is the confidence level

The results from Table 3-1 show that the micro-grid could select an array size of 2000 kW and expect to stay with the acceptable tolerance level for the occurrence of faults per operational year. This array size would result in 12 faults per operational year and a mean PV penetration of 30.8%.

In theory, increasing the number of rings should increase the conservativeness of the PV forecast, and therefore it should also drive up diesel fuel consumption as any load not carried by the PV system must be supported by the gensets. However, it can be seen from Figure 3-8 that the fuel cost of increasing the number of rings is statistically insignificant, as indicated by the overlapped 95% confidence intervals. Therefore, the analysis indicates that 10 rings should be used in all cases.

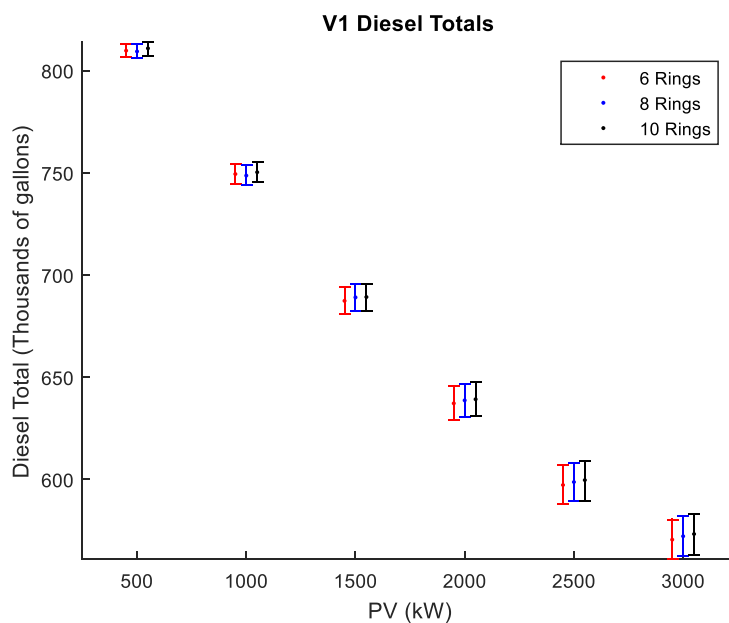


**Figure 3-8: Diesel totals for various array sizes and ring settings**

The statistical insignificance of the impact of increasing the number of rings on diesel consumption can be attributed to the fact that increasing the number of rings only slightly increases

the conservativeness of the PV forecast. This makes the impact on the amount of PV utilized minimal and therefore, the impact on diesel consumption minimal.

Next, the PV utilized relative to the total PV available will be evaluated to determine if increasing the number of rings in the forecast has a significant impact. Equation 3-3 shows how to calculate the fraction of PV energy utilized,  $\kappa$ , relative to the total PV energy available for utilization,  $PV_{avail}$ .

**Equation 3-3:**

$$\kappa = \frac{\int_0^{t_e} PV_a(t) dt}{\int_0^{t_e} PV_{avail}(t) dt}$$

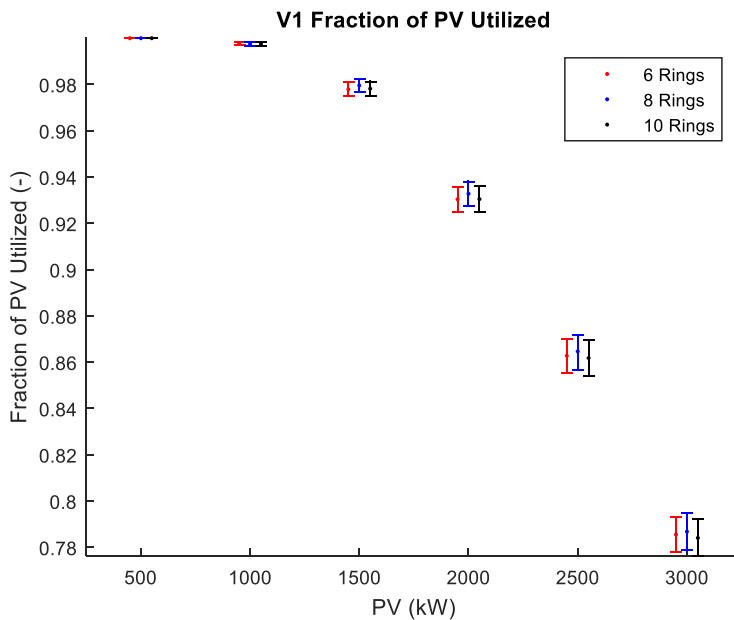


**Figure 3-9: Fraction of PV utilized for various ring settings**

Figure 3-9 shows that the fraction of PV utilized decreases as the array size is increased for all ring settings. It is also noted that the rate at which PV is discarded increases at array sizes  $\geq 2000kW$  because the micro-grid experiences a load of 2500 kW for 73% of the year. Therefore, at array sizes  $\geq 2000kW$ , the system must start curtailing PV to maintain stable operation with a single generator online on a larger number of days (when load is  $< PV$  size).

### *3.1.1 Analysis of PV Forecast Errors*

Overall, increasing the number of rings decreased the occurrence of faults because it increased the conservativeness of the PV forecast. However, it had no statistically significant impact on diesel consumption and a minimal impact on energy discarded at all array sizes because the PV forecast was not modified in such a way that the system was required to curtail large amounts of PV to prevent faults. Therefore, small changes in the PV forecast are ultimately what will optimize the performance of this system. To better understand the underlying drivers which reduced the fault count, faults were grouped into five types. Fault types 1-4 are related to errors with cloud detections and are shown in Figure 3-10. Fault type 5 is a case where a cloud was detected for the entire duration of the fault, but the PV forecast was overestimated. The interval of 900 seconds was used to get a clear understanding of exactly when cloud detections occurred.

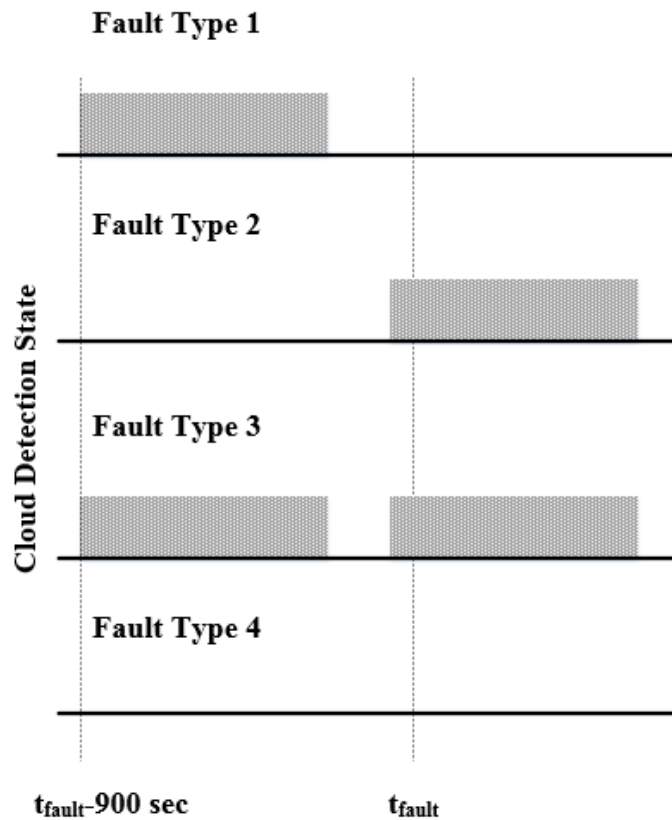


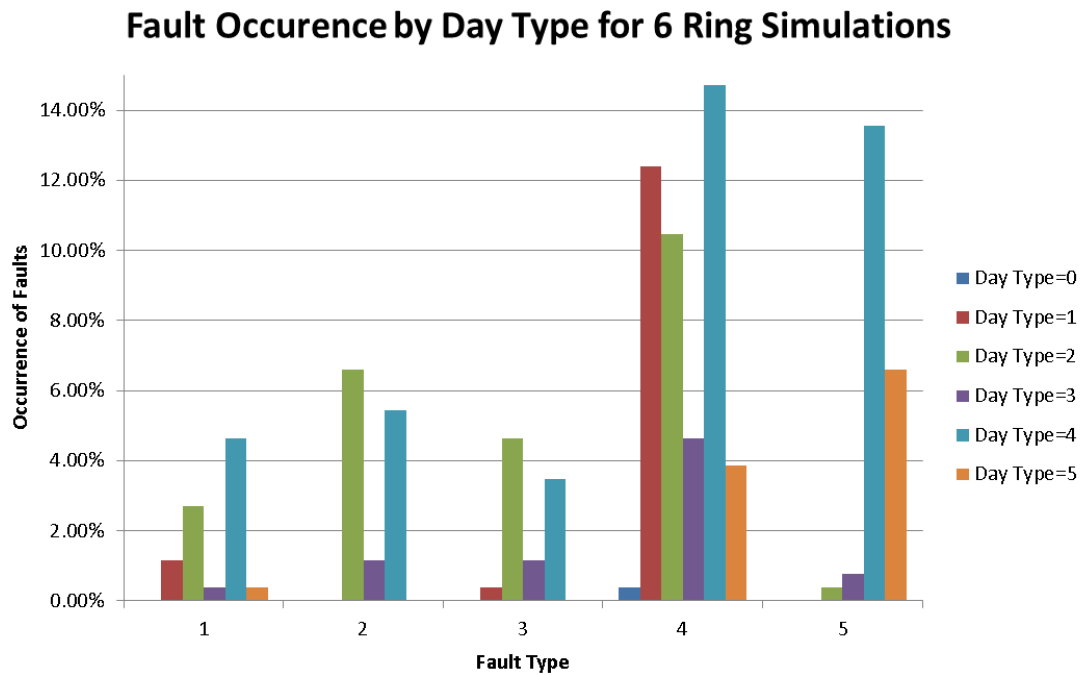
**Figure 3-10: Event Classification**

- 1) **Insufficient Hold:** A cloud detection occurred shortly before the fault, but the cloud detection, including the downstream jitter filter, failed to hold the detection long enough.
- 2) **Detected Too Late:** A cloud was successfully identified. However, this cloud detection did not give a generator adequate time to prepare for a drop in PV output.
- 3) **Detection Gap:** This is a combination of types 1 and 2. Clouds were detected early, the detection cleared, and was not restarted with sufficient time for more generation to come online.
- 4) **Miss:** The cloud was never identified.
- 5) **PV Forecast Overestimate:** This is not pictured in Figure 3-10, as it is unrelated to a cloud detection error. In other words, the jitter filter stayed on for all 900 seconds in advance of

the fault. In this case, the fault was due to the fraction of PV estimated when a cloud is detected,  $f_c$  in Equation 2-1, being set too high. In other words, the PV forecasted overestimated the amount of PV to expect when a cloud shades the array.

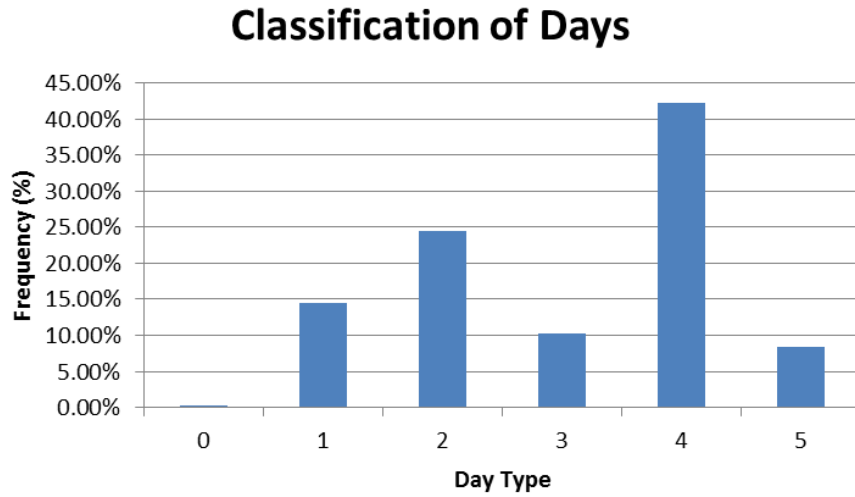
Day types are an indicator that of cloudiness for a given day. A lower day type indicates that this day was mostly sunny and a higher day type indicates that the day was mostly cloudy.

Figure 3-11 shows the classification of faults for 6 ring simulations by day type.



**Figure 3-11: Fault occurrence by day type for 6 ring simulations**

From this bar plot, it is observed that the majority of the faults were types 2, 4, and 5. This means that the majority of the faults experienced by the system were a result of a late cloud detection, no cloud detection or an overestimate in the PV forecast. Additionally, it is observed that the majority of the events occur on day types two and four. This is a result of the way the days were initially classified. Figure 3-12 shows that 24% of the days run were classified as type 2 and 42% were classified as type 4.



**Figure 3-12: Classification of days**

After the faults have been classified for the six ring trials, it is necessary to evaluate how the faults are handled in trials utilizing eight and ten rings. Figure 3-13 illustrates the changes in cloud detections that lead to the elimination of a fault.

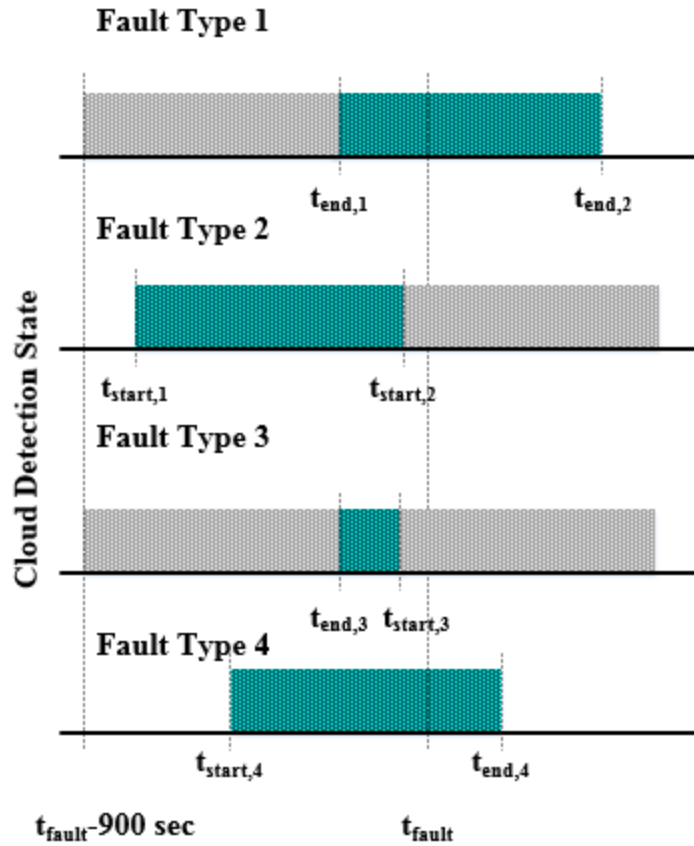


**Figure 3-13: Solutions for fault types 1-4**

For fault type 1, the cloud detection occurred shortly before the event. However, the jitter filter didn't hold the detection long enough to cause a generator to start up. Equation 3-4 specifies the difference in time from the end of the first cloud detection to the end of the second cloud detection, which caused the generator to start.

**Equation 3-4:**

$$t_{f,1} = t_{end,2} - t_{end,1}$$

For fault type 2, the cloud detection occurred too late to give adequate time for a generator to start. Equation 3-5 quantifies the amount of time for which a cloud detection occurred in advance of the original cloud detection at a lower ring setting.

**Equation 3-5:**

$$t_{f,2} = t_{start,2} - t_{start,1}$$

For fault type 3, there was a detection gap. Therefore, this could be resolved by increasing the hold time of the jitter filter. Equation 3-6 indicates exactly what the required hold time would need to be to sustain the cloud detection.

**Equation 3-6:**

$$t_{f,3} = t_{start,3} - t_{end,3}$$

Lastly, fault type four occurs when a cloud detection never occurred. Equation 3-7 indicates exactly how long the cloud was detected.

**Equation 3-7:**

$$t_{f,4} = t_{end,4} - t_{start,4}$$

Figure 3-14 shows the faults that were cleared by increasing the number of rings in the forecast from 6 to 8 rings. This shows that the majority of the faults that were able to be cleared were type 4, which means that a cloud detection never initially occurred.

### Overview of Faults Cleared by Increasing to 8 Rings

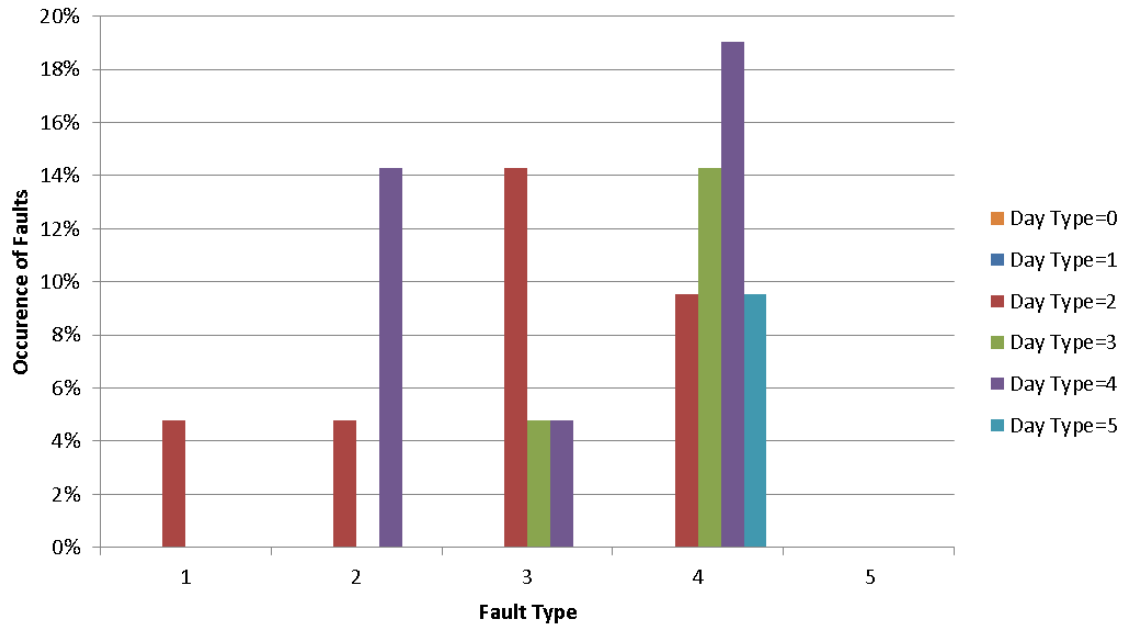


**Figure 3-14: Faults cleared by increasing number of rings in forecast from 6 to 8 rings**

Figure 3-15 shows the faults that were cleared by increasing the number of rings in the forecast from 8 to 10 rings. This bar plot shows that the majority of events cleared were either types 2 or 4.

## Overview of Faults Cleared by Increasing to 10 Rings

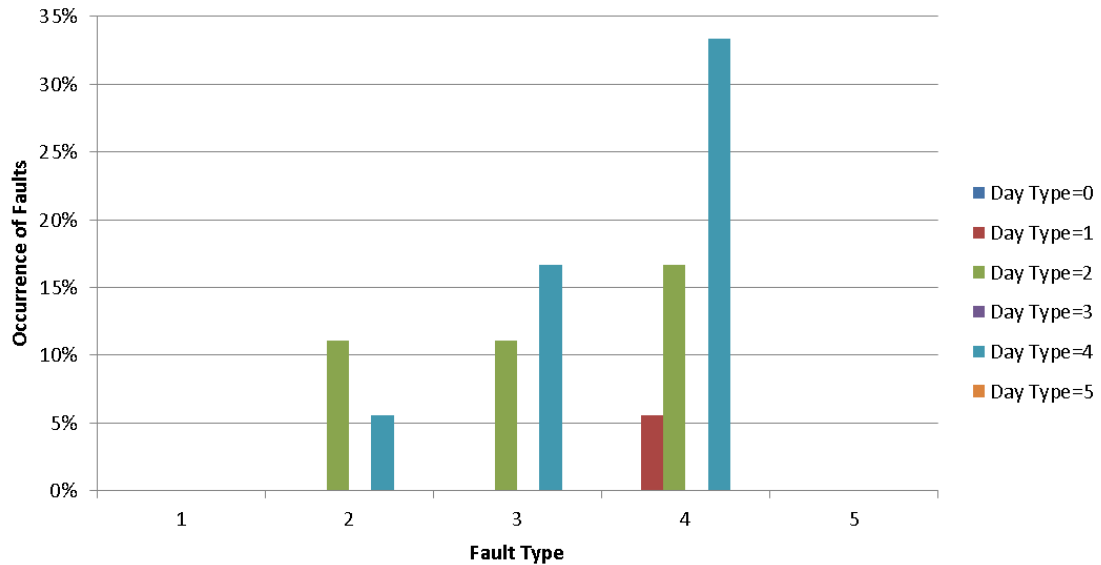


**Figure 3-15: Faults cleared by increasing number of rings in forecast from 8 to 10 rings**

Table 3-3 quantifies the values outlined in Equation 3-4 to Equation 3-7. From this table, it is shown that for fault type one, detections are extended for approximately 9246 seconds longer if the number of the rings in the forecast are increased from six to eight rings. For faults of type 2, detections occurred 282 seconds in advance of the fault if the rings in the forecast were increased from six to eight rings and 95.7 seconds if the number of rings was increased from eight to ten rings. For faults of type 3, the jitter filter would be required to extend the hold time by 121-200 seconds to prevent a fault from occurring. Although this sounds like a realistic approach, increasing the hold time on the jitter filter for every cloud detection is not ideal because it will ultimately result in more fuel burned to eliminate very few faults. That is why increasing the number of rings is preferable.

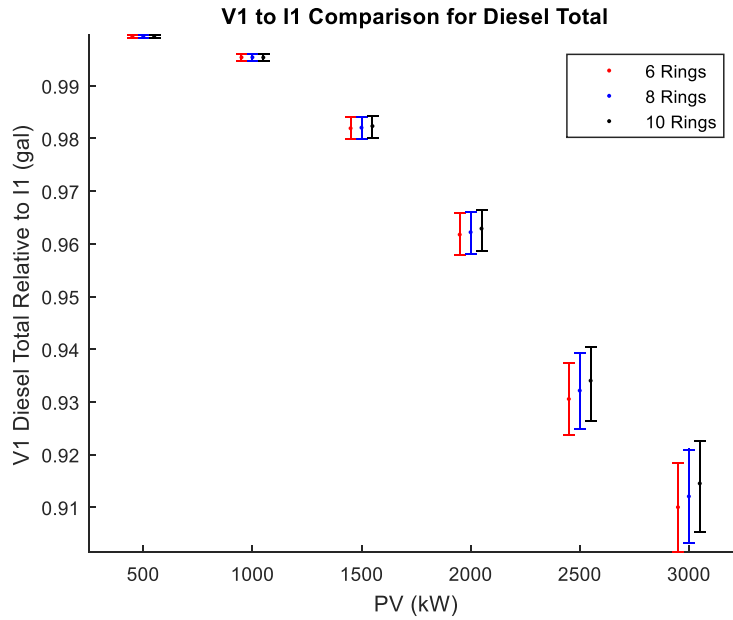
**Table 3-3: Results for fault types 1-4**

Rings Compared		Fault Type			
		1	2	3	4
		Extended forecast Time	New detect time in advance of event	Extended forecast time	Total Detect Time
6	8	9246 sec	282 sec	200 sec	10606 sec
8	10	N/A	95.7 sec	121 sec	7382 sec

*3.1.2 Comparison to “Industry Standard”*

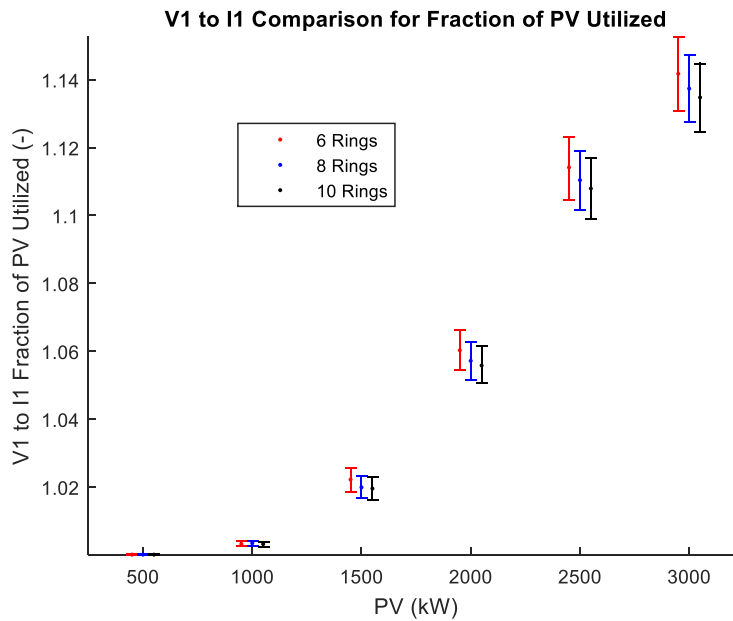
Next, the results from the V1 system will be compared to the “industry standard” to compare performance in diesel consumption, PV discarded, and the occurrence of faults. Section 1.7 goes into further detail on how the industry currently utilizes PV. Having an industry comparison is important because it tells the micro-grid owner how their system performs in comparison to a conventional control system.

Figure 3-16 shows how our system performs relative to the industry standard controller for diesel consumption at various array sizes. From this figure, it is evident that the V1 system outperforms the industry at array sizes  $> 1000kW$ . At array sizes  $< 1000kW$ , there is little benefit in choosing the V1 system. Additionally, the industry consumes more diesel than the V1 system at every array size because it consistently forecasts a lower value than the actual PV output (see Equation 1-7). Therefore, it forecasts a higher planning load for the generators and keeps more generators online than the V1 system.



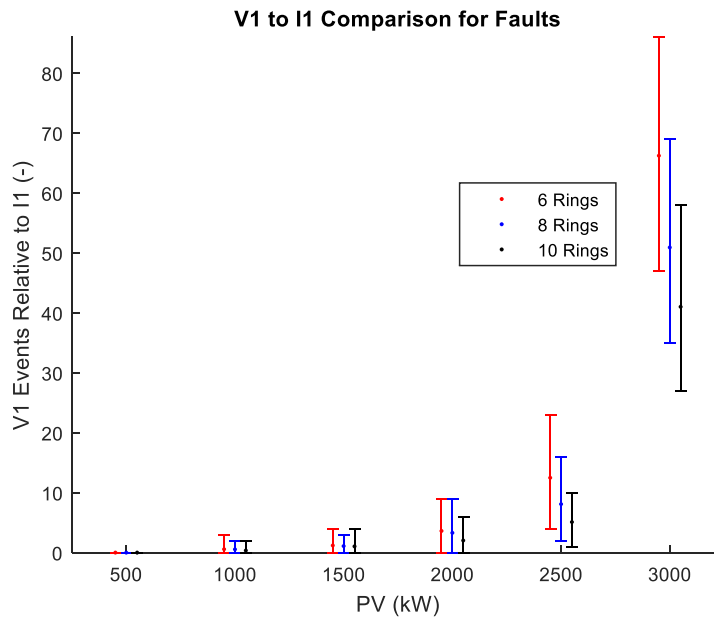
**Figure 3-16: V1 to I1 comparison for diesel total**

Figure 3-17 shows how our system performs in comparison to the industry for the fraction of PV utilized. From this plot, it is evident that the V1 system utilizes more PV across all array sizes.



**Figure 3-17: V1 to I1 fraction of PV utilized**

Figure 3-18 shows the V1 to industry comparison for the total number of faults. The total number of faults relative to industry does increase as array size also increases, but many of these events are able to be eliminated by increasing to 10 rings. At an array size of 2000 kW, the V1 system produces 1.71 faults per year more than the industry on average. However, the V1 system is still able to remain within the tolerable level for the acceptable fault occurrence if the micro-grid is willing to tolerate more faults to consume less diesel relative to the industry system.



**Figure 3-18: V1 to I1 comparison for number of faults**

### 3.1.3 Comparison to “No PV” Case

Next, a comparison was done to evaluate how much fuel would be saved in the case that the micro-grid had not yet installed a PV array. This is shown in Figure 3-19. At a large array size such as 2500 kW, the micro-grid can expect to consume 73.3% of the amount they would normally consume. Comparisons for faults and the total energy discarded were not done for the “No PV” case because it is assumed that the micro-grid site is not experiencing (PV-related) faults if no PV is connected.

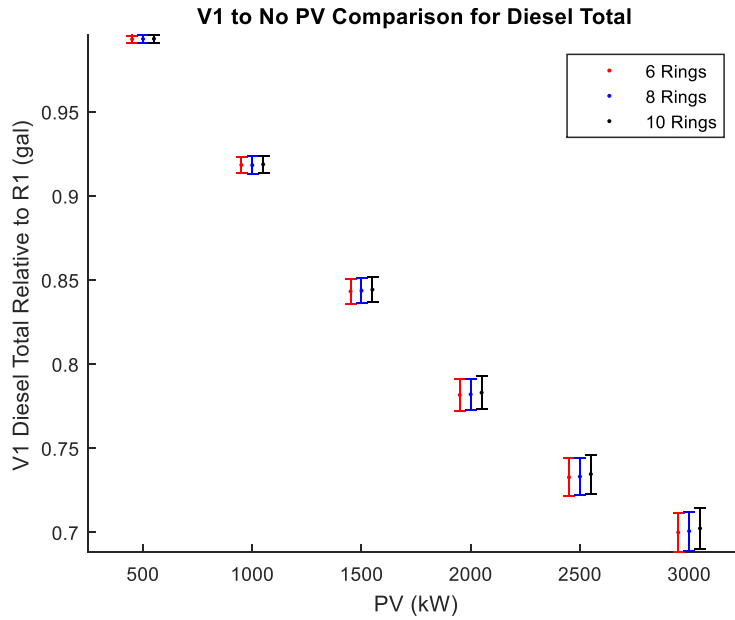


**Figure 3-19: V1 to “No PV” comparison for diesel total**

Figure 3-20 shows amount of diesel saved per kilowatt of PV that is added to the system. From this figure, it is observed that the highest amount of diesel savings per kilowatt of PV is achieved at an array size of 2000 kW. When the array size is greater than 2000 kW, the return on investment begins to decrease.

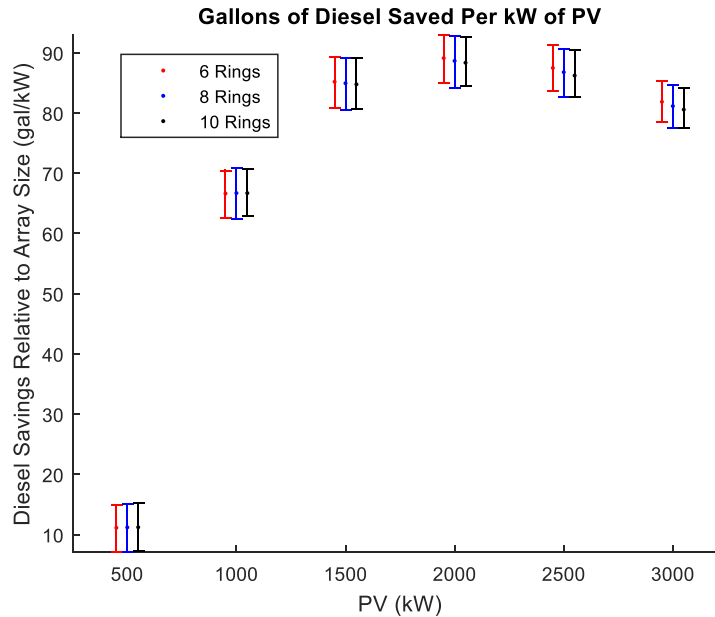


**Figure 3-20: Diesel Savings per kW of PV Added**

After the array size is increased beyond 2000 kW, the return seen begins to decrease because the amount of energy discarded to keep the system operating under stable conditions increases. However, it is important to note that the point at which the micro-grid will achieve the maximum return on investment is dependent on the load that is most frequently experienced. For instance, the micro-grid used for this paper most often sees a load of 2500 kW, and therefore the maximum return on investment is achieved at an array size of 2000 kW because there is enough PV while still retaining one generator online. At array sizes  $> 2000kW$ , the system must curtail PV to sustain a single generator online, regardless of the PV forecasted.

From the results discussed in this section, it is concluded that the micro-grid should invest in a 2000 kW array. With this array size, the micro-grid can expect to see 12 faults per year on average if 10 rings are used in the forecast. Additionally, with a 2000 kW the micro-grid will see the maximum return on the investment with an average diesel savings of 88.6 gal per kilowatt of PV installed. This exceeds the daytime diesel savings with the “industry standard” system by

approximately 3.65%. Lastly, it is recommended that the micro-grid owner chooses an array size  $> 1000kW$ , as an array size smaller than this would provide little benefit relative to the “industry standard” when diesel consumption for both systems is compared.

### **3.2 Increasing Generator Count**

Equations 1-15 through 1-17 show that the maximum PV that is able to be utilized by the V1 system is limited by the number of generators online because PV must be curtailed to keep the generators above their minimum rated relative loading and below their maximum rated relative loading. Therefore, using a large generator such as the 1 MW generators currently utilized by the micro-grid results in large amounts of PV curtailment. The following sections will describe trials were performed to evaluate if increasing the generator count could reduce the overall diesel consumption for the V1 system.

#### *3.2.1 Results Assuming No Variance in Trend Lines*

To evaluate whether generator count alone could reduce the diesel consumed by the micro-grid, a trial was performed with two generator sizes (300 kW and 1000 kW) assuming the same relative fuel consumption across 0-100% relative loading. The diesel consumption results for three and ten generators using the same trend line are shown in Figure 1-6. For all PV levels, it can be observed that using smaller generators with the same trend line had a small impact on diesel consumption. On average, there was an 8,500 gallon reduction in diesel consumed by using ten generators in comparison to only using three generators.

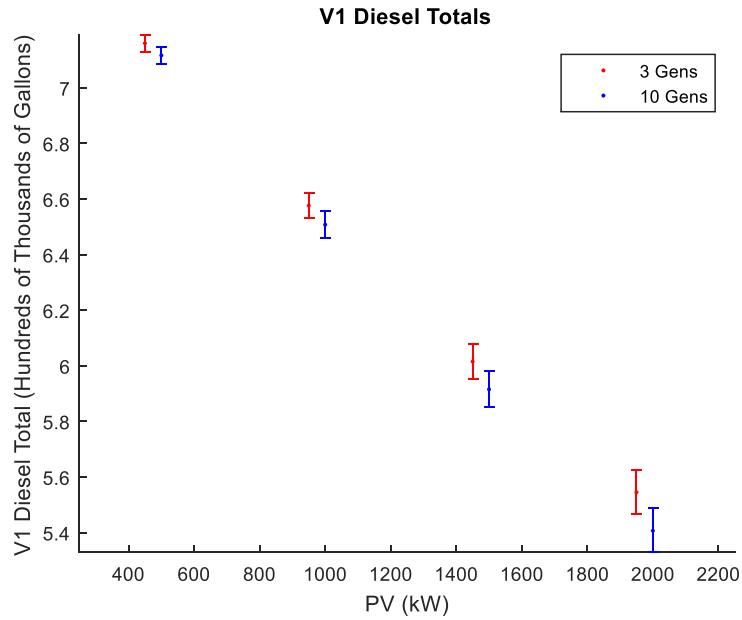


**Figure 3-21: V1 Diesel Totals for three and ten generators**

Using ten generators allowed for less diesel consumption because it allowed for loads <300 kW to be removed from the generators and satisfied by the PV system. The increased utilization of PV with ten generators is illustrated in Figure 3-22.

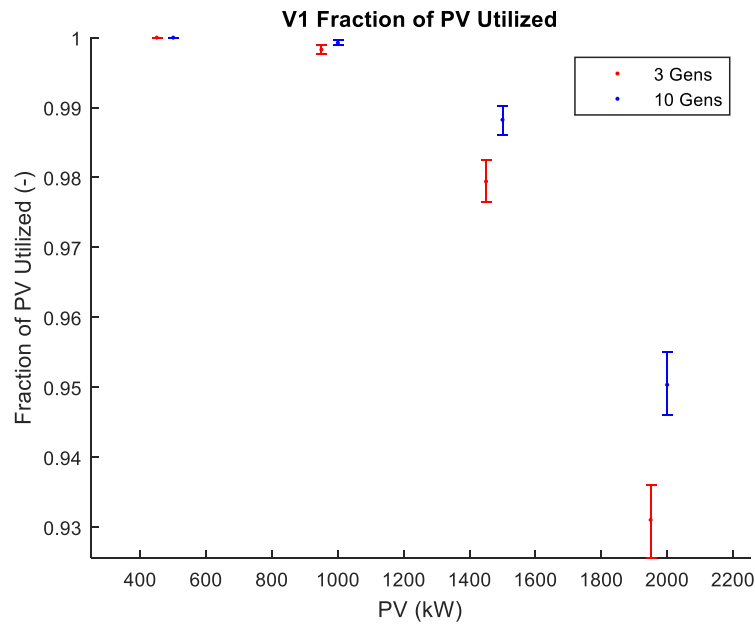


**Figure 3-22: V1 fraction of PV utilized for three and ten generators**

At array sizes  $> 1000kW$ , the system sees the largest benefit by switching to a 10 generator system. At array sizes smaller than this, difference in amount of PV utilized is small. The increased utilization of PV at array sizes  $> 1000kW$  results in an increased number of “generator cycles”. A “generator cycle” is defined as a single instance where a generator comes online and eventually transitions to being offline as a result of shedding load. An increased number of generator cycles indicate that there were more frequent generator startups and shutdowns.

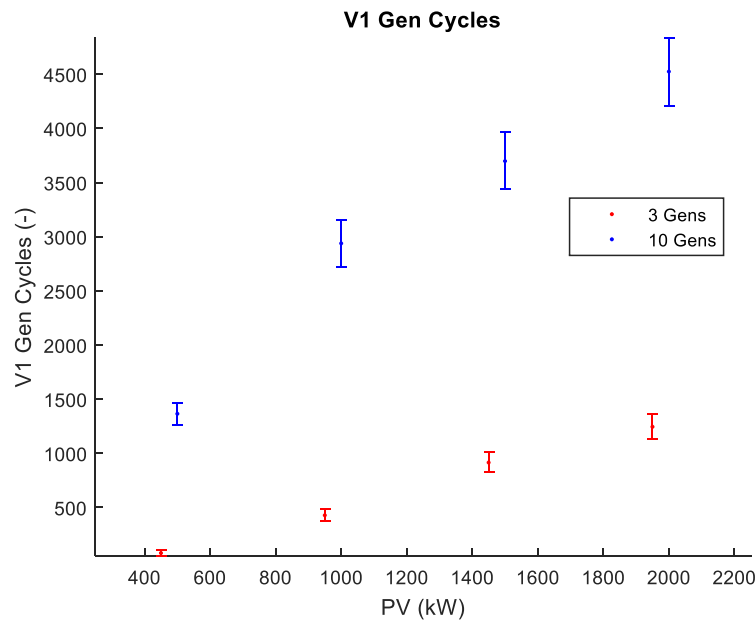


**Figure 3-23: V1 generator cycles for three and ten generators**

Next, it’s important to compare the occurrence of faults when three and ten generators are utilized. Although an increased number of generator cycles can result in lower fuel consumption, it’s important to investigate if adding generators to the system increases occurrence of faults and therefore, has the potential to jeopardize the integrity of the system.

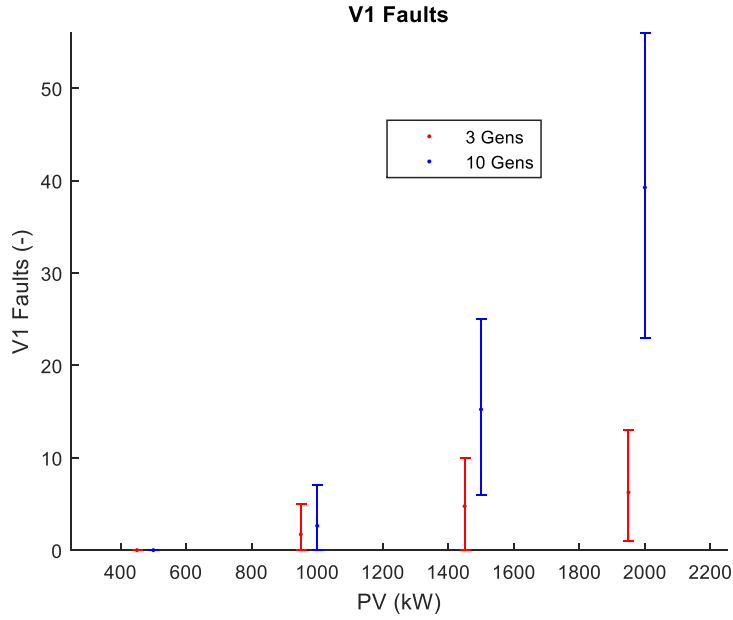


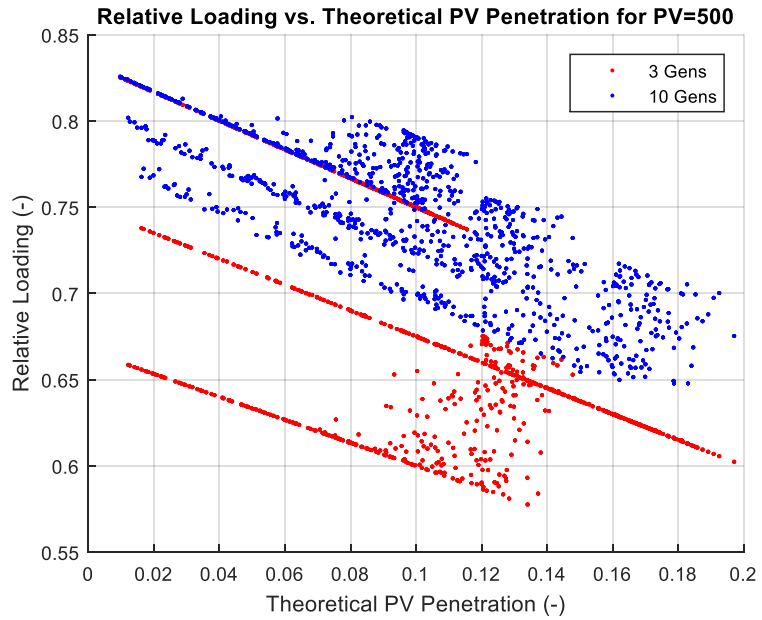
**Figure 3-24: V1 Faults for three and ten generators**

From Figure 3-24, it is evident that at all levels, using ten generators results in an increased number of faults. This could mean that generators are not able to start in time to avoid faults. Additionally, the system is unable to synchronize multiple generators when the instantaneous increase in net power demanded from the generators increases. Therefore, if the increase in net power demanded is greater than 300 kW, it will result in the generators being overloaded. To resolve this problem, the generation reserve can be increased.

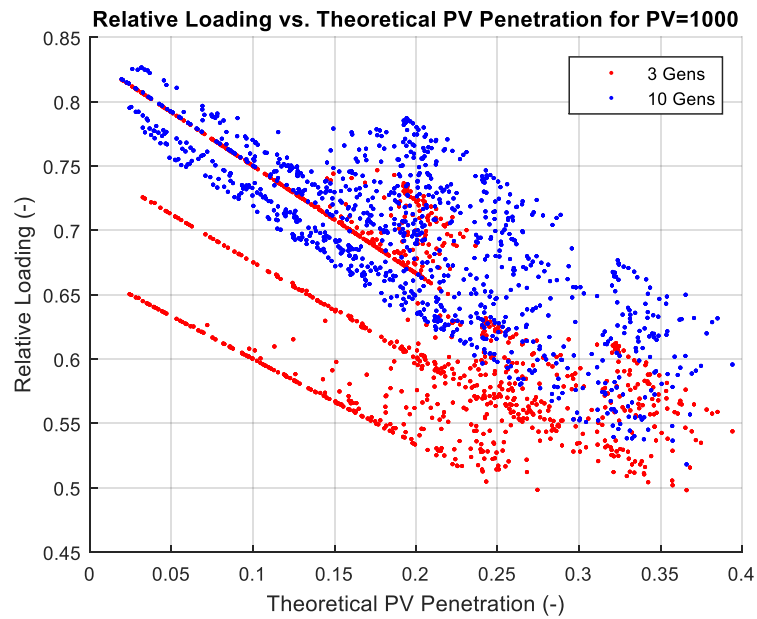
Figure 3-25 to Figure 3-28 show the relative loading vs the theoretical PV Penetration for array sizes ranging from 500 kW to 2500 kW. Equation 3-8 defines theoretical PV penetration,  $\chi_t$ , which is the resulting PV Penetration if all available PV were utilized.

**Equation 3-8:**

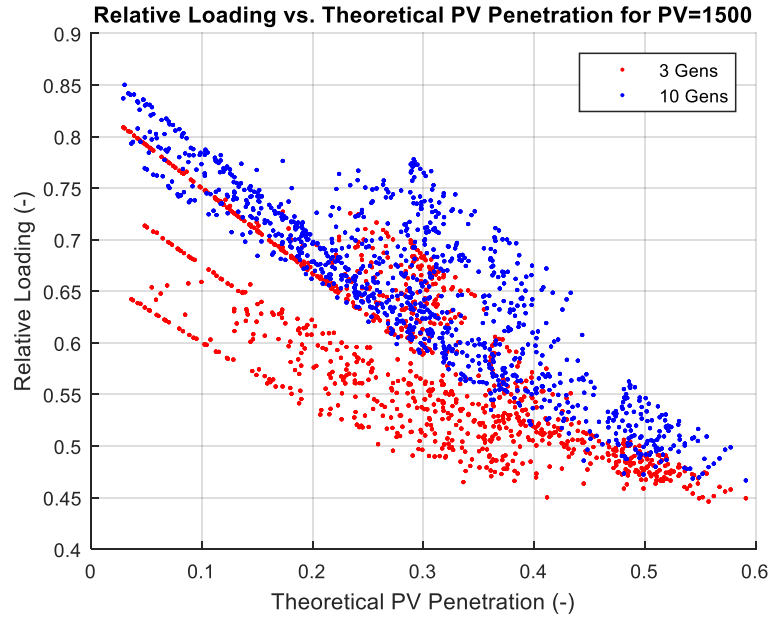
$$\chi_t(t_e) = \frac{\int_0^{t_e} PV_{avail}(t) dt}{\int_0^{t_e} L(t) dt}$$



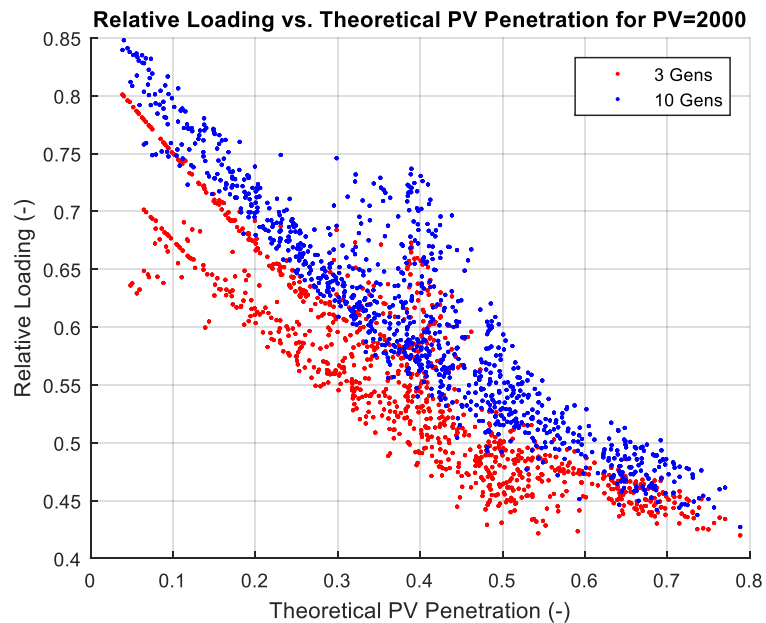
**Figure 3-25: Relative Loading vs. Theoretical PVPen PV=500 kW**



**Figure 3-26: Relative Loading vs. Theoretical PVPen PV=1000 kW**



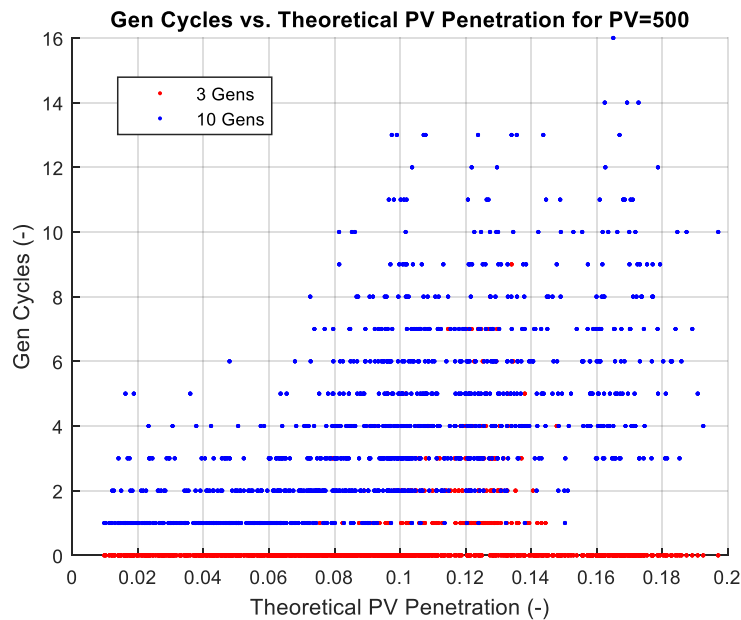
**Figure 3-27: Relative Loading vs. Theoretical PVPen PV=1500 kW**



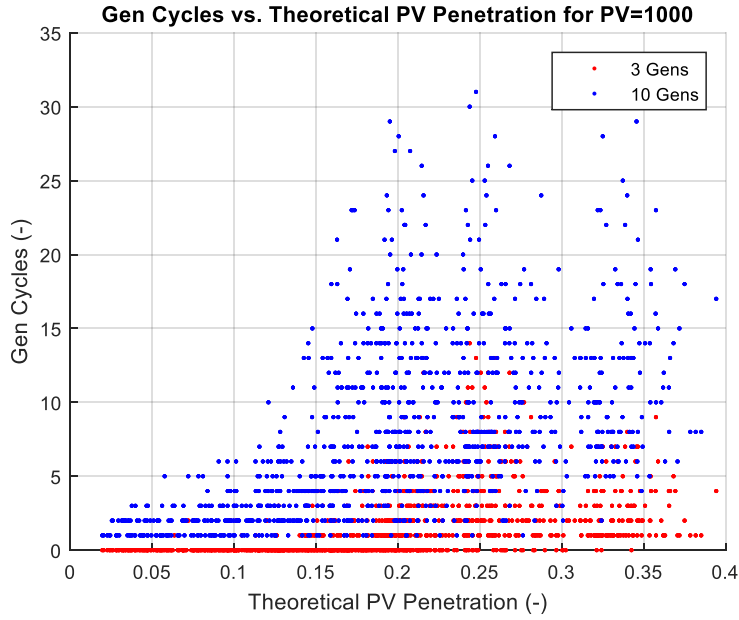
**Figure 3-28: Relative Loading vs. Theoretical PVPen PV=2000 kW**

In Figure 3-25, the relative loading appears to be linear for all levels of theoretical PV penetration. The three lines in this figure represent the three load islands in the MTM shown in Figure 2-15. Additionally, it is clear that these lines are more distinct when only three generators

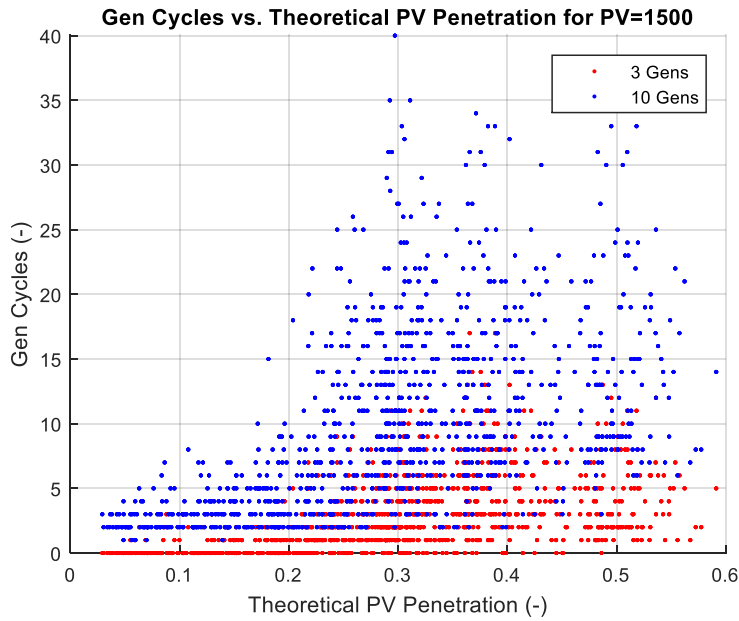
are utilized in a simulation and when an array size  $< 1500kW$  is selected. This is due to the fact that the number of generator cycles are more constrained, as shown in Figures 3-30 through 3-33. The constraints on the generator cycles are due to constraints on the net power commanded from the gensets. For example, if the array size is 1000 kW, the generator system can expect to see  $>1500$  kW of load for the majority of the year because the load most frequently seen by the micro-grid is 2500 kW for 73.3% of the year. Therefore, the system will maintain a minimum load on the generators that would be higher than the minimum load on the generators at an array size of 2500 kW. This results in fewer generator cycles.



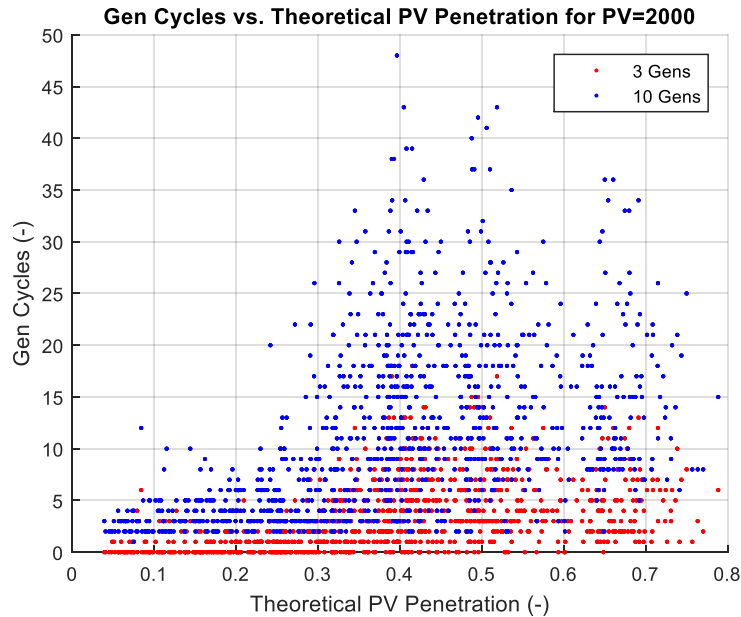
**Figure 3-29: Gen Cycles vs. Theoretical PVPen for PV=500 kW**



**Figure 3-30: Gen Cycles vs. Theoretical PVPen for PV=1000 kW**



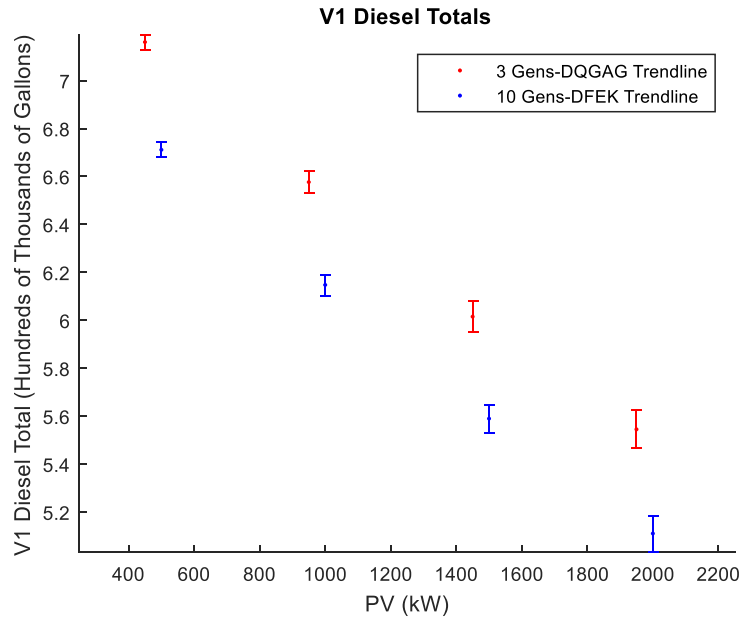
**Figure 3-31: Gen Cycles vs. Theoretical PVPen for PV=1500 kW**



**Figure 3-32: Gen Cycles vs. Theoretical PVPen for PV=2000 kW**

### 3.2.2 Results Assuming Separate Trend Lines

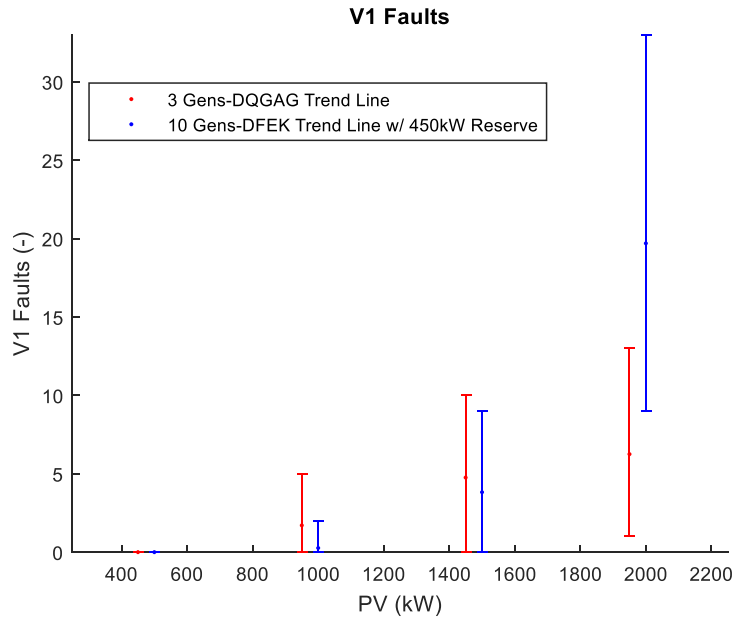
In the previous runs, the same trend lines were used for both the three and ten generator runs to isolate the impact of generator count alone on diesel consumption. However, the Cummins DFEK generator (rated at 400 kW, scaled down to 300 kW) is more efficient than the Cummins DQGAG generator (rated at 1232 kW, scaled down to 1000 kW). This is also illustrated by the specific fuel consumption curves in Figure 2-19. Therefore, the utilization of a smaller and more efficient generator such as the DFEK will result in lower annual diesel consumption. On average, using the DFEK trend line for the ten generator simulation saved 40,000 gallons in comparison to the three generator simulations using the DQGAG trend line.



**Figure 3-33: Fuel consumption results using DFEK and DQGAG trend lines**

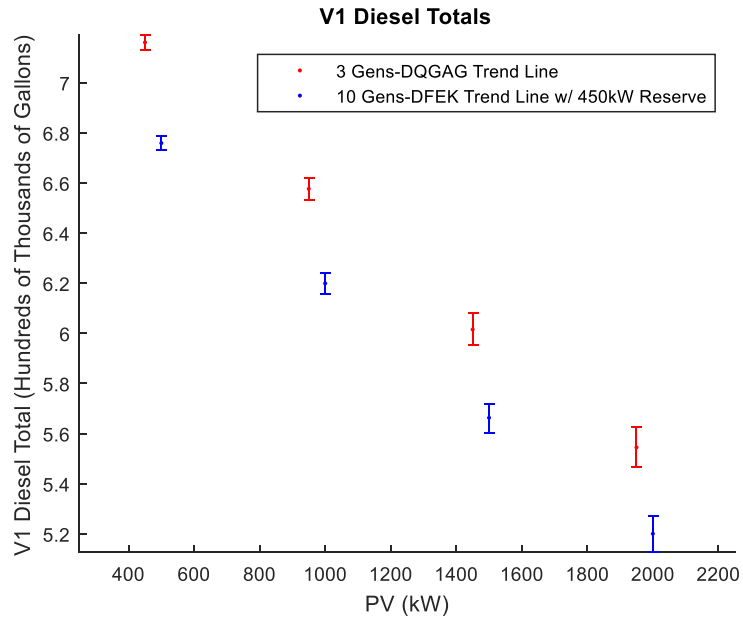
### 3.2.3 Results for Ten Generators with Varied Reserve Settings

Figure 3-24 shows that the utilization has the potential to triple or quadruple the occurrence of faults seen by the micro-grid, depending on the array size. Therefore, to utilize ten generators, the issue of increased fault count must be addressed. After increasing the reserve to 450 kW for the ten generator runs (previously set to 200 kW), the occurrence of faults decreased significantly, as shown in Figure 3-34. Compared to Figure 3-24 (results if 200 kW reserve is used), the faults are reduced by more than half at all array sizes.



**Figure 3-34: V1 Annual fault counts for 3 generator simulations and 10 generator simulations using 450 kW reserve**

From Figure 3-34, it is evident that the 10 generator simulation outperformed the 3 generator simulation at array sizes  $\leq 1500kW$  because the fault counts are lower if 10 generators are used with a 450 kW reserve. For array sizes  $> 1500kW$ , the reserve would need to be increased further to outperform the three generator simulations. Therefore, it is clear that for array sizes  $\leq 1500kW$ , it is best to use ten generators with 450 kW of reserve. Additionally, Figure 3-35 shows that using 10 generators a reserve setting of 450 kW saves approximately 37,000 gallons of fuel on average. Therefore, it is evident that using 10 generators with 450 kW reserve is acceptable for array sizes  $\leq 1500kW$ .



**Figure 3-35: V1 diesel totals for 3 generator simulations and ten generator simulations using 450 kW reserve**

## 4 CONCLUSION

The work presented in this paper examined the optimization of daytime diesel fuel consumption for a hybrid diesel and photovoltaic (PV) industrial micro-grid with no energy storage. The micro-grid utilized a control system developed to forecast PV transients and manage the diesel generators providing electrical supply to the micro-grid. The work focused on optimization of daytime fuel consumption when PV generation is available. Simulations were utilized to minimize diesel consumption while maintaining secure operations by controlling both PV curtailment and diesel generation. The control system utilized a cloud forecast system based upon sky imaging, developed by CSIRO (Australia), to predict the presence of cloud cover in concentric “rings” around the sun’s position in the sky. The control system utilized these cloud detections to establish supervisory settings for PV and diesel generation. Work included methods to optimize control response for the number of rings around the sun, studied the use of two different sizes of generators to allow for increased PV utilization, and modification of generator controller settings to reduce fault occurrence.

Results showed that using 10 rings to formulate the PV forecast achieved the greatest fault reduction, while having a minimal impact on diesel fuel consumption across all array sizes. Additionally, for three generator simulations, the greatest return on investment was achieved an array size of 2000 kW with a diesel savings of approximately 85 gallons per kilowatt of PV installed. However, it is important to note that the point at which the micro-grid sees the maximum return on investment is dependent on the most frequently observed load.

To see a return on investment relative to the industry, it is recommended that the micro-grid selects an array size  $>1000$  kW, as anything smaller than this results in nearly the same diesel consumption.

Next, it is recommended that the micro-grid utilizes 10 generators, as this allows for increased PV utilization relative to 3 generators. Equations 1-15 through 1-17 show that the maximum PV output is dependent on the generator size and the minimum/maximum rated relative load of a generator, as exceeding these limits puts the generators at risk for faults. It is also important to note that in every hybrid diesel-PV micro-grid, the amount of PV that is able to be utilized will always be limited by the generator size, as fault definitions for generators are defined based on their levels of relative loading. Considering that introducing higher PV utilization also increases the risk of faults with 10 generators, it is recommended that the reserve be increased to 450 kW. For array sizes  $\leq 1500$  kW, the system will always experience less faults than the 3 generator system with an average of 37,000 gallons of diesel saved. Therefore the final recommendations for the micro-grid are to use 10 generators, a PV forecast with 10 rings, and 450 kW of reserve.

Lastly, it is important to state that this paper is not specific to a single micro-grid location. If given a single-diagram, equipment specifications, three months of load data, and several months of irradiance recordings for a test site, these results can be reproduced for any micro-grid, and thus recommendations for array sizes can be made for various sites.

#### **4.1 Recommendations for Future Work**

In future versions of this system, it would be ideal to have battery storage for the discarded PV output. This will lead to further energy savings for the owner of the micro-grid site. However, battery life as a result of depth of discharge will need to be taken into account. Considering that

battery life can decrease very fast if the battery is drained at a high depth of discharge, there will need to be a system to control this. This system may work best to make use of excess PV energy that is curtailed on sunny days (i.e. PV previously needed to be curtailed to avoid damage of other equipment on that day). The stored energy could be used during the nighttime hours. The penetration of the stored energy can be held low enough where damage to the generators would not be inflicted and battery life would be extended. Planning for how to use the energy during the nighttime hours could be done using the Clear Sky Model, which would tell you the number of daytime hours of PV and one could also estimate the number of nighttime hours from this model. In addition to battery storage, other storage options can include (but are not limited to): a flywheel or a hydrogen electrolysis/fuel-cell system. However, before deployment, a cost-benefit analysis should be done to evaluate which of these (or other storage options) is the best option. Aside from using energy during the nighttime hours, the stored energy could also be used to supplement the PV during times when PV drops occur. This would benefit the system greatly because it could prevent the fuel cost that bringing another generator online would require. This system would most likely not be utilized for extended periods at a time. However, it could delay a generator start up for several minutes at a time and could interface with the scheduler to bring another generator online when necessary.

Aside from optimizing storage options, the PV forecasting system could be improved by including information about cloud vector information. This would give a more accurate PV forecast, which would in turn lead to less PV being discarded at the time it is available. When forecasting PV with the vector information, several cloud vector layers should be considered to obtain the most accurate forecast. This is important because different cloud layers move at different rates.

## APPENDICES

### 4.2 Load Management

This section will detail the requirements for various conditions in the load management state machine, as previously discussed in section 2.3.

#### 4.2.1 Load-Dependent Start

The load dependent start setting forces a generator to synchronize when the following conditions are met:

1.  $P_{avail} < LD_{start}$
2.  $n_1 > t_{LD\ start}$
3.  $N_f = N_o$

Where:

$LD_{start}$  is the load dependent start threshold

$n_1$  is the number of consecutive time steps where the power available has exceeded the load dependent start threshold

$t_{LD\ start}$  is the number of consecutive time steps where the power available must fall below the load dependent start threshold for a 'START' command to be sent

##### 4.2.1.1 'Non-Connected Gens' Parameter

This parameter will stop a generator from synchronizing if load dependent start was previously triggered and the following conditions have been met:

1. Requirements in section 2.3.2 for load dependent start have been met
2.  $N_{min} \leq N_o$  (*generator has not synchronized*)

3.  $P_{avail} > LD_{start}$
4.  $n_2 > t_{NonnConnGens}$

Where:

$n_2$  is the number of consecutive time steps where the power available as exceeded the load dependent start threshold after a ‘START’ command has been sent

$t_{NonnConnGens}$  is the number of consecutive time steps where the power available must exceed the load dependent start threshold after the initial ‘START’ command to force the generator into the ‘COOLDOWN’ state

#### 4.2.2 Load-Dependent Stop

For the load dependent stop function to be activated, the following criteria must be satisfied:

1.  $P_{avail} - P_g > LD_{stop}$
2.  $N_{min} < N_o$
3.  $n_3 > t_{LD Stop}$

Where:

$LD_{stop}$  is the load dependent stop threshold

$n_3$  is the number of consecutive time steps where the power available has exceeded the load dependent stop threshold

$t_{LD Stop}$  is the number of consecutive time steps where the power available minus the rated power for one generator (theoretical new power available) must exceed the load dependent stop threshold for a ‘STOP’ command to be sent

### 4.3 Configuration Parameters

```
conf.Step = 1; % step size of load & PV
conf.InitN = 1800; % settling time
conf.RandomSeed = 0;

% Transient reserve with load step forecast
load.Load = 1e6; % default load if non other is provided.
load.LoadExpectedStep = 900e3; % reserve if a load step is expected.
load.NoWarnReserve = 200e3; % reserve if a load step is not expected
load.HCThreshold = 400; % Heavy consumer threshold for warning (W)
load.HCTime = 300; % warning period load step to warn
load.VaryLoad = true; % if true, load variation is superimposed on load
load.TanzLevels = [659 1581 2377]; % load levels at probability peaks in Tanz data
load.TanzProb = [0.1197 0.1480 0.7323]; % Probability which Tanz load levels occur
conf.Load = load;
Gen.GenSize = 1000e3; % full load rated capacity of generators
Gen.IdleFuelRate = 12.4/3600; % fuel rate when idling (gal/s or equivalent)
Gen.FuelRateSlope = 66.32/3600; % rate of fuel increase by fraction of load (gal/s)

% Estimated behavior of individual generators in the generator cluster
Gen.StartingTime=30; % Starting time of generator
Gen.SyncTime=180; % Time to synchronize with grid
Gen.CoolDownTime=300; % Cool down time when stopping
Gen.CoolToSyncTime=60; % Time it takes for a gen to go from cooldown to sync states
Gen.UpStep=.2; % Ramp rate when loading a generator (fraction/s)
Gen.DownStep=.2; % Ramp rate when unloading a generator (fraction/s)

% DEIF Load controller parameters
Gen.LoadDepStart=200e3; % Load margin at which another generator is started (W)
Gen.LoadDepStop=300e3; % Gen stopped if running reserve > gen size + this parameter (W)
Gen.HeavyConsumer=600e3; % Reserve to add when heavy consumer warning is active
Gen.LoadDepStartTimer=10; % Delay before a generator is started (s)
Gen.LoadDepStopTimer=60; % Delay before a generator is stopped (s)
Gen.LoadDepStopNonConnGens=60; % Wait time before stopping a non-connected
% generator (before cool down) (s)

PV.ArraySize = PVSize; % peak clear sky power in watts
PV.InverterResponseRate = 0.15; % Speed at which controller responds to
% curtailment commands; SMA parameter
PV.FractionIfCloudy = 0.3; % PV output as fraction of clear sky if clouds

% perfect forecast window in seconds
PV.ForecastWindow = Gen.StartingTime + Gen.SyncTime + 30;

% Slew rate from Cormode, Daniel, et al. "Comparing ramp rates from large and
% small PV systems, and selection of batteries for ramp rate control."
% 39th IEEE Photovoltaic Specialist Conference. 2013.

% Rates for 99.99 percentile
rate2kW = 0.16; % Conservative
rate1600kW = 0.08; % Conservative
rate600kW = 0.09; % From Munich data from Ankur
PV.RampRate = rate600kW; % Fractional rate at which PV array changes (fract/s)

% Fraction of clear sky is adjusted dynamically. If PV drops below starting fraction,
% then the future level is adjusted on each time step was Gain*(observedFraction- %
curFraction)+curFraction

CL.StartFractionOfClearSky = PV.FractionIfCloudy;
% Fraction of estimated PV if clouds are seen.
```

```

% Starting value that is tuned later
CL.LevelStartTrackingFraction = 0.3;    % Level of PV output as fraction of clear sky
                                         % irradiation, where tracking starts/ends
CL.FractionGain = 0.1;                  % f_c: Proportional gain when
                                         % adjusting the fraction setting

% Base threshold levels on which all of the ensemble forecasts are based
% Chicken little thresholds for max rings
CL.Thresholds = [0.5 0.1 0.1 0.1 0.1 0.1 0.1 0.1 0.1 0.1];

% Main forecast used when at low risk
CL.MainKt = 1;
CL.MainKm = 30;
CL.MainT = CL.Thresholds(1:6);    % Use the base threshold values
CL.MainRisk = inf;                % Always trigger on this forecast
CL.MainHold = 1200;               % Hold time if this forecast is tripped

% Forecast engaged when risk drops near the likely error in FractionOfClearSky
CL.F1Kt = 2;
CL.F1Km = 30;
CL.F1T = CL.Thresholds(1:8) * 0.5; % 1/2 threshold values + 2 additional rings
CL.F1Risk = 0.05; % Engage if gens could be overloaded, but not in crisis overload
CL.F1Hold = 900;

% Forecast engaged when serious risk of a critical overload if cloud missed
CL.F2Kt = 3;                      % Allow three hits to stabilize
CL.F2Km = 30;                      % Smoothing
CL.F2T = CL.Thresholds(1:10) * 0.25; % 1/4 of threshold values + 4 additional rings
CL.F2Risk = -0.15;                % Engage if gens at risk of a crisis overload
CL.F2Hold = 600;

CL.RiskArray = [CL.MainRisk CL.F1Risk CL.F2Risk];
CL.HoldArray = [CL.MainHold CL.F1Hold CL.F2Hold];

% Forecast to clear holds faster. Currently does not work. Disabled
CL.ClearKt = 3;
CL.ClearKm = 240;
CL.ClearT = CL.Thresholds*0.01;
CL.ClearSkyDropRate = 5;          % Clear holds at 5 seconds per cycle of controller
                                   % if a clear sky is detected

% Load leves in fraction of generator full load
CL.CrisisMinLoad = 0.05; % below this level, controller takes immediate action
CL.MinLoad = 0.3;        % decreases generation if persistently below this level
CL.MaxLoad = 0.90;       % increases generation if persistently above this level
CL.CrisisMaxLoad = 0.99; % above this level, controller takes immediate action
CL.WaitToDecrease = 120; % sec to wait before commanding decrease in generators on
CL.WaitToIncrease = 10;  % sec to wait before commanding increase in generators on
CL.PVPerSecond = 0.1;    % max PV movement allowed per second, relative to gen size
CL.StartAtPV = 0.2;      % level at which controller starts, relative to gen size

Ind.MinLoad = CL.MinLoad; % minimum load on generators (fraction)
Ind.MaxLoad = CL.MaxLoad; % maximum load on generators (fraction)
Ind.ActiveHours = [7 17]; % hours when controller is active
Ind.PVRampRate = 0.2;     % Maximum PV ramp range as fraction of generator size
Ind.DBWidth = 0.1;       % Dead band for start/stop of generators, as fraction of gen size

```